

Volt-VA control using multi-port converters for voltage management in low voltage feeders

R.V. Prins

Volt-VA control using multi-port converters for voltage management in low voltage feeders

by

R.V. Prins

to obtain the degree of Master of Science
at the Delft University of Technology,
to be defended publicly on Wednesday, 28 July 2021 at 9:00 AM.

Student number:	4317580	
Thesis committee:	Prof. dr. ir. P. Bauer,	TU Delft, chair
	Dr. ir. G.R. Chandra Mouli,	TU Delft, supervisor
	Dr. ir. R. Remis,	TU Delft
	Prof. dr. ir. T. Kevickzy,	TU Delft

An electronic version of this thesis is available at <http://repository.tudelft.nl/>.

Abstract

The increase in quantity and electrification of energy in residential areas pushes the existing distribution network to its limits. If left unchanged, the network will suffer from voltage violations caused by the increase of electric vehicle (EV) charging, energy generation by Photovoltaics (PV) panels and the phasing out of natural gas. Typically, cables are reinforced to cope with increased demand, but upgrading large parts of the Dutch electricity network is expensive. By not expanding the network, the remaining capacity of the network needs to be optimally used. This situation encourages the switch to an active distribution network, which opens up a new possibility for voltage management and optimal use of the distribution network.

One of these prospects is the multi-port converter. This converter combines the usually separate converters of EV, PV and battery energy storage system (BESS) to a single entity. Combined with an optimal charging algorithm, the energy management system (EMS) of the multi-port converter decides when to (dis)charge the BESS and EV, using a moving horizon window. By controlling the previously non-dispatchable loads, flexibility is generated on the demand side. Using a network of multi-port converters on its own is insufficient to cope with voltage problems in the distribution network due to the overlap of (dis)charging schedules and lack of communication.

A Voltage management system (VMS) is used to coordinate the EMS of all the multi-port converters in the network to stay within the voltage range. This controller aims to prevent and correct voltage problems by varying the input or output of the multi-port converter. The prevention is done by actively reserving energy and changing prices to encourage changes in the (dis)charge schedule of the multi-port converter. The correction of the voltage profile is achieved by active power (Volt-Watt), reactive power (Volt-VAR) and apparent power (Volt-VA) control.

Due to the stochastic nature of solar energy and load demand, the actual battery capacity and voltage profile may deviate. To combat the change in battery capacity, a reference tracker is installed. For the change in voltage, a real-time controller is implemented, used for rapid response. These controllers are placed inside the EMS under the optimal charging algorithm.

The main focus of this thesis is to design a control structure, which can be gradually deployed, to prevent and correct voltage problems in a low voltage feeder in various time scales. By using multiple intertwined controllers, the proposed hierarchical control structure achieves fast operation, prevention and correction of the voltage profile over an extended period.

The simulations have been validated on the IEEE European low voltage test feeder. Results demonstrate that a limited number of multi-port converters is needed to keep the voltage profile within limits. The various correction methods have been tested for effectiveness to correct voltage deviations. Both active (Volt-Watt) and apparent (Volt-VA) power show capabilities of voltage control. Furthermore, the real-time controller is capable of removing individual load usage from the network and prevent voltage violations caused by uncontrolled PV and EV.

Acknowledgements

Achtendertig jaar geleden heeft mijn vader op dezelfde faculteit (toen nog Technische Hogeschool) zijn studie elektrotechniek afgerond. Nu, na iets meer dan 7 jaar, kan ik zeggen dat ik hetzelfde heb bereikt. Toch is wat hij toentertijd op papier heeft gezet voor mij onbegrijpelijk. De regelsystemen van toen waren enorm gecompliceerd, uitgebreid en analoog. Nu zou met een algoritme veel betere resultaten worden geboekt in slechts een fractie van de tijd. Dit is niet om mijn pa te bekritisieren, maar om aan te tonen dat we in de afgelopen veertig jaar een gigantische vooruitgang hebben geboekt in de techniek. Ik hoop dat mijn zoon en/of dochter na het lezen van mijn thesis er over 40 jaar er hetzelfde over denkt. Met een terugkijkende blik: "Wat wisten we toen eigenlijk nog maar weinig".

I want to thank my weekly-supervisor ir. Wiljan Vermeer for guiding me through my thesis project. You always approached every subject positively, encouraged me and gave insight into the fundamentals of the energy network. I also want to thank my monthly supervisor, dr. ir. Gautham Ram Chandra Mouli for asking critical questions and giving his expertise on possibilities for voltage regulations. Lastly, I would like to thank prof. dr. ir. Tamas Kevickzy, prof. dr. ir. Pavol Bauer and dr. ir. Rob Remis of my thesis committee for taking the time to evaluate my performance.

Graag zou ik ook mensen uit mijn privé-omgeving willen bedanken. Ten eerste wil ik mijn ouders bedanken, die mij tijdens mijn studie, maar in het bijzonder in het laatste deel van mijn scriptie, hebben geholpen. Ten tweede wil ik mijn vrienden bedanken, waarmee ik een geweldig leuke tijd in Delft en omstreken beleefd heb. Als laatste wil ik mijn vriendin bedanken, die mij altijd heeft gesteund en geholpen in de moeilijke tijd voor en tijdens mijn scriptie.

*R.V. Prins
Delft, July 22, 2021*

Contents

Abstract	iii
Acknowledgements	v
1 Introduction	1
1.1 Changes in distribution network	2
1.2 Multi-port converter and Energy management system	4
1.3 Challenges for the Distributed Service Operator (DSO)	5
1.4 Research goals	5
1.5 Thesis contribution	6
1.6 Outline of the thesis	6
2 Background	7
2.1 Background	7
2.2 Control methods voltage mitigation	9
2.2.1 Voltage control methods in passive distribution network	9
2.2.2 Voltage control methods in active distribution network	11
2.3 State of the art	16
2.3.1 PV inverters	16
2.3.2 (Multiple-stage) coordinated PV inverters	16
2.3.3 Distributed control	16
2.3.4 Cost minimisation	16
2.3.5 Summary state of the art	17
3 Active distribution network model	19
3.1 The distribution network	19
3.2 Data inputs	21
3.2.1 PV	21
3.2.2 Load profile	22
3.2.3 EV	25
3.2.4 Electricity Price	25
4 Energy Management System	27
4.1 Energy Management System	27
4.2 AC Power balance	30
4.3 Multi-port converter interactions	31
4.3.1 PV	32
4.3.2 Battery energy storage system dynamics	32
4.3.3 EV dynamics	33
4.4 Battery degradation	35
4.5 Cost analysis	36
5 ADN control mechanism	39
5.1 Control structure	39
5.2 Control model for correction	41
5.2.1 Volt-Watt	42
5.2.2 Volt-VAR	43
5.2.3 Volt-VA	48
5.2.4 Volt-VA optimisation problem	48
5.2.5 Summary	50

5.3	Prevention measures	51
5.4	Power Reservation	56
6	Reference tracking and real-time control	57
6.1	Need for real-time control	57
6.2	Reference tracker.	58
6.3	Real-time controller	60
6.3.1	Capacity availability	62
6.3.2	Sector 1 (no hazard)	62
6.3.3	Sector 2 (Overvoltage hazard)	65
6.3.4	Sector 3 (Undervoltage hazard).	67
7	Results	69
7.1	Selection procedure	69
7.2	Summer day	70
7.2.1	Summer day with many multi-port converters (45)	71
7.2.2	Summer day with few multi-port converters(20)	82
7.3	Winter day	93
7.3.1	Winter day with many multi-port converters (45)	94
7.3.2	Winter day with few multi-port converters(20)	105
7.4	Moving horizon window	106
8	Conclusion and Future work	109
8.1	Conclusions	109
8.2	Future Work	109
A	IEEE European Low Voltage Test Feeder	111
B	Newton-Raphson Power flow equations	113
	Acronyms	115
	Bibliography	121

Introduction

From the start of the industrial revolution until now, most of the energy demand is based on the use of fossil fuels [1]. These fossil energy sources were for a long time thought to be irreplaceable and are used in all major energy sectors (e.g. transportation, housing and electricity generation). Generating electricity through fossil fuels has several advantages. These include easiness of scaling, flexible operation at the generation side and a foreseeable supply of energy. The downside is the production of vast amounts of CO₂ and other greenhouse gasses. As rising levels of these gasses result in an increased greenhouse effect, the unsustainable use results in an undesired climate change.

To combat this climate change, the Dutch parliament goal is to reduce the output of CO₂. This goal, named "het klimaataakkoord", aims to reduce the production of CO₂ by 80–95%, in the EU, by the year 2050 [2]. At this date, the energy generation must also consist entirely out of renewable energy sources (RES) [2]. These agreements will impact the residential housing sector as households are responsible for 27% of the final energy consumption [3]. Furthermore, the residential housing sector will undergo considerable changes in the coming decades:

- By 2050, the consumption of natural gas will be phased out [4]. To date, 71% of the energy consumption in dutch households is from natural gas [3]. This termination will lead to an increased load as the replacements are (partly) electrified.
- Increase in EV charging due to the increase in EV sales and phasing out of combustion engine cars (2030 in the UK) [5, 6]. As the transport sector contributes 31% of the global energy consumption, it also requires to be green [7]. To fully charge a modern EV (80 kWh) from 50% to full requires the energy of 3 daily households worth of energy [8]. If not properly controlled, the considerable energy demand will inflict peak loads [9].
- The rise of distributed generation (DG), predominantly achieved by the intermittent and uncontrollable PV [10]. If the generation of the DG exceeds the load, a bidirectional power flow occurs. During summer, when generation reaches peak power, the output may result in a high voltage in the network and requires the PV inverter to shut off. Due to an increase in penetration level and reliance on RES for electricity generation, disconnecting RES will no longer be eligible.

Furthermore, there is the possibility of the liberalisation of the energy market. Instead of a fixed price, a flexible rate per time unit is used to improve supply and demand. When cost minimising charging schemes are implemented, this will result in peak demand during low energy prices.

This increase in quantity and electrification of energy will cause complications to the conventional power infrastructure due to possible overvoltage, undervoltage and current violations. The distribution system operator (DSO) is responsible for the long term ability and feasibility to meet reasonable electricity demands in the network [11]. The DSO is at a critical stage to invest heavily in the distribution network as it increases energy at both demand and generation sides. Furthermore, the demand side contains the intermittent and uncontrollable factors of DG.

Ideally, the changes in the housing sector should cause minimal modification to the existing infrastructure. Replacing, reinforcing or expanding parts of the distribution network in all of the Netherlands to cope with larger loads and distributed energy resources (DER)(generators, loads and storage) is a costly, polluting and time-consuming process. Therefore, it is preferable to use the current AC distribution network and only modify parts of it to comply with the integration of DER. As the peak capacity is not increased, the remaining capacity should be optimally used. Improvements in power electronics, data communications

and advancement in network control can increase capacity usage [12]. However, this requires a change in the current distribution network.

1.1. Changes in distribution network

These changes will alter the structure of the traditional power system. The conventional power system, as seen in Figure 1.1, consists of three parts. These are generation, transmission and distribution using a unidirectional power flow from generation to distribution.

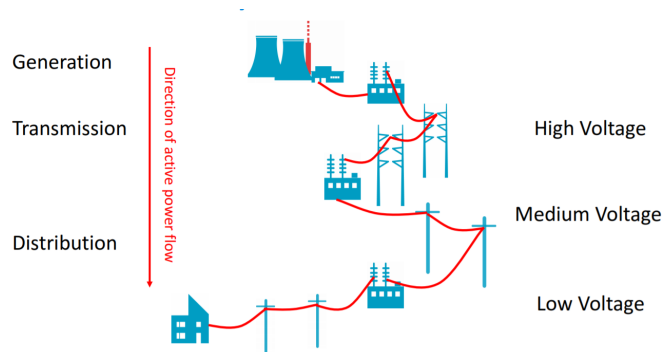


Figure 1.1: An overview of the traditional power system structure. This conventional structure uses large scale power plants for electricity generation, transmission lines for transportation, and a distribution feeder to provide to the end-consumer. Various voltage levels are used to decrease losses and provide stability and safety. (DCES, TU Delft)

These traditional power systems were designed to ensure sufficient and stable energy supply and do not integrate high levels of RES penetration. This is due to the bidirectional power flow at the distribution level, negatively affecting voltage regulation, protection, and installed equipment of the power system higher up [13].

Additionally, this traditional power system has no flexibility on the demand side. The power plants at the generation site are entirely responsible for the matching of generation and consumption. This centralised approach is wasteful as the last 10% of the generating capacity is only used 1% of the time [14].

In recent years, developments have been made to evolve the power system to handle bidirectional power flows and be flexible in operation on the generation and demand-side. To deliver these properties, the distribution network has to change from passive to active. An active distribution network (ADN) is described as:[15]

ADN are distribution networks that have systems in place to control a combination of DER (generators, loads and storage). DSO have the possibility of managing the electricity flows using a flexible network topology. DER take some degree of responsibility for system support, which will depend on a suitable regulatory environment and connection agreement.

A schematic representation of the upcoming power system, as an ADN, is given in Figure 1.2.

In literature, ADN and smart grid overlap in many aspects. A smart grid has the capability for consumers to use their energy supply. Consumers can coordinate when to buy or sell energy and, therefore, play a part in network optimisation [16]. ADN and smart grid are seen as interchangeable in this study and will implement the profound monitoring and information exchange and consumer interaction capabilities [17]. Similar, a microgrid can be seen as a subset of an ADN. The microgrid has the possibility to go in an islanded state, while the ADN will always remain in grid-connected mode. As the Netherlands has a strong grid, an option for an islanded state is not needed.

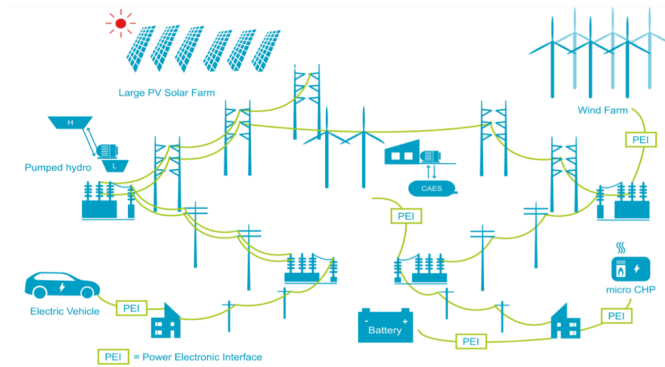


Figure 1.2: An illustrative example of the upcoming power systems. Using this ADN, integration of DER become possible. These include various energy storage systems, EV and the widespread use of RES. (DCES, TU Delft)

The change to an ADN has its ups and downs. The RES as DG can be quickly added to the network. This is beneficial for the DSO as locally generated energy decreases distribution losses. Furthermore, using techniques like demand side management (DSM), controllable loads can be moved to a more desired time slot. This can change the charging patterns of energy storage system (ESS) and EV to a more optimal time slot. A considerable disadvantage of the ADN is the need for (real-time) reliable communication and coordination between transmission system operator (TSO), DSO and end-consumers. Without coordination, DER may cause voltage violations. To avert these hazards, additional monitoring is needed to monitor the voltage at the distribution level, where traditionally, this is mainly done at the transmission and generation levels.

The monitoring is needed as the voltage is seen as a local signal, which can be locally controlled, and should be kept within a minimum and maximum. As stated by EN50160, the voltage at each bus should be $230V \pm 10\%$ 100% of the time to be acceptable. Due to the change to ADN, not only a voltage sag ($<207V$) but also a voltage swell ($> 253V$) can occur due to the increase in DER. As seen in Figure 1.3, not all users face the same consequences by the voltage deviation. The further you are away from the Point of common coupling (PCC) at the transformer, the more the voltage deviates.

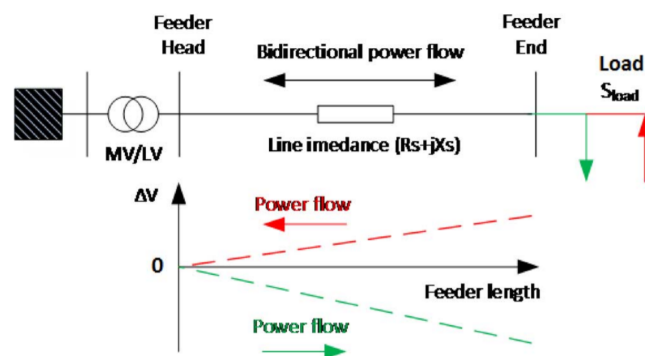


Figure 1.3: The deviation of the voltage across the length of the feeder. The voltage problems will occur at the end of the feeder as the voltage deviates further down the network [18].

Frequency, as a global signal, is assumed to be constant. This is due to the limited size of a single distribution network and the continuous grid connection. Its small influence would therefore not be able to inflict variations.

1.2. Multi-port converter and Energy management system

During the transition to ADN, the amount of DG, ESS, and EV will increase, making monitoring and control more complex. This increased complexity in local control and internal control results in longer computation time, and due to the unpredictable nature of RES, it can still inflict instability. To improve efficiency and controllability, a multi-port converter with energy management system (EMS) is proposed. By using this converter, it is possible to combine all previously separate converters into a single one. An overview of the multi-port converter is given in Figure 1.4.

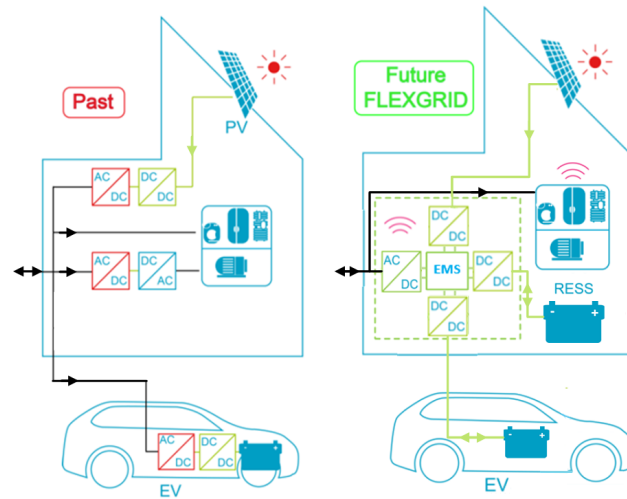


Figure 1.4: A schematic description of the change from multiple converters into a single multi-port converter. All previously separated converters are integrated into a single one. (DCES, TU Delft)

Using EMS and supervisory control and data acquisition (SCADA), all the components are individually controlled, and the usage can be tracked and presented to the consumer.

The potential benefits of using a multi-port converter with an EMS for either the DSO or the consumer are:

- **Efficiency:** BESS, EV and PV are inherently Direct Current (DC). Charging the BESS and EV from the PV power increases efficiency as the DC/AC step is removed. The removal of these DC/AC steps make a simpler, more compact and possible cheaper converter.
- **Voltage control:** From the definition of the ADN as stated in Section 1.1, this multi-port converter has to take a degree of responsibility for system support. System support can lower or increase the voltage by letting the DSO set limitations of active power or setting reference points for reactive power support. Although DER can also achieve this, the multi-port converter only requires a single connection, limiting communication. Furthermore, as the multi-port converter uses a 3-phase inverter, it removes any DER voltage unbalance.
- **Resilience:** The use of BESS in the multi-port converter, as seen in Figure 1.4, removes the direct connection of the PV to the distribution network. This eliminates the possible voltage sway created by either a large surplus or forecasting errors. Using a BESS, the multi-port converter can respond instantly to power changes if an imbalance occurs due to the fast power switches.
- **Optimisation:** The merging of each DER EMS to a single centralised EMS removes the need for coordination between the DER. If the DER elements were previously uncoordinated, which is currently the case, the merged EMS will optimally control charging patterns and improve load flexibility (during possible curtailments). Furthermore, a more detailed summary of information can be given to the end-consumer.

A downside of the multi-port converter is the cost of installation for people who already have already invested in individual converters. Using a multi-port converter, the integration of PV, EV and energy storage systems ESS has improved efficiency, economic performance and controllability [19]. Furthermore, the uncontrollable and unpredictable nature of RES is partly diminished by the direct connection to the BESS. However, if not monitored or controlled, the multi-port converter could still cause problems in a technical, financial and operational way.

1.3. Challenges for the Distributed Service Operator (DSO)

The arrival of ADN and the multi-port converter brings novel opportunities for the DSO. Using these developments, applications as power flow, voltage management and ancillary services as DG and load control become possible [15].

These opportunities imply that the DSO has to monitor and control the distribution network actively and account for the influence of the multi-port converter on the network voltage. To prevent hazards, the DSO needs to model the voltage in the network and perform control limitations (setpoints active/reactive power) accordingly.

The modelling of voltage can be negatively influenced by uncertainty. To minimise these effects, the DSO can use the following techniques:

- **Forecasting:** The elements which are bound to uncertainty in an ADN are:
 - Loads: Although for individual users hard to predict, load patterns are already used by DSO and TSO to match supply and demand. They vary day to day between users and are seasonally dependent
 - PV generation: The generation of PV can vary due to weather conditions and seasonal changes
 - EV departure/arrival time: People could arrive late or leave early and therefore disrupting the (dis)charging
- **Prediction and prevention:** By using horizon prediction or day-ahead scheduling, many hazards can be predicted using the data of the multi-port converters in combination with forecasting. By using the system support of the multi-port converter, prevention methods can be applied to remove the hazards prematurely.

With the techniques and capabilities offered by the development of technology, the DSO can increase the capacity efficiency of the distribution network within the voltage limits.

1.4. Research goals

This study focuses on developing a control system in an active distribution network that can utilise the benefits of the multi-port converter and can help the DSO prevent voltage deviation. This is needed to be able to use the distribution network for the coming decades reliably.

Therefore, the research goal is:

"Designing a control structure, which can use a network of multi-port converter energy management systems, to prevent and correct voltage deviations in a low voltage feeder"

As the transition in the distribution network is gradual, two additional sub-goals are set:

1. Designing a control structure that is capable of both gradual deployment and full occupancy
2. To create an EMS which is capable of removing real-time hazards under partial and complete occupancy

1.5. Thesis contribution

In this research, a hierarchical control structure is developed capable of preventing and correcting voltage violations in a distribution network (in advance). This control structure uses the multi-port converter to accomplish the correction and prevention of violations on multiple time scales. Intertwined controllers inside the multi-port converters' EMS have been developed to realise real-time control and optimal charge schemes. Gradual deployment is considered to incorporate the control structure into an existing distribution network.

This thesis distinguishes itself by providing the combination of (active power control (APC)) and (reactive power control (RPC)) for voltage management. Furthermore, various existing voltage management methods are combined, where usually only a single correction method is used.

1.6. Outline of the thesis

- **Chapter 1: Introduction**

A brief introduction of the current challenges in the distribution network and the corresponding opportunities that arrive by changing to an active distribution network. Additionally, the multi-port converter is introduced and the research goal is stated.

- **Chapter 2: Background**

This chapter covers the background on a wide range of present and upcoming voltage regulators in the distribution network. Moreover, the state of the art in voltage deviation techniques are discussed.

- **Chapter 3: Active distribution network model**

The IEEE European low voltage feeder is introduced, and the corresponding inputs are defined. These include the real-life data input of PV, load profile, EV arrival/departure time and electricity price. Furthermore, the error in the PV forecast and load data is discussed.

- **Chapter 4: Energy management model**

This chapter formulates the optimisation scheme of the multi-port converter EMS. This formulation includes the energy balance, battery degradation, constraints and cost function.

- **Chapter 5: Active distribution network controller**

Chapter 5 debates the chosen control structure and its model implementation. The interaction between the various control layers is explained and debated. The various methods to prevent and correct voltage deviations on a large time scale are described and reviewed on effectiveness.

- **Chapter 6: Reference tracker and real-time controller**

Chapter 6 focuses on the real-time controller and reference tracker. It explains why a real-time controller is needed and the additional data required to do so. Furthermore, it gives the mathematical formulations of the reference tracker and the real-time controller.

- **Chapter 7: Results**

This chapter shows the overall performance of the implemented control scheme. Several correction methods are compared based on the number of multi-port converters and seasonal changes. Furthermore, the impact of real-time control on the voltage deviation is shown.

- **Chapter 8: Conclusions and Future Work**

In the last chapter, a summary of the findings of the thesis is given. The research goal is reviewed, and conclusions are made. Recommendations are made on possible future work.

2

Background

Arising problems in the low voltage passive distribution feeders have gained a lot of attention due to the increase in DER. Firstly, this chapter explains how voltage changes occur in a distribution network with active and reactive power. Secondly, the various voltage control techniques in both passive and active distribution networks are discussed. Lastly, state of the art on voltage mitigation and prevention techniques are mentioned.

2.1. Background

Voltage problems occur by exceeding the load and generation capacities of the distribution network. From Figure 1.3, the voltage drop in a distribution network with loads is given by:

$$V_H = V_E + I(R + jX) \quad (2.1)$$

where V_H and V_E are the feeder head and feeder end bus voltage, R is the resistance, X is the reactance of the distribution line and I is the current through the distribution line determined by:

$$I = \frac{P - jQ}{V_E^*} \quad (2.2)$$

where P is the active load, Q is the reactive load and $*$ is the complex conjugate.

Filling in Equation 2.2 in 2.1 yields:

$$V_H = V_E + \left(\frac{P - jQ}{V_E^*} \right) (R + jX) = V_E + \frac{RP + XQ}{V_E^*} + j \frac{XP - RQ}{V_E^*} \quad (2.3)$$

Equation 2.3 can be approximated by only the real part as the angle difference between V_E and V_H is small.

$$\begin{aligned} V_H &\approx V_E + \frac{RP + XQ}{V_E^*} \\ V_H - V_E &\approx + \frac{RP + XQ}{V_E^*} \\ \Delta V &\approx \frac{RP + XQ}{V_E^*} \end{aligned} \quad (2.4)$$

Equation 2.4 shows that besides active power, reactive power can be used to change the voltage favourably. This can be done by injecting/absorbing reactive power in the opposite direction to active power.

However, the result of this injection/absorption, compared to active power, is less due to the reactance being low in a distribution feeder (high R/X ratio) [20]. Furthermore, there is a tradeoff between reactive power to create a voltage difference and power losses. The power loss is defined as:

$$I^2 R = \left(\frac{P^2 + Q^2}{V_R^2} R \right) \quad (2.5)$$

The losses increase when reactive power is used. Besides the losses, there are certain limitations on reactive power, both regulatory and physical. Regulatory, reactive power in DG has to oblige to a particular power factor. The power factor can be seen in Figure 2.1 and is described as:

$$\cos(\theta) = pf = \frac{P}{S} \quad (2.6)$$

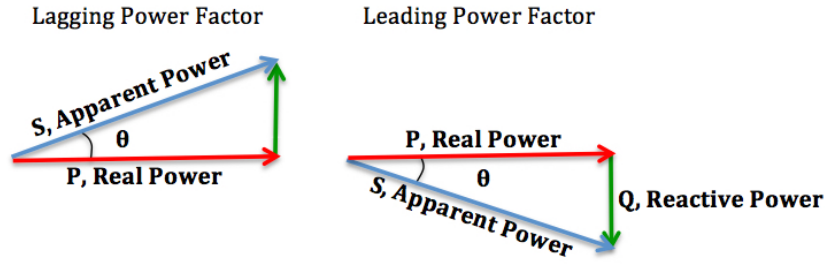


Figure 2.1: A representation of the power triangle with real, reactive and apparent power. Under current regulations the power factor θ can not exceed a certain angle [21].

where pf is the power factor, θ is the phase angle, P is the real power, and S is the apparent power. The current regulations are a maximum pf of 0.9 [22]. This means the max reactive power is limited by:

$$Q_{max} = P \sqrt{\frac{1 - pf^2}{pf^2}} \quad (2.7)$$

Physically, the amount of reactive power is limited by the inverter apparent power rating (S_{max}) and the active power usage of the inverter. The physically maximum amount of reactive power is:

$$Q_{max} = \sqrt{S_{max}^2 - P^2} \quad (2.8)$$

A schematic representation can be seen in Figure 2.7a. This limitation in operation range may result that reactive power alone is not enough to improve the voltage profile [23].

The reactive power itself is generated by the phase between the network voltage and the current. The switches inside the multi-port converter can alter the phase. By actively changing this phase, more or less reactive power can be injected or absorbed.

2.2. Control methods voltage mitigation

Now that the basics of voltage changes have been explained, the focus shifts to the techniques preventing voltage violations. Various studies have been performed to prevent or mitigate voltage problems. In [13, 20, 23–25], overviews are given of the different methods in low voltage feeders with (high) penetration of PV panels. A composition of techniques is presented in Figure 2.2.

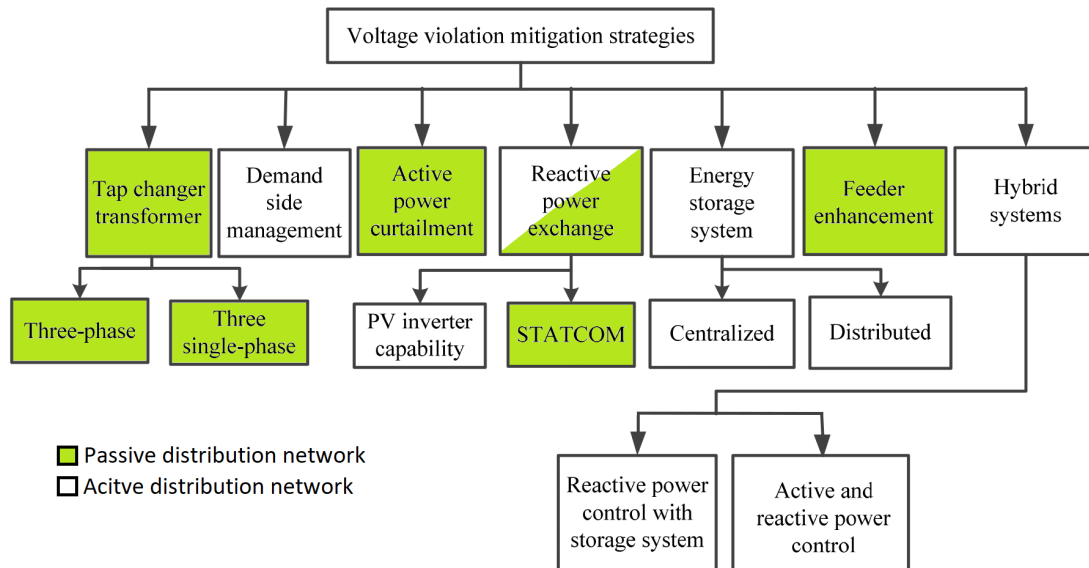


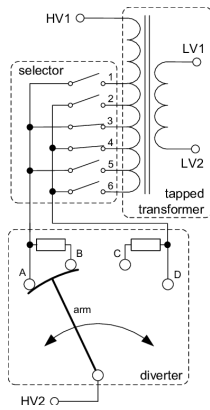
Figure 2.2: Overview of methods for voltage violation mitigation [23].

Each of the methods shown in Figure 2.2 will be discussed to give a broad view of the methods available to prevent voltage violation.

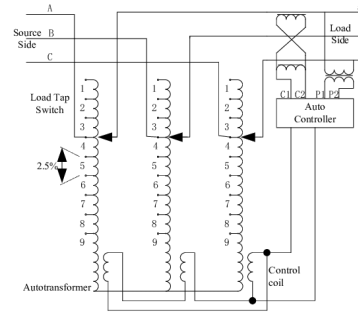
2.2.1. Voltage control methods in passive distribution network

The methods marked green in Figure 2.2 are the methods that currently are used in the distribution network. These can be controlled or uncontrolled. The only one without any possibility for control methods is feeder enhancement. Feeder enhancement is replacing cables to cope with higher energy demand. As stated previously, replacing a large part of the feeder is not economical or ecological justifiable, and the problem can quickly reoccur if penetration of DG increases. The traditional methods for voltage mitigation, which can use a form of control, is on-load tap changer (OLTC) transformer, (automatic) step voltage regulators (SVR), (voltage-controlled) capacitor bank (CB), static compensators (STATCOM) and active power control (APC).

An OLTC is a transformer that adjusts its secondary voltage based on the distribution network's voltage level or power consumption. The voltage or current can be either measured or estimated [23]. The voltage on the secondary side is changed by moving the tap position of the secondary coil, as seen in Figure 2.3a. Similar to OLTC, the (automatic) SVR changes the voltage using transformers but is located alongside the distribution feeder and is primarily used when the network distances are long. The schematic representation can be seen in Figure 2.3b.



(a) A schematic representation of the mechanical OLTC. It can change from tap position 3 to 4 by moving (increasing the turn ratio) the diverter and thereby decreasing the voltage [26].



(b) Schematic diagram of an automatic SVR [27]. Changing the turn ratio can be used to increase the voltage of one of the three phases.

Figure 2.3: Two implementations of tap changing voltage regulators

A voltage-controlled CB switches on to increase the voltage as needed. Besides the change in voltage, the capacitance of the CB can improve the power factor as it becomes less lagging. STATCOM is a reactive power compensating device capable of generating and absorbing reactive power using a switching converter. The output can be varied and accurately controlled by the operator. STATCOM is mainly used to compensate large consumers such as factories.

The use of methods like OLTC transformers, automatic SVR and voltage-controlled CB no longer suffice for controlling the voltage [13, 25]. For OLTC and (automatic) SVR, the main reason is frequent operation due to rapid voltage changes and slow switching times. CB only works when there are loads in the distribution network but fail to improve voltage level or power factor when generation occurs. Furthermore, it is difficult to estimate how much capacitance is necessary and where it should be placed. Recent improvements of the OLTC decrease the switching time to a few microseconds [18]. However, the inclusion of a modernised OLTC would require additional changes to the transformer, which we want to minimise. STATCOM is mainly intended for large users, and adding them to each distribution network is costly.

The best performing method in a passive distribution network is APC by curtailing, decreasing distribution losses and improving voltage [25]. If uncoordinated, the method curtails the amount of active power based on the bus voltage and the droop curve, as seen in Figure 2.4.

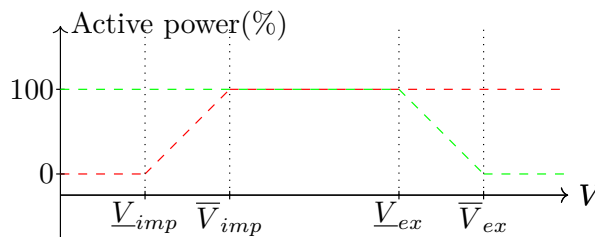


Figure 2.4: An overview of the droop curve used in APC. The control method reacts to the voltage at the bus by curtailing the amount of active power. In this figure, the red line is for the curtailment of dispatchable loads. With ADN, the green line is used for the generation of energy which is exported to the distribution network

The method is seen as wasteful and economically unattractive as it directly impacts PV performance. However, using the multi-port converter, the energy from the PV can be directly stored in the BESS [13, 25]. If not properly coordinated, this droop curve implementation of APC will mainly impact houses at the end of the distribution network as the voltage deviates more, as seen in Figure 1.3.

2.2.2. Voltage control methods in active distribution network

Now the methods marked white in Figure 2.2 are discussed. The ADN can combine these various voltage-mitigation methods such as DSM, (smart) PV inverters and BESS.

The DSM technique can control dispatchable loads (e.g.(water)heating and BESS) to a more desired time slot. The technique can be used for peak shaving, load shifting and valley filling, as seen in Figure 2.5 [23].

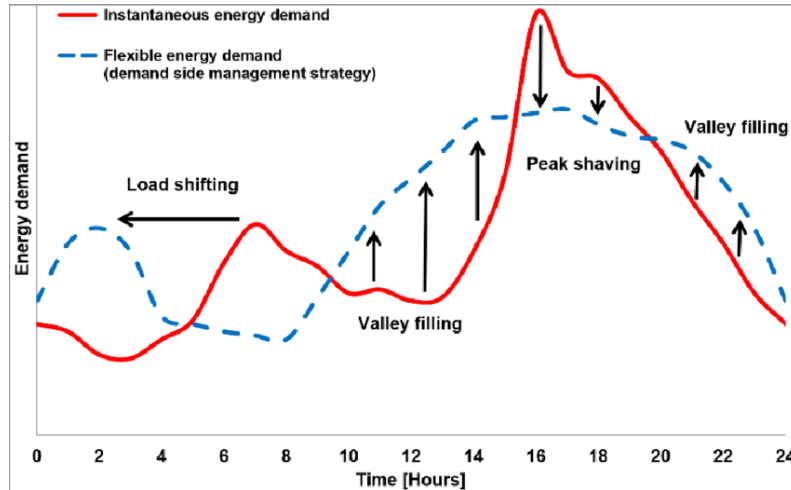
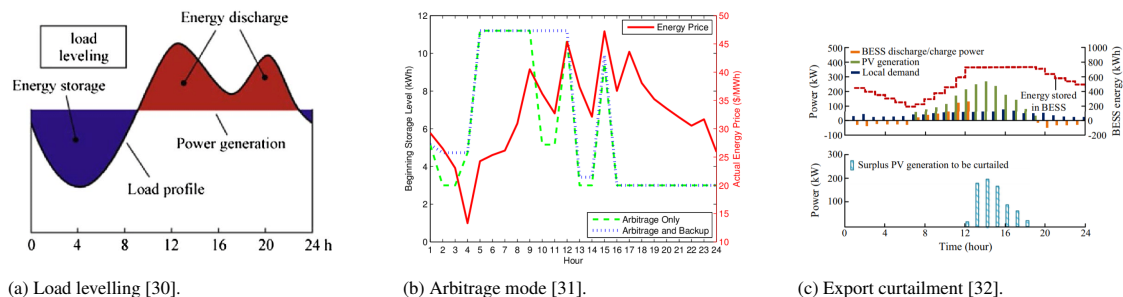


Figure 2.5: The implications of DSM using peak shaving, load shifting and valley filling [28].

An example of DSM would be to charge the EV at a different time to get a lower energy price or to prevent peak currents based on energy demand in the network. The load shifting in an ADN with liberalised energy markets is not always performed out of necessity but is often done out of economic aspects. To help mitigate voltage problems using DSM, a limit of power import/export can be set [29].

To accomplish valley filling and peak shaving capabilities, BESS can be used. BESS has been picked as the best way to mitigate voltage problems due to high energy density and rapid response [20]. It provides the DSO benefits and cost savings by raising flexibility in power generation, delivery and consumption [12]. It does this by providing continuous and reliable power generation and can be used for active power balancing and voltage regulation at the same time [12]. The application of BESS has increased due to the rise in DG by PV. BESS can be used centralised (e.g. community battery) or distributed (each individual has a smaller unit). The distributed BESS outperforms the centralised BESS and can directly store PV power [23].

BESS can be used for load levelling, arbitrage mode and export curtailment mode, as seen in Figure 2.6.



(a) Load levelling [30].

(b) Arbitrage mode [31].

(c) Export curtailment [32].

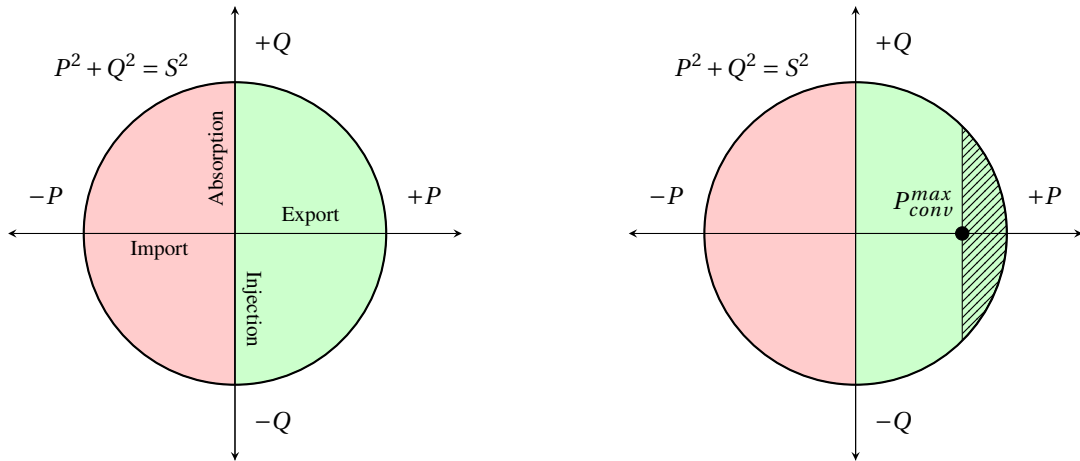
Figure 2.6: Three possible implementations of using an BESS in an ADN

In load levelling, as seen in Figure 2.6a, the energy is stored during periods of low demand and used during peak hours. In arbitrage mode, as shown in Figure 2.6b, the energy is bought during low price hours

and is sold back to the distribution network when the price is high. Export curtailment in Figure 2.6c stores the energy, of the PV, in the BESS when local generation exceeds local demand but does not sell back to the distribution network. With the liberalisation of the energy market, it is more common to export energy from BESS when the price is high. Combining arbitrage and export curtailment methods in the ADN is vital to prevent voltage violations while maintaining profits for consumers. To avoid additional curtailment of the PV, the export curtailment method should allow the energy export when the PV generation level decreases.

The DC/AC inverter needed to convert the DC solar-PV power to AC power can be an effective mean for continuous voltage regulation due to the significant amount of reactive power support [24, 25]. Currently, inverter interfaced DG are not permitted to control voltage locally [13]. This is done as DG by PV is at the moment too small to impact the voltage, and it could interfere with OLTC and SVR controllers [33]. The addition of reactive power shows improvement in the amount of energy the distribution network can handle. Expanded use of reactive power is expected [13, 34].

The continuous voltage regulation of a PV system can be seen as the green part of Figure 2.7a. It is capable of injecting and absorbing reactive power but only capable of exporting active power. The voltage regulation can be improved upon if the PV is coupled with an BESS. This adds the import capability seen in Figure 2.7a as the red part. The combination of PV and BESS make a four-quadrant operation possible. In Figure 2.7b, an example is given using APC to limit the amount of possible export.



(a) A four-quadrant operation of a bidirectional inverter.

(b) A four-quadrant operation of a bidirectional inverter limited by APC. In this example, the amount the PV-inverter can export is limited. This is needed when an overvoltage situation appears.

Figure 2.7: The four-quadrant operation of a bidirectional inverter with (2.7b) and without (2.7a) APC. The green part of the positive P is the generation of energy exported to the distribution network. The negative P in red is importing energy from the distribution network.

An uncoordinated bidirectional AC/DC inverter can be used in several ways. A conservative implementation is zero current injection, limiting the output to match the load but never injects any power back into the distribution network. This results in a decline of the PV generation capacity and is therefore unfavourable. APC based on the local voltage and the droop curve, similar to Section 2.2.1, can be applied to curtail active power in the inverter, as seen in Figure 2.8a. Using RPC based on the local voltage level and the droop curve, reactive power can be absorbed/injected, as seen in Figure 2.8b.

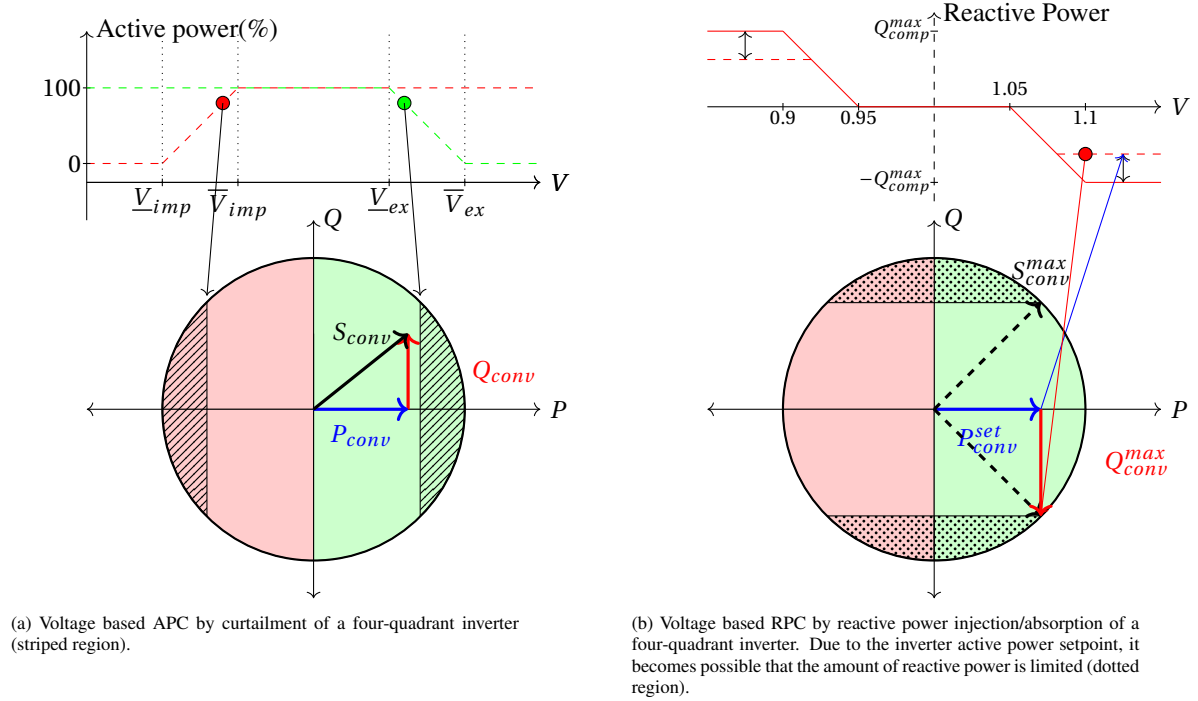


Figure 2.8: Two uncoordinated methods of controlling voltage in the distribution network by using bidirectional inverters

As RPC is not always capable of controlling the voltage,[24] the combination of APC and RPC becomes necessary for voltage management.

The challenge stated for inverters using PV is proper coordination [25, 35]. The coordination in existing voltage regulators gives the best result for both active and reactive power [36].

A method of implementing coordination is a fair curtailment dispatch via a centralised controller, as seen in Figure 2.9a. This aims to curtail via APC every house equally. A similar method curtailing the active power via voltage "sensitivities" in the distribution network is shown in Figure 2.9b. These voltage "sensitivities" reflect the change in voltage level based on the active and reactive power of each house. Voltage sensitivities will be further discussed in Section 5.2.2.

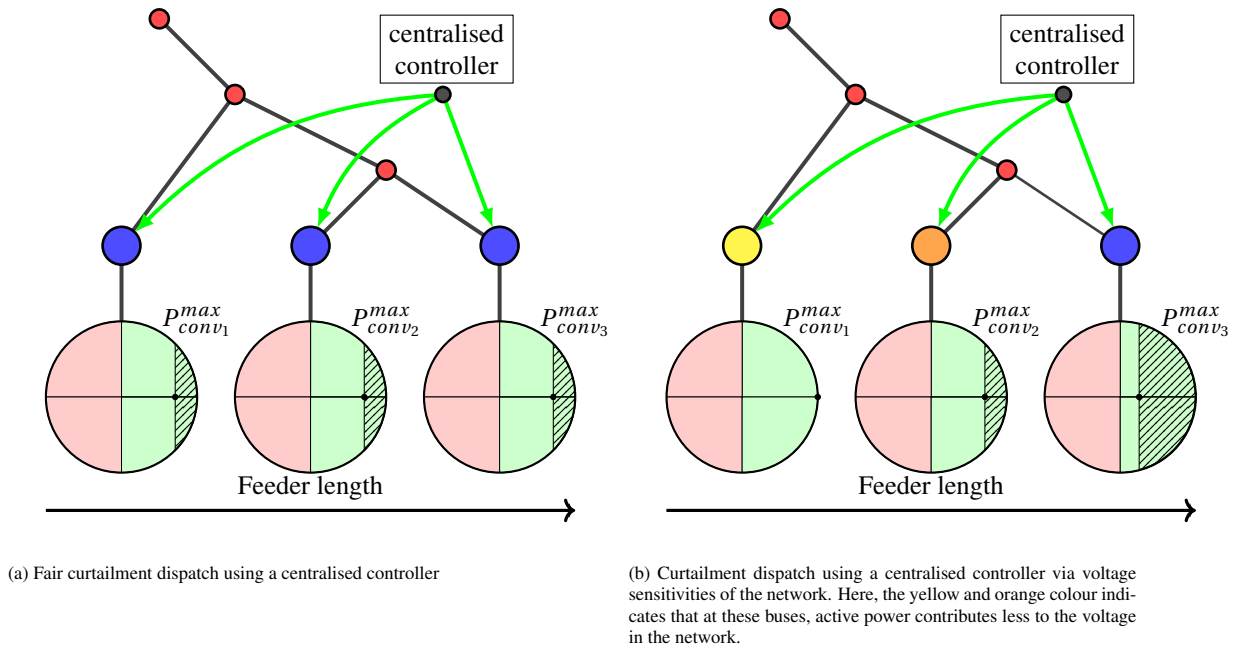
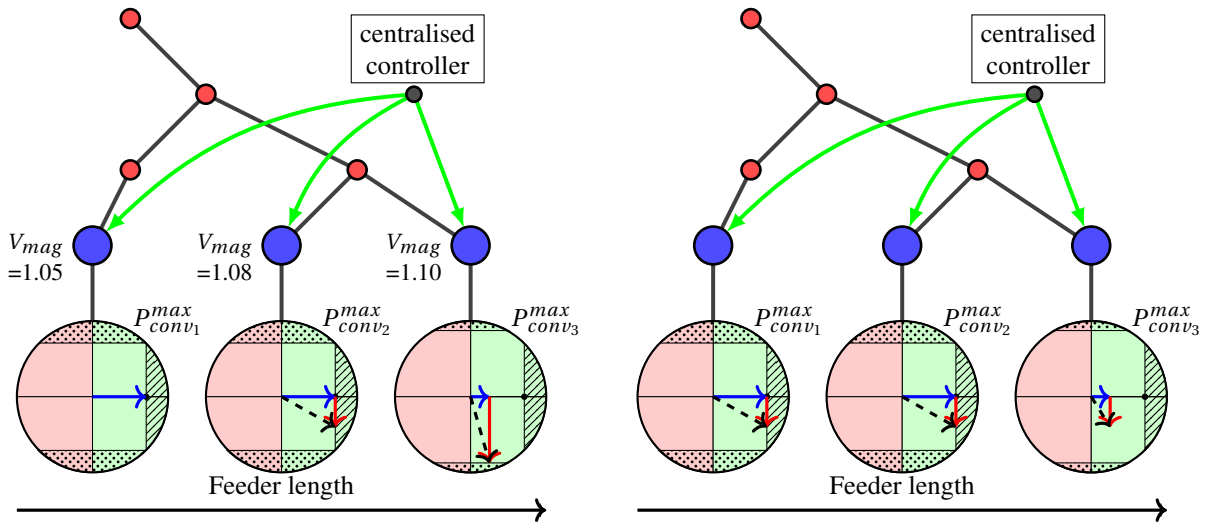


Figure 2.9: Two methods of implementing APC in a coordinated way.

Although APC based on voltage sensitivity performs well [36], curtailing active power based on location would discriminate against users. It results in certain areas failing to meet energy demand for EV charging and needing to buy power at a higher price at a different time.

Improved results can be expected by a coordinated hybrid model of APC and RPC [23]. Using the fair curtailment dispatch as a base, a couple of implementations could emerge. The first uses a droop curve for the reactive power flow based on local bus voltage, as seen in Figure 2.10a. The second possible implementation uses an equal amount of reactive power output determined by a power flow model in the centralised controller, as seen in Figure 2.10b. The third implementation is based on nodal sensitivity, and the power flow model determines which houses should use their reactive power support, as seen in Figure 2.11 [35].



(a) Hybrid mode with RPC based on voltage droop curve. Here, the centralised controller computes the APC, but the RPC is done based on bus voltage.

(b) Hybrid mode where reactive power control is equally distributed.

Figure 2.10: Two methods of implementing a combination of APC and RPC.

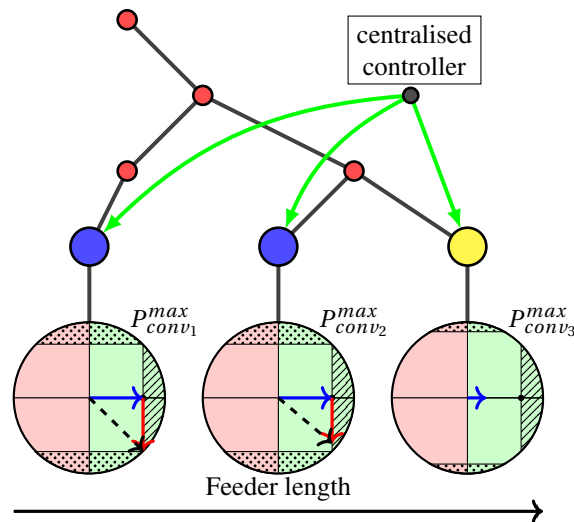


Figure 2.11: Hybrid mode where reactive power is based on bus sensitivity. Here, the yellow colour indicates that at this bus, reactive power contributes less to the voltage in the network.

The disadvantage of the hybrid model with a droop curve RPC is the consumption of too much reactive power at the end of the distribution network. It will result in more significant distribution losses. The method that uses an equal amount of reactive power will use more reactive power to achieve the same voltage change than the sensitivity method. The disadvantage of the sensitivity method is that the shift in P_{conv} in real-time can result in a decrease of reactive power due to inverter limits

2.3. State of the art

This section focuses on state of the art in voltage mitigation and prevention techniques. Each subsection is focused on a specific method or implementation.

2.3.1. PV inverters

To keep modifications to a minimum, the easiest control method is RPC by PV inverters/multi-port converters without coordination as done in [37, 38]. In [38] an adaptive algorithm is used for loss minimisation. In this loss minimisation, a maximum voltage sway is proposed. The voltage sway by PV generation and the lack of increasing/reducing the voltage enough due to inverter limits removes this as a single solution option. In [37] coordination is added with additional clustering to prevent voltage violation at critical buses. The addition of clustering doesn't improve cost.

2.3.2. (Multiple-stage) coordinated PV inverters

In [39–45] coordination between PV inverters is added to improve performance. In [40, 42, 43] multiple-stage optimisation are used for PV inverters. In [40] hierarchically RPC is proposed where the upper layer calculates the PV inverter output and the lower layers respond to real-time variation via droop control. However, the model is based on linearisation of distribution lines which only work on small systems. In [42, 43] the linearisation of the model is replaced by an AC power flow model convexified by second-order cone programming. In [42] it is used for a two-stage robust centralised RPC with APC capabilities, which tries to maximise the generation capacity taking into account network losses. In [43] a multi-objective adaptive Volt-VAR control (VVC) is used to minimise voltage deviation and power loss simultaneously. They prioritise big loads to achieve this, which would be an unfair approach in a residential area. In [39, 41, 44, 45] in addition to the PV inverter variations of OLTC SVR and CB are installed. In [39] a multi-time scale coordinated stochastic VVC is used for voltage fluctuations and deviations. It uses optimal dispatch for OLTC and CB each hour, and 15 min intervals for PV using a mixed integer quadratic programming. The goal of the VVC is to minimise distribution losses. The model computation uses linearisation of distribution lines and uses uncontrollable stochastic loads. In [41] OLTC, SVR and PV are used. They dispatch OLTC and SVR for 15 min intervals and the PV for fast response under moving cloud conditions. In [44] OLTC and smart inverters using a mixed integer linear programming. It proposes a system to minimise voltage deviation for unbalanced systems. In [45] a three-stage robust VVC using OLTC, CB and PV is proposed. The first stage is optimal dispatch of CB and OLTC in a rolling horizon, the second stage is the smart inverter output dispatch, and the third stage is the reactive droop controller in the smart inverter. All of the papers focus on using PV inverters to solve the voltage deviation but lack taking into account the voltage mitigation and prevention effort of DSM, EV or BESS.

2.3.3. Distributed control

In [46, 47] distributed solutions are proposed. In [46] a distributed cooperative framework using consensus-based droop control is proposed, which regulates the voltage and power-sharing amongst DG. The restoring of the voltage is done by exchanging data with only the neighbour (distributed) to reach a common goal (consensus). The network used is small, and if expanded, convergence time would increase. In [47] a distributed cooperative control of a multi-agent system is proposed. It is using the relation between the dynamics of the output and the control input (input-output feedback linearisation). It is also performed on a small scale and does not easily converge to a bigger one. Both do not take into account the voltage mitigation effort of DSM, EV or BESS as options.

2.3.4. Cost minimisation

In [48–55] methods have been found to optimise the cost for the houses. In [51] EV charging using DSM is proposed but leaves out the contribution of PV. In the remaining papers, a model predictive controller (MPC) is used for optimisation. In [53] a cooperative MPC framework is used for sharing between DER using DSM. It does not take generation by PV into consideration. In [52] users can change their load strategy to comply with power consumption constraints. However, it does not consider uncertainty. In [54] a receding horizon MPC as a mixed integer linear programming is used as a multi-energy operational flexibility assessment. The paper looks at how houses can help solve the voltage issue in a microgrid. No

EV or BESS is used. In [55] a hierarchical MPC is used for EV charging based on power constraints and the PV prediction. They do not look at the voltage level. In [50], an MPC for vehicle-to-grid (V2G) to regulate voltage. It uses the EV inverter for reactive power support and uses a linearisation of the network. This paper assumes no PV in the distribution network, and therefore the promising results would diminish if a high penetration of PV would be introduced. In [48, 49] an MPC as mixed integer linear programming in mixed logical dynamical formulation[56] is used. This is used for the optimisation of DG, BESS and DSM. They do not take into account EV charging and do not measure the voltage in the network.

2.3.5. Summary state of the art

To summarise the state of the art, there are various methods available to mitigate or prevent voltage violation. Most literature only focuses on a few techniques, as seen in Table 2.1.

Table 2.1: Comparison of components that can be used in voltage management in the state of the art. The CB in the BESS column stands for capacitor bank.

Paper	RPC	APC	RPC & APC	DSM	PV/DG	Real-time	BESS	EV	Battery degradation
[40]	x				x(PV)	x			
[43]	x			x	x(PV)	x			
[49]		x		x	x(DG)		x		
[48]		x		x	x(DG)		x		
[37]	x	x	x		x(DG)		x(CB)		
[46]	x	x			x(DG)	x			
[41]	x				x(PV)		x(CB)		
[42]	x				x(PV)				
[38]	x				x(PV)	x			
[44]	x				x(PV)	x			
[50]								x	
[39]	x				x(PV)	x	x(CB)		
[45]	x				x(PV)	x	x(CB)		
[55]				x	x(PV)	x		x	
[53]		x		x	x(DG)	x	x		
[47]		x					x		
[51]		x			x(DG)	x		x	
[35]	x				x(PV)	x			
[52]		x		x	x(DG)		x		

This thesis implements all of the above mentioned components and methods. Using the EMS of the multi-port converters and a control scheme by the DSO, the combination of DSM, APC, RPC, and BESS become possible. This creates a system that can prevent and correct voltage violations (DSM, APC, and RPC) and can limit the line power losses (APC and distributed BESS).

3

Active distribution network model

This chapter introduces the model of the low voltage feeder as the distribution network and the corresponding external parameters. Firstly, in Section 3.1, a description of the low voltage feeder’s layout, operation limits, and operational behaviour is given. Secondly, section 3.2 shows the external parameters and their errors. The external inputs consist of EV arrival and departure time, EV arrival and departure state of charge, PV generation, load demand, and electricity price.

3.1. The distribution network

With the introduction of DER and control structure for voltage control, a test feeder is needed to show medium to long term dynamic behaviour in a residential area. The IEEE European Low Voltage Test Feeder, as seen in Figure 3.1, is picked to provide a benchmark for this type of dynamic behaviour [57].

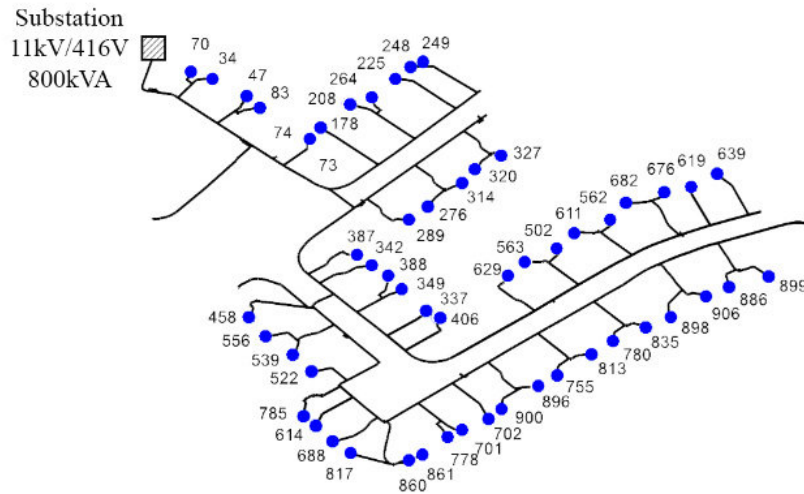


Figure 3.1: A single line diagram of the IEEE European LV Test Feeder [58]. Each blue dot represents a house with the corresponding bus number. The substation, connected to the transmission network, is a transformer positioned in the top-left corner of the network.

As observed in Figure 3.1, the structure of the feeder is radial, and it consists solely of three-phase cables. The PCC at the substation is a step-down transformer with a capacity of 800 kVA, which transforms the voltage from 11 to 0.416kV at 1.05 per unit (p.u.). The p.u. is calculated as: [59]

$$\text{Quantity per-unit} = \frac{\text{Quantity}}{\text{base value of Quantity}} \quad (3.1)$$

The low voltage feeder consists of 55 houses, each having a load and being capable of having a maximum of one multi-port converter. If the house has no multi-port converter, it is replaced by a combination of PV and EV, which are both uncontrolled. The EV and PV converter are assumed to have the same charging constraints, generation capacity and efficiencies as the multi-port converter (Table 4.3). An overview of the grid specifications is given in Table 3.1.

Table 3.1: Network specifications of the IEEE European Low Voltage Test Feeder

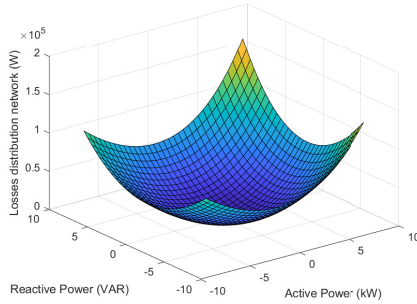
Symbol	Quantity	Value
S_{tran}^{max}	Maximum capacity transformer	800 kVA
$V_{0,l \rightarrow l}$	Line to line voltage at bus 1 (transformer)	416 V (1.05 p.u.)
N	Amount of houses	55
$V_{l \rightarrow l}^{max}$	Upper limit line to line voltage	436 V (1.1 p.u.)
$V_{l \rightarrow l}^{min}$	Lower Limit line to line voltage	357 V (0.9 p.u.)

The test feeder is simulated using OpenDSS. OpenDSS is open-source software designed specifically to represent electric power distribution circuits and distributed planning with DG [60].

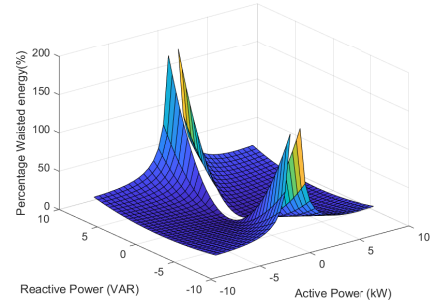
The following assumptions have been made while simulating the voltage profile of the IEEE European low voltage feeder:

- All energy exchange between the network and the houses is assumed to be balanced. No voltage unbalance should occur.
- The balance of supply and demand of energy is expected to be upheld by the DSO. It is assumed that the excess generation can be sold back to the feeder at every moment, and enough generation capacity is available for consumption.
- Current limitations are out of the scope of this thesis and therefore ignored.
- Uncontrollable loads only consume active power ($pf = 1$). These include AC loads and, if no multi-port converter is attached to the house, the EV and PV.

Certain specifications of the system are summarised in Appendix listing A. These include line codes and line characteristics. An overview of the dynamic behaviour of the distribution network is shown in Figures 3.2 and 3.3.

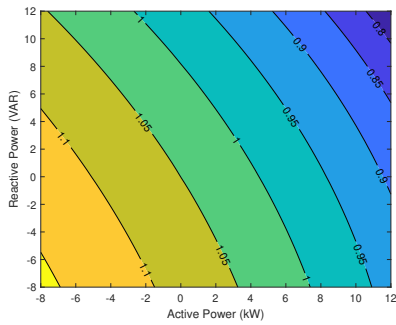


(a) Losses in the distribution network based on the use of Active and Reactive power.

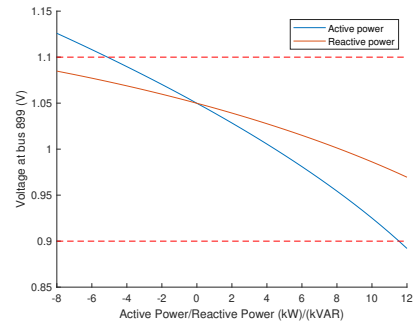


(b) Added losses, in percentage, in the distribution network based on the active and reactive power used.

Figure 3.2: The loss characteristics of the IEEE LV Test Feeder. In both figures, all houses use the same amount of active and/or reactive power.



(a) Voltage profile at furthest bus (bus 899) with a combination of Active and Reactive power.



(b) Voltage deviation when only active or reactive power is used at the furthest bus (bus 899). Active and reactive power numbers are per house.

Figure 3.3: Voltage characteristics of the IEEE LV Test Feeder. In all figures all houses use the same amount of active and/or reactive power.

Figure 3.2 shows the additional losses generated by the use of active and reactive power. Figure 3.2a highlights the total losses. Reactive power increases losses, and the consumption of apparent power is more demanding than the generation of apparent power. If, e.g. 10 kW of energy is generated at the house, distribution losses are made, and less than 10 kW arrives at the transformer. If 10 kW of power is consumed at the house, more than 10 kW is needed at the transformer. The increase in power in the distribution for consumption adds additional losses. Figure 3.2b shows the additional losses, in percentage, in the distribution network. Notably, a lot of energy is lost when little active power is used.

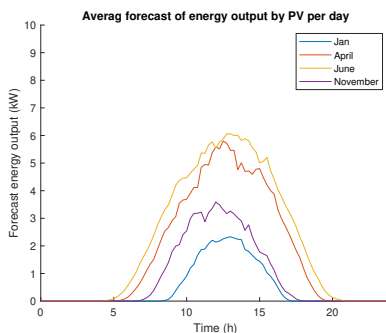
Figures 3.3a and 3.3b show the influence of active and reactive power on the voltage of the bus furthest away (see position bus 899 Figure 3.1). Although reactive power has a more negligible effect on the network, it can still raise or lower the voltage significant.

3.2. Data inputs

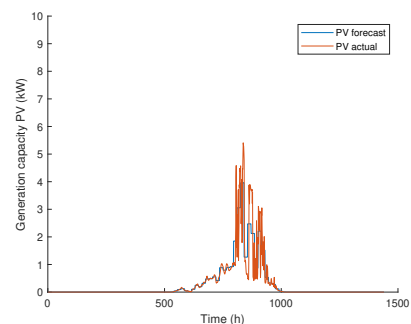
With the introduction of ADN, additional inputs of DER are added to the distribution network.

3.2.1. PV

The generation of energy by the Maximum power point tracking (MPPT) using PV can vary by generation capacity and seasonal demand. The data used is collected by a Dutch DSO. The seasonal variation in production can be seen in Figure 3.4a. The difference between the forecast and actual generation of a single day is given in Figure 3.4b.



(a) Seasonal variation in PV generation. The data shown is the average over the whole month.



(b) The difference between forecasting and actual PV generation on 1 Jan.

Figure 3.4: These figures show the intermittent generation of PV. Figure 3.4a shows the seasonal change, and Figure 3.4b the daily variation.

To simulate a real-life scenario, each house has a varying PV generation capacity, shown in Figure 3.5. A normal distribution with the mean (μ) of 8 kW is used, and the forecast of generation is scaled accordingly. Besides the scaling of the generation, it is assumed that there is no variation in output between the houses due to the limited size of the network.

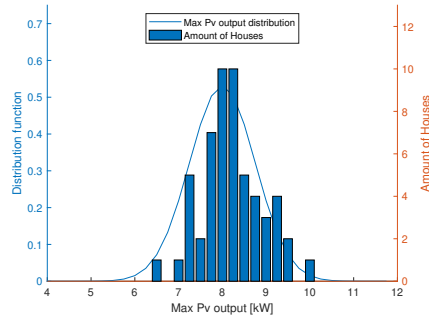
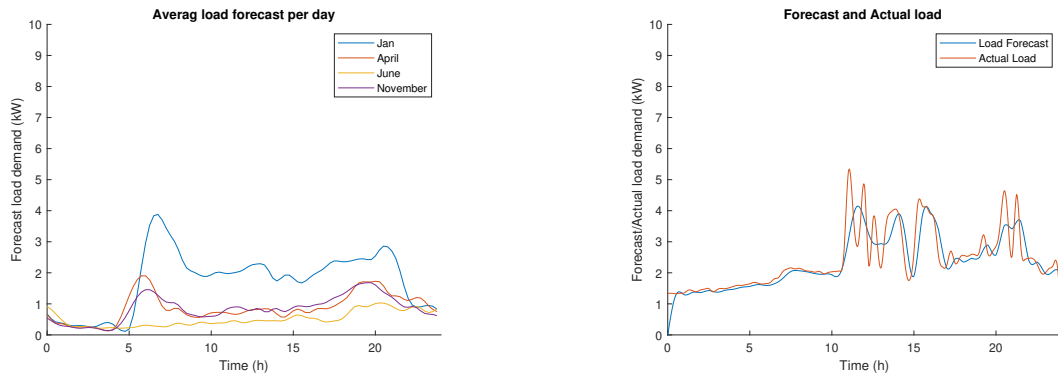


Figure 3.5: The distribution of maximum PV generation for each house.

The error of PV generation is compensated in the real-time controller, which is discussed in Chapter 6.

3.2.2. Load profile

The load demand of appliances is the sole element used in the passive distribution network. The load consists of the energy demand used by the electrical appliances and the heat pump. Using record data of load demand combined with data of electricity use of the heat pump, a profile of average demand during the year can be made, as seen in Figure 3.6a. The data is collected by a Dutch DSO. The difference between the forecast of the average load profile and the actual load profile in a single day is shown in Figure 3.6b.

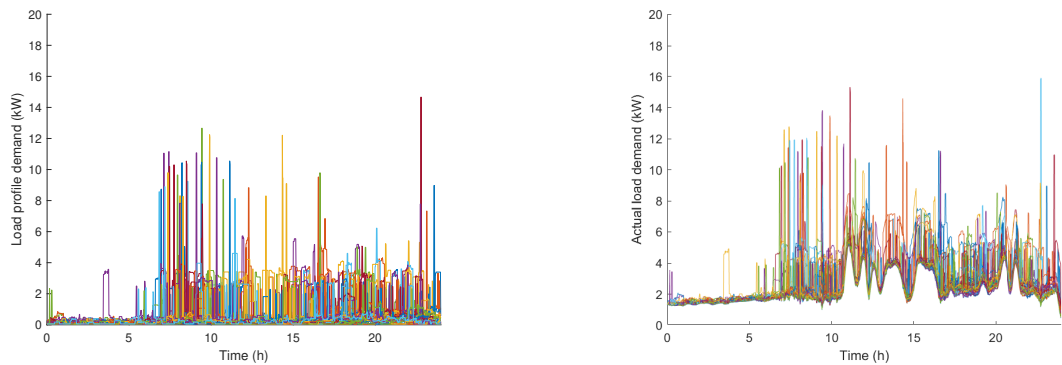


(a) The seasonal variation of the average load demand. Each line represents the average load, of all the houses, over a whole month.

(b) The variation and mismatch between the average forecast and actual load over a whole day.

Figure 3.6: Varying load demands due to different seasons (3.6a) and the daily mismatch between forecast and actual demand (3.6b).

However, the load demand usage varies amongst individual users. To give a better representation, the IEEE European Low voltage test feeder includes load demand profiles, as seen in Figure 3.6a. Scaling these individual load profiles with the average actual load demand from Figure 3.6b results in a more accurate load demand in Figure 3.7b.



(a) The combined load demand profile of 55 houses. These are randomised for each day.

(b) The actual load profile for individual users consisting of the load demand profiles (Figure 3.7a) scaled to the average actual profile (Figure 3.6).

Figure 3.7: The transformation of the average actual profile to a more representing actual load profile (3.7b) by using load demand profile from the IEEE European low voltage feeder test set.(3.7a)

The profiles are generated per day by randomly assigning a unique profile out of the 100 load profiles available and scaling it to the average profile.

When Figure 3.7b is summed and then averaged, it would result to the actual profile of Figure 3.6b. Figure 3.8 shows the limited influence of the individual load profiles on the minima and maxima of the voltage. Still, the individual loads influence the decisions made inside the real-time controller of the multi-port converter (more in detail in Chapter 6) and are therefore important to take into consideration.

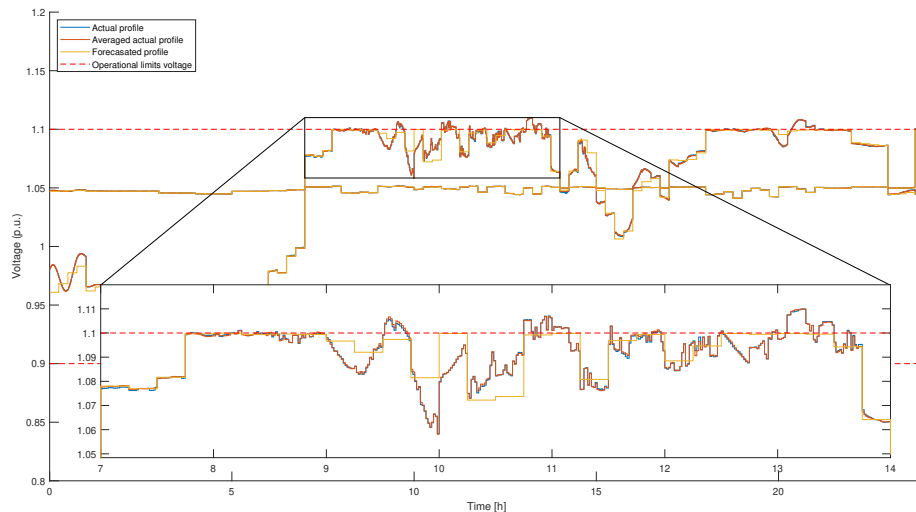


Figure 3.8: The average variation in forecast and actual load.

Figure 3.9 shows the error between the forecast and actual load.

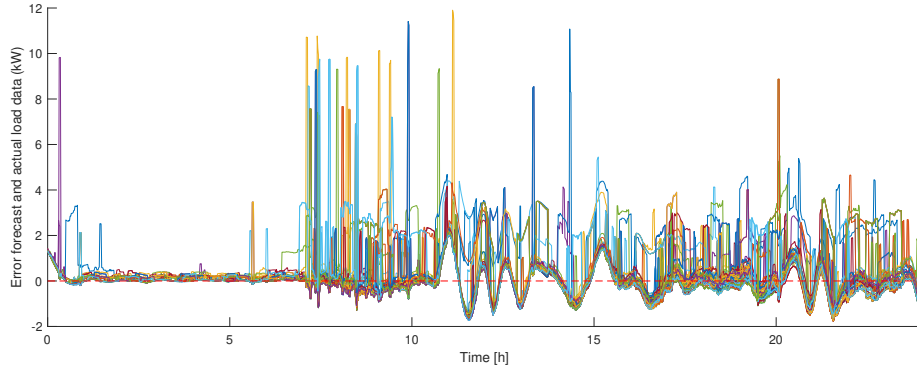
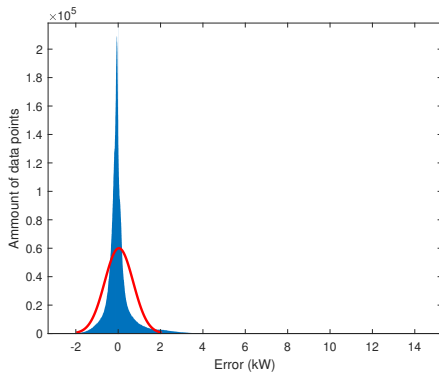
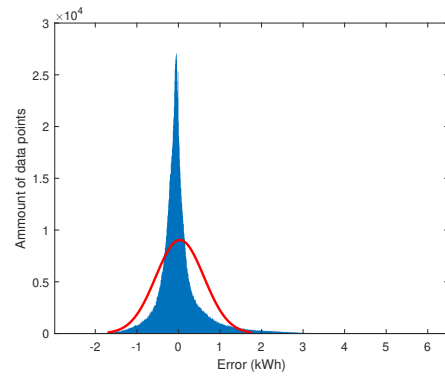


Figure 3.9: The error between the average forecast of the load and the actual load. Each line represents the error between the average forecast and the actual load.

A positive variation ($P_{load,act} - P_{load,fc} \geq 0$) results in a larger voltage drop than anticipated, resulting in an undervoltage if close to the operational voltage limit. Similar, a lack of consumption ($P_{load,act} - P_{load,fc} \leq 0$) during high PV generation will cause an overvoltage. The distribution of load error is given in Figure 3.10. It appears that the majority of the errors are between -2 and 2 kW. Figure 3.10b and Table 3.2 display that the mismatch in terms of energy usage (kWh) is essentially within 3 kWh over a 15-minute interval.



(a) Error load (kW) over 1-minute interval (blue) and distribution of error (red)



(b) Total error load (kWh) over 15-minute interval (blue) and distribution of error (red)

Figure 3.10: Distribution of errors during the whole year for both short duration (Figure 3.10a) and interval (Figure 3.10b)

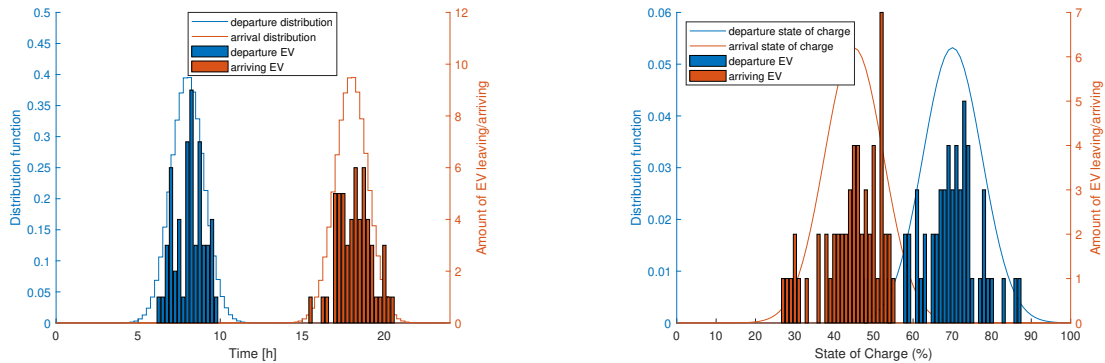
Table 3.2: Percentage of average error covered in a 15 min interval.

Absolute error (kWh)	Percentage covered (%)
0.5	79.24
1	92.28
2	98.30
3	99.660

Although the forecasting is not perfect, the implications of the increased load due to forecasting error are controllable. This is because the distribution network is only a fraction of the time at capacity limits, mainly during the summer or winter. To compensate for the load error, the real-time controller, which will be discussed in Section 6.3, can adjust the control inputs of the multi-port converters.

3.2.3. EV

The individual EV can vary by arrival/departure time and state of charge, as seen in Figure 3.11. All 55 houses have an EV connected to them, either through the multi-port converter or through a separate converter. The capacity of the EV has been picked at 100 kWh, similar to popular EV models. A normal distribution is taken for the arrival and departure times of the EV, as seen in Figure 3.11a. The mean (μ) of the EV is 8 AM and 6 PM. To decrease cost, users can specify the state of charge for departure. A normal distribution is taken at 70% for departure and 45% for arriving, as seen in Figure 3.11b. These minor variations are expected as charging at work will be more available in the future.



(a) Arrival and departure time of the EV. The normal distribution is on an interval as the car only start charging on the next time step of 15 min.

(b) The state of charge when departing and the corresponding arrive state of charge. The departure state of charge is a minimum.

Figure 3.11: The arrival/departure time and state of charge of the EV.

If the EV arrives at the house with no multi-port converter, the car is immediately charged to the state of charge level ($E_{bat,dep}$) at maximum charging level (P_{ev}^{max}).

3.2.4. Electricity Price

Caused by a change in demand per hour and seasonal influence, the prices in the ADN are dynamic. An overview of the seasonal price changes used is shown in Figure 3.12. With the possibility to sell energy back (feed-in) to the network, this could yield a profit for consumers. The feed-in tariff in the distribution network is set two percent lower than the purchase price.

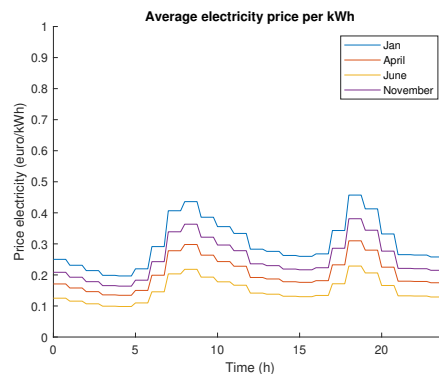


Figure 3.12: The variation of electricity price during the seasons.

4

Energy Management System

This chapter formulates the energy management system (EMS) of the multi-port converter. The EMS is based on the smart charging system [19]. Starting , Section 4.1 introduces the structure of the EMS, its function in the multi-port converter and its objective goal. Secondly, Section 4.2 models the AC energy balance between the house and the distribution network. In Section 4.3, the energy balance inside the multi-port is analysed. Furthermore, the formulations of individual components are discussed. In Section 4.4, the battery degradation models for both EV and BESS are shown. Section 4.5 presents the cost analysis of the multi-port and the objective function.

4.1. Energy Management System

The primary function of the EMS is to optimise cost by incorporating data elements. This is necessary to enhance the versatility and usability of the multi-port converter. These data elements include the forecast data and user inputs, as mentioned in Chapter 3, and the output of the VMS controller and continuous updates of state (E_{bat} and E_{ev}) and input ($P_{load,act}$ and $P_{fc,act}$) variables. The VMS controller, which will be further elaborate on in Chapter 5, can set (a combination of) energy import and export restrictions (APC), reactive power set-points (RPC) and price alterations based on the voltage magnitude of the network. The continuous update of the state and input is needed to prevent exceeding capacity limits (E_{bat}^{max} and E_{ev}^{max}) and determine forecast errors. These data elements make it possible to calculate optimal control inputs for charging schedules while maintaining the multi-port converter's distribution network limits and operational limits. A visualisation of the data elements and streams of the multi-port converter system is given in Figure 4.1.

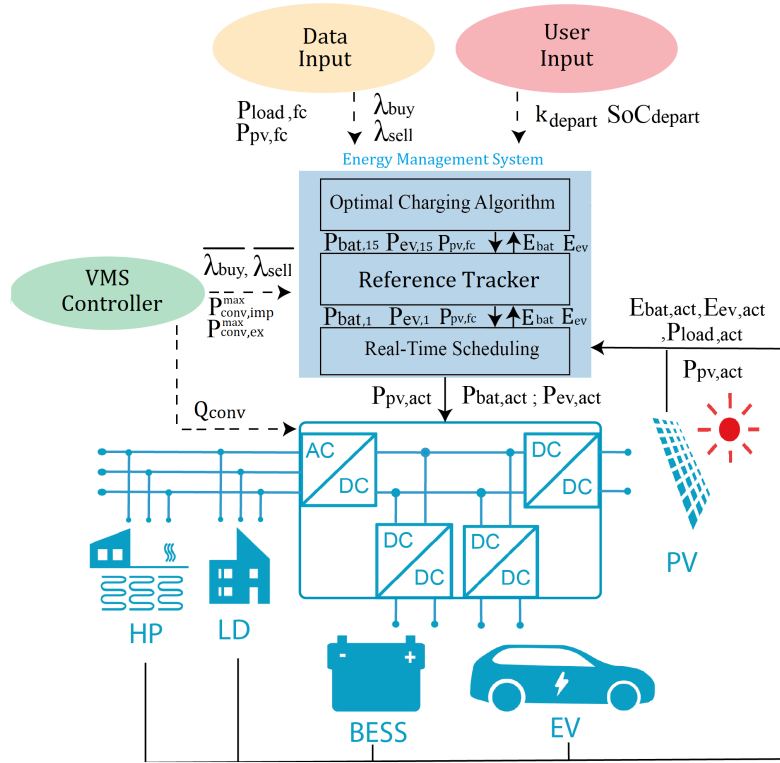


Figure 4.1: Overview of the EMS and corresponding data inputs needed for the optimal operation. These consist of the forecast data, user input, data from the VMS controller, and the multi-port converter's feedback. The multi-port converter control on the DC side, as the physical part of the EMS, consist of an EV (dis)charger, BESS (dis)charger and an MPPT for PV. The AC side consist of non-flexible load demand, containing appliances and the heat pump. The dashed lines are external data inputs, on which the EMS has no control. The solid lines are data from components surrounding the house.

The various operational limits of the multi-port converter are summarised in Table 4.1.

Table 4.1: System parameters multi-port converter

Symbol	Quantity	Value
P_{pv}^{rated}	Installed PV capacity power	10 kWp
P_{ev}^{max}	Maximum EV (dis)charging power	10 kW
P_{bat}^{max}	Maximum BESS (dis)charging power	10 kW
S_{conv}^{max}	Maximum apparent power rating	10 kVA
θ_{pf}	Power factor range	0-1
E_{ev}^{max}	Maximum EV capacity	100 kWh
E_{bat}^{max}	Maximum BESS capacity	10 kWh

Each of the converter blocks in Figure 4.1 is capable of handling 10 kW. This means when the PV provides 10 kW, the converter imports 10 kW and the battery and EV charge with 10 kW the maximum capacity of 20 kW can flow through the multi-port converter.

The goal of the EMS is to minimise the total operational cost within the limitations of the converters and storage elements. This is achieved by optimising the control inputs of its DC converter components. These Components are the (dis)charging rate of the bidirectional BESS (P_{bat}), (dis)charging rate of the bidirectional EV (P_{ev}) and the maximum generation of the MPPT (P_{pv}) by PV. Although the EMS has the additional task of preventing and correcting voltage deviations, this is not specified in the operational cost. The EMS knows nothing about the voltage magnitude in the distribution network nor its influence on the distribution network. These are all computed in the VMS, which will be discussed in Chapter 5.

Optimising a large set of control inputs is computationally expensive. Furthermore, with constant updates of state variables and forecast errors, the computation must be recomputed regularly to stay optimal. However, the period must be significant enough to enable EV charging (long period) and precise enough to remove forecast errors (short period). Therefore, the challenge is to combine fast response, high accuracy with a large prediction horizon. By breaking down the EMS into various time scales, as seen in Figure 4.1, the highly responsive and long prediction horizon can be kept while decreasing the computational burden.

The EMS consists of a three-stage strategy for cost-minimisation (top), correction (middle) and responsiveness (bottom). In this chapter, only the top layer will be discussed. The top layer consists of an optimal charging algorithm, which determines the set-points on a 15-min interval for a full day (96 time steps). This cost minimisation is integrated into a moving horizon window, as seen in Figure 4.2. The moving horizon window implementation helps correct forecast errors by updating control inputs each iteration to the current state. By only implementing the first step of the computed control sequence, the charging scheme can quickly adapt to changing constraints or set-points after only 15 min.

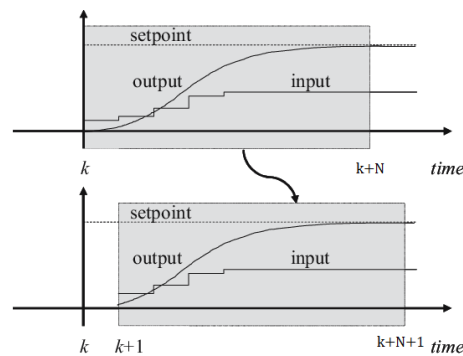


Figure 4.2: This figure shows the moving horizon window principle. In the top figure, the control input is computed over a prediction horizon with length N to get the output to a predefined set-point with minimal cost. While the control input is calculated from time k till $k+N$, only the control input from k till $k+1$ is implemented. At $k+1$ the prediction horizon is moved one step to the right. From here, the optimal control input is calculated again, within the new horizon, to get to the output to the (new) set-point with minimal cost [61].

The second and third stages fulfil the purpose of reference tracking and real-time control on a one-minute interval and real-time, respectively. These actions are computed within the 15 minute time frame of the optimal charging algorithm, as seen in Figure 4.3. The reference tracking and real-time controller are explained in depth in Chapter 6.

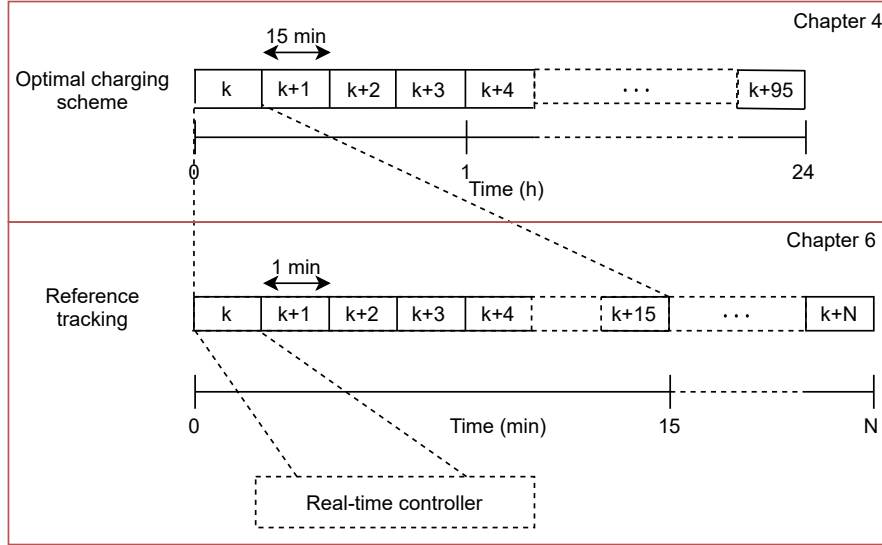


Figure 4.3: The different time schemes of the different layers in the EMS. The optimal charging scheme computes over a 96 step prediction horizon of 15 minute intervals. Inside the 15 minute interval, the reference tracking computes on the interval of 1 minute with a prediction horizon N. Within that 1 minute interval, the real-time controller continuously computes and updates.

The following assumptions are made in the EMS for simulation purposes:

- The EV arrival charge ($E_{ev,arr}$) is known by the EMS. This value can be continuously estimated and transmitted from the EV to the EMS.
- No unexpected departure. If the EV is available (EV_{avail}) for (dis)charging at the multi-port converter, it will remain until the departure.
- The stated arrival and departure times are expected to be upheld. The EMS can satisfy this assumption by disabling the (dis)charging 30 minutes before departure (k_{dep}) and only start 30 minutes after the expected arrival time step (k_{arr}).
- The forecast data and user input remain constant between iterations of the moving horizon. The $P_{pv,fc}$ and $P_{load,fc}$ will not change.
- The battery cells of BESS and EV are assumed to be made out of the same material. Therefore the same degradation method can be used.
- Only the cost of the battery degradation is taken into account. The battery will remain at its peak capacity ($E_{bat}^{max}/E_{ev}^{max}$) as the simulation period is short (2 days).

The rest of the chapter look at all the individual components needed for computing the optimal charging scheme.

4.2. AC Power balance

Besides a multi-port converter (P_{conv}), each house possesses an additional AC load (P_{load}), consisting of the energy demand of the household appliances and the heat pump. These AC loads are assumed to be non-flexible. As mentioned in Section 3.1, it is assumed the generation/feed-in capacity of the distribution network is sufficient to match the power at all times. The power balance, on the AC side, is modelled as:

$$P_{grid}(k) = P_{conv}(k) - P_{load}(k) \quad , \forall k \quad (4.1)$$

where k is the optimisation time step, and P_{grid} is the amount of power exchanged between the distribution network and the house. If P_{grid} is positive, the combined load of the multi-port converter and AC load is feeding energy to the distribution network. An overview of the energy flows is shown in Table 4.2.

Table 4.2: Indication of power flows regarding the multi-port converter.

Symbol	Meaning
$P_{grid}(+)$	Energy from the multi-port converter to the distribution network (exporting)
$P_{grid}(-)$	Energy from the distribution network to the multi-port converter (importing)
$P_{conv}(+)$	Feeding power into the distribution network (exporting)
$P_{conv}(-)$	Draw power from the distribution network (importing)
$P_{ev}(+)$	Energy to the EV from the multi-port converter (charging)
$P_{ev}(-)$	Energy from the EV to the multi-port converter (discharging)
$P_{bat}(+)$	Energy to the BESS from the multi-port converter (charging)
$P_{bat}(-)$	Energy from the BESS to the multi-port converter (discharging)
$P_{pv}(+)$	Energy from the solar panels to the multi-port converter.

The following constraints are added to P_{grid} :

$$P_{grid,ex}(k) \leq P_{grid,ex}^{max}(k) \quad , \forall k \quad (4.2a)$$

$$P_{grid,imp}(k) \leq P_{grid,imp}^{max}(k) \quad , \forall k \quad (4.2b)$$

$$P_{grid}(k) = -\frac{1}{\eta_{grid}} P_{grid,imp}(k) + \eta_{grid} P_{grid,ex}(k) \quad , \forall k \quad (4.2c)$$

Here, "imp", "ex", and "max" stand for import, export and maximum. η_{grid} is the efficiency of the cables running from the distribution network to the house, and $P_{grid,ex/imp}^{max}$ is the capacity limits of the distribution lines. An overview of the efficiencies is shown in Table 4.3. Equation 4.2c is split into two parts, and the efficiencies are added to prevent importing and exporting simultaneously.

Table 4.3: Efficiency of converter blocks and components in the multi-port converter.

Symbol	Meaning	Value
η_{mppt}	Efficiency of MPPT	98%[62]
η_{ev}	(Dis)charging efficiency EV	97.5%[63]
η_{bat}	(Dis)charging efficiency BESS	97.5%[63]
η_{conv}	Importing/Exporting Converter efficiency	97%[64]
η_{grid}	Cable efficiency importing/exporting	99%

4.3. Multi-port converter interactions

The equilibrium consists of the DC part of the AC/DC converter and the 3 DC/DC converters seen in Figure 4.1. The DC-part of the multi-port converter is balanced as:

$$P_{conv}(k) = P_{pv}(k) - P_{bat}(k) - P_{ev}(k) \quad , \forall k \quad (4.3)$$

Here, P_{bat}/P_{ev} are the energy exchange between the converter and the BESS/EV, and P_{pv} is the generated electricity by the MPPT obtained from the PV. The constraints of the converter on the DC side are as follow:

$$P_{conv,ex}(k) \leq P_{conv,ex}^{max}(k) \quad , \forall k \quad (4.4a)$$

$$P_{conv,imp}(k) \leq P_{conv,imp}^{max}(k) \quad , \forall k \quad (4.4b)$$

$$P_{conv}(k) = -\frac{1}{\eta_{conv}} P_{conv,imp}(k) + \eta_{conv} P_{conv,ex}(k) \quad , \forall k \quad (4.4c)$$

Here, $P_{conv,ex/imp}^{max}$ are the capacity limits of the AC/DC converter. When the DSO, via the VMS controller, needs to limit the exchange capabilities of the multi-port converter, the $P_{conv,imp/ex}^{max}$ can be lowered accordingly. Furthermore, the splitting can accommodate limiting only the import or export of energy, thereby maximising the possible control input.

As the elements of Equation 4.3 are controllable, further explanation of these dynamics are necessary.

4.3.1. PV

The expected MPPT generation by PV is based on the forecast of the PV. It is formulated as:

$$P_{pv}(k) \leq \eta_{mppt} P_{pv,fc}(k) \quad , \forall k \quad (4.5)$$

where η_{mppt} is the MPPT efficiency and $P_{pv,fc}$ is the forecast of PV power, as shown in Chapter 3. The \leq -sign in Equation 4.5 is used to accommodate the curtailment of PV power in the optimisation. If an excess of PV power could result in exceeding battery limits or an increase in cost, the optimisation can pick a lower P_{pv} to remain feasible and optimal.

4.3.2. Battery energy storage system dynamics

The charging and discharging dynamics of the BESS are implemented as:

$$P_{bat}(k) = \eta_{bat,ch} P_{bat,ch}(k) - 1/\eta_{bat,dis} P_{bat,dis}(k) \quad , \forall k \quad (4.6a)$$

$$0 \leq P_{bat,ch}(k) \leq 10 \quad , \forall k \quad (4.6b)$$

$$0 \leq P_{bat,dis}(k) \leq 10 \quad , \forall k \quad (4.6c)$$

Here, "ch" and "dis" stand for charging and discharging. $P_{bat,ch}$ and $P_{bat,dis}$ are the (dis)charging rate of the BESS.

The state charge is modelled as:

$$E_{bat}(k+1) = E_{bat}(k) + P_{bat}(k)\Delta k \quad , \text{ for } 1 \leq k \leq N-1 \quad (4.7)$$

where E_{bat} is the battery charge, N is the prediction horizon length, and Δk is the 15 minute time interval. The initial and final value of the state are defined as:

$$E_{bat}(k) = \begin{cases} E_{bat,init} & , \text{ for } k = 1 \\ E_{bat,final} & , \text{ for } k = N \end{cases} \quad (4.8)$$

Here "init" stands for initial. To give a fair price comparison the initial charge is set equal to the final charge.

$$E_{bat,init} = E_{bat,final} \quad (4.9)$$

To extend battery lifetime, a minimum charge of 10% and a maximum charge of 90% is picked. To prevent problems regarding real-time control, soft constraints ($E_{bat,soft}^{(+/-)}$) are added. These soft constraints make exceeding the previously set limits possible at a very high cost, as shown in Figure 4.4. The benefit of these soft constraints is that the model does not become infeasible if slightly exceeded. If they do exceed, the optimisation will prioritise them to get within the state boundaries as quickly as possible due to the high cost. The state constraints with soft constraints are formulated as:

$$E_{bat}(k) \leq 9 + E_{bat,soft}^{(+)}(k) \quad , \forall k \quad (4.10a)$$

$$E_{bat}(k) \geq 1 - E_{bat,soft}^{(-)}(k) \quad , \forall k \quad (4.10b)$$

$$0 \leq E_{bat,soft}^{(+)}(k) \leq 0.5 \quad , \forall k \quad (4.10c)$$

$$0 \leq E_{bat,soft}^{(-)}(k) \leq 0.5 \quad , \forall k \quad (4.10d)$$

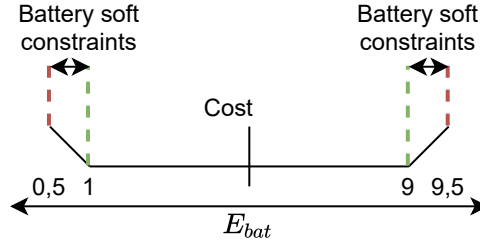


Figure 4.4: The cost function of the battery state (E_{bat}) per charge level. Only if the 10% or 90% is exceeded cost are added. If the red line is exceeded at 0.5 or 9.5 the model becomes infeasible.

An example of battery state E_{bat} over the prediction horizon is shown in Figure 4.5. The blue line indicates the optimal battery charge E_{bat} . The light green and light red planes indicate the possible optimisation range. The dark green and dark red strips show the potential (dis)charging. If the battery is empty, discharging is impossible, and the red strip diminishes (e.g. at 9 PM). In a full battery, charging becomes impossible (e.g. at 5 AM). The range of the (dis)charging per time step differs based on the battery's current state E_{bat} . If the battery is already charging (e.g. 3 PM), the potential charging decreases while the discharging increases.

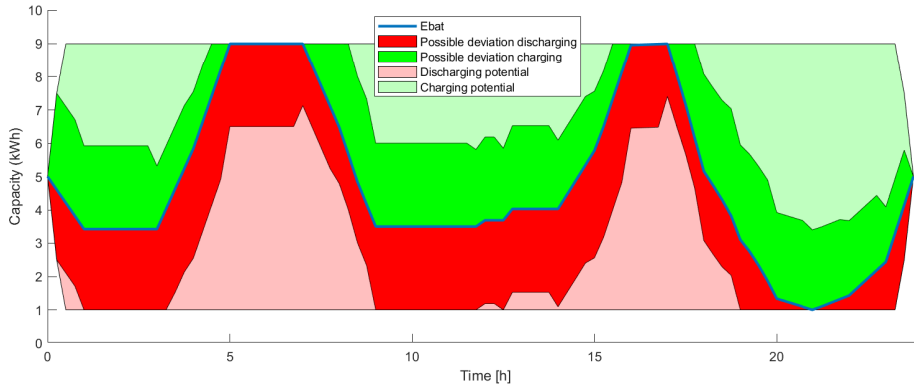


Figure 4.5: An example of E_{bat} over the prediction horizon.

4.3.3. EV dynamics

The EV is modelled similar to the battery. These include the same maximum (dis)charging power and converter efficiency. EV, if compatible, can be charged up to 240 kW [65]. However, the capacity limit of the distribution network can not cope with this high peak demand for EV charging. Furthermore, the investment cost would increase significantly. The difference in (dis)charging dynamics between BESS and EV is the availability of the EV. With this slight alteration, the (dis)charging dynamics are modelled as:

$$P_{ev}(k) = EV_{avail}(k)(\eta_{ev,ch}P_{ev,ch}(k) - 1/\eta_{ev,dis}P_{ev,dis}(k)) \quad , \forall k \quad (4.11a)$$

$$0 \leq P_{ev,ch}(k) \leq 10 \quad , \forall k \quad (4.11b)$$

$$0 \leq P_{ev,dis}(k) \leq 10 \quad , \forall k \quad (4.11c)$$

Where $EV_{avail} = 1$ means the EV is available for (dis)charging and $P_{ev,ch}$ and $P_{ev,dis}$ are the corresponding positive and negative charging capabilities.

The EV state charge does not include the EV_{avail} variable, as the EV uses power for driving and can dis(charge) at a different location. This state dynamic of the EV is modelled as:

$$E_{ev}(k+1) = E_{ev}(k) + (P_{ev}(k) - P_{drive}(k))\Delta k \quad , \forall k \quad (4.12a)$$

where E_{ev} is the charge of the EV, P_{drive} is the power usage of the EV when not connected to the multi-port converter.

The value of P_{drive} is determined by the difference of expected arrival and departure charge ($E_{ev,arr/dep}$) over the period that the EV is not available for (dis)charging at the multi-port converter ($EV_{avail} = 0$):

$$P_{drive}(k) = \begin{cases} \frac{E_{ev,arr} - E_{ev,dep}}{k_{arr} - k_{dep}} & , EV_{avail}(k) = 0 \\ 0 & , EV_{avail}(k) = 1 \end{cases} \quad (4.13)$$

Here, "dep" and "arr" stands for departure and arrival. $E_{ev,arr}$ is the arrival charge, $E_{ev,dep}$ is the departure charge, k_{dep} is the time step on which the EV departs, and k_{arr} is the arrival time. These inputs are defined by the user and vary between users, as shown in Section 3.2.3.

The operating range of the EV has been set between 20% and 80%. Furthermore, a minimal charge for the departure time step is set. Similar to the battery, soft constraints are added. The state constraints are formulated as:

$$E_{ev}(k) \leq 80 + E_{ev,soft}^{(+)}(k) \quad , \forall k \quad (4.14a)$$

$$E_{ev}(k) \geq 20 - E_{ev,soft}^{(+)}(k) \quad , \forall k \quad (4.14b)$$

$$0 \leq E_{ev,soft}^{(-)}(k) \leq 2.5 \quad , \forall k \quad (4.14c)$$

$$0 \leq E_{ev,soft}^{(+)}(k) \leq 2.5 \quad , \forall k \quad (4.14d)$$

$$E_{ev}(k) \geq E_{ev,dep} - E_{ev,dep,soft} \quad \text{for } k = k_{dep} \quad (4.14e)$$

Here, $E_{ev,soft}^{(+/-)}$ is the soft constraint for the state variable, and $E_{ev,dep,soft}$ is the soft constraint for the departure state. The departure soft constraint is added to keep the model feasible even when the E_{ev} is not at the required level. This may occur due to significant forecast errors. Suppose the moving horizon continues and k_{dep} is close to the start of the moving horizon window (e.g. $k_{dep} = 3$). In that case, a considerable forecast error could result in discharging the EV to prevent voltage violation. To prevent $E_{ev,dep,soft}$ from being used without the necessity for it, a high penalty is added to the soft constraints, so only in emergency scenarios would the system opt for going under the predefined set-point.

To give a fair cost evaluation, similar to the battery, the initial charge is set equal to the final by:

$$E_{ev,init} = E_{ev,final} \quad , \text{ if } k = 1 \quad (4.15)$$

This is only done for comparing the cost over a whole day (the first iteration of the moving horizon), but not when using the moving horizon starts ($k > 1$). If used in the moving horizon and the EV is unavailable during the final step ($k = 96$), the charge can not be changed. If an error occurs to the state E_{ev} , this will result in an infeasible solution. An example of the charging pattern of the EV (E_{ev}) is shown in Figure 4.6

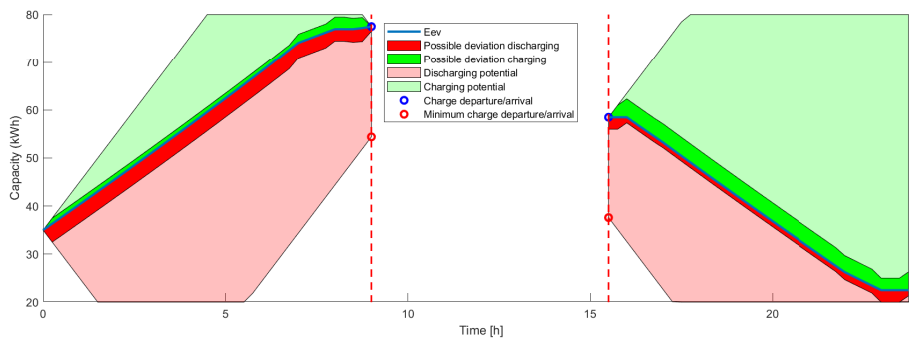


Figure 4.6: An example of E_{ev} over the prediction horizon. A gap in the optimisation range occurs due to the absence of the EV at this time. The red dots indicate the minimum charge needed for the EV, as set by the user. In this example, the EV chooses a different path, as seen by the blue line and blue dots, and departs with a higher charge. When the EV arrives back at the house, the optimisation is free to choose its path instead of going to a fixed final point.

4.4. Battery degradation

The (dis)charging of the EV and BESS is a vital part of the multi-port converter. These components enable opportunities as real-time control, demand side management (DSM) and direct PV to BESS capability. Therefore, to have a realistic operational cost, a battery degradation model is included in the optimisation. This model is used for both EV and BESS. Both models are based on the lithium-ion Nickel-Manganese-Cobalt cells. Besides its compact size, it has a high power density, fast (dis)charging rate, relatively long life and is resaleable. For operation characteristics, the cells of the batteries are assumed to be operating at 35 degrees Celsius. The constant operation at this temperature can be considered, as modern EV possesses active cooling. The temperature in the house is always around 20 degrees Celsius due to the heat-pump cooling and heating capabilities.

To compute the operational cost due to battery degradation, the daily capacity loss $\Delta E_{bat,dCap,tot}$ is determined. To determine the daily capacity loss of a single cell, the following model is used: [66]

$$\Delta E_{bat,dCap}(k) = B_1 e^{B_2 I_{bat}(k)} I_{bat}(k) \Delta k \frac{E_{bat}^{max}}{100}, \forall k \quad (4.16a)$$

$$\Delta E_{bat,dCap}^{tot} = \sum_{k=1}^N \Delta E_{bat,dCap}(k), \forall k \quad (4.16b)$$

Here, I_{bat} is the current rate, $I_{bat} \Delta k$ is the ampere-hours processed, and $\Delta E_{dCap}(k)$ is the lost capacity per time interval. The pre-exponential factor B_1 and exponential factor B_2 are constants as the temperature remains at the same level. Table 4.4 summarises all the pre-exponential and exponential factors. To go from percentage to actual capacity loss, in Equation 4.16a, $\frac{E_{bat}^{max}}{100}$ is added [66].

In Equation 4.16a, the current rate I_{bat} is unknown. The current from or to the battery cells can be computed as:

$$I_{bat}(k) = \frac{|P_{bat}(k)|}{N_{parallel,bat} V_{oc,bat}(k)}, \forall k \quad (4.17)$$

Here, $V_{oc,bat}$ is the battery's open-circuit voltage, and $N_{parallel}$ is the number of cells set in parallel. The $V_{oc,bat}$ is fitted to a curve determined by: [67]

$$V_{oc,bat}(k) = p_1 e^{\alpha_1 SoC_{bat}(k)} + p_2 e^{\alpha_2 SoC_{bat}(k)} + p_3 SoC_{bat}(k)^2, \forall k \quad (4.18)$$

Here, p_{1-3} and α_{1-2} are fitting parameters, shown in Table 4.4. To get an open-source voltage comparable to existing batteries, the cells have been set in a series of 100 (N_{series}). These cells are put in parallel ($N_{parallel}$), to reach the predefined capacity (E_{bat}/E_{ev}). The only difference in the degradation model between BESS and EV is the number of battery cells in parallel, as seen in Table 4.4.

The state of charge in Equation 4.18 can be calculated as:

$$SoC_{bat}(k) = \frac{E_{bat}(k)}{E_{bat}^{max}}, \forall k \quad (4.19)$$

Table 4.4: Constants of the battery degradation model.

Symbol	Quantity	Value
$N_{bat}^{parallel}$	Number of battery cells in parallel for BESS	14
$N_{ev}^{parallel}$	Number of battery cells in parallel for EV	145
N_{cell}^{series}	Number of battery cells in series	100
p_1	$V_{oc}(k)$ curve fit parameter	3.679
p_2	$V_{oc}(k)$ curve fit parameter	-0.2528
p_3	$V_{oc}(k)$ curve fit parameter	0.9386
α_1	$V_{oc}(k)$ curve fit parameter	-0.1101
α_2	$V_{oc}(k)$ curve fit parameter	-6.829
B_1	Ageing curve fit parameter	0.00054
B_2	Ageing curve fit parameter	0.35

4.5. Cost analysis

The cost analysis of the multi-port converter is in three categories: the operational cost of components, the cost of energy demand and the cost of the soft constraints.

The operating cost is the battery degradation of EV/BESS and the investment cost of the PV. The BESS cost C_{bat} is calculated by the decreasing value per kWh (V_{bat}) due to battery degradation. This is modelled as:

$$V_{bat} = V_{bat}^0 \frac{E_{bat}^{max} - \Delta E_{bat,dCap}^{tot}}{E_{bat}^{max}} \quad (4.20a)$$

$$C_{bat} = V_{bat}^0 E_{bat}^{max} - V_{bat} (E_{bat}^{max} - \Delta E_{bat,dCap}^{tot}) \quad (4.20b)$$

Here, V_{bat} is the current value per kWh of BESS, V_{bat}^0 is the initial value, and C_{bat} is the cost of BESS operation.

The second-hand value of the EV deteriorates faster if its capacity drops. In this thesis, it is assumed that at 80% of its original capacity, the value of the batteries is only 50% of its original value. To incorporate this increased devaluing, the cost of the EV is:

$$C_{ev} = (V_{ev}^0 - V_{ev}^{2nd}) \frac{\Delta E_{ev,dCap}^{tot}}{0.2 E_{ev}^{max}} (E_{ev}^{max} - \Delta E_{ev,dCap}^{tot}) \quad (4.21)$$

Here C_{ev} is the cost of operation of the EV, V_{ev}^0 is the initial value per kWh, and V_{ev}^{2nd} is the second-hand value per kWh.

To incorporate the investment cost of the PV panels, a cost function for the energy generated by the PV is added:

$$C_{pv} = \sum_{k=1}^N \lambda_{pv} P_{pv}(k) \Delta k \quad , \forall k \quad (4.22)$$

The cost of holding a rooftop PV panel is set to 0.097 euro/kWh [68].

The cost of the energy is calculated by the price and the amount consumed or generated. The cost is split into import and export (feed-in) as varying prices are used. The cost for the energy is calculated as:

$$C_{grid,imp} = \sum_{k=1}^N P_{grid,imp}(k) \Delta k \lambda_{buy}(k) \quad , \forall k \quad (4.23a)$$

$$C_{grid,ex} = \sum_{k=1}^N P_{grid,ex}(k) \Delta k \lambda_{sell}(k) \quad , \forall k \quad (4.23b)$$

$$C_{grid} = C_{grid,imp} - C_{grid,ex} \quad (4.23c)$$

Here $C_{grid,imp}$ is the cost from buying energy from the distribution network to the multi-port converter, $C_{grid,ex}$ is the profit from the energy sold back to the distribution network, $\lambda_{buy}(k)$ is the buying price of energy at time step k , and $\lambda_{sell}(k)$ is the selling price of energy at time step k .

The cost of the soft constraints are formulated as:

$$C_{bat,soft} = \alpha_1 \sum_{k=1}^N E_{bat,soft}^{(-)}(k) + \alpha_2 \sum_{k=1}^N E_{bat,soft}^{(+)}(k) \quad , \forall k \quad (4.24a)$$

$$C_{ev,soft} = \alpha_3 \sum_{k=1}^N E_{ev,soft}^{(-)}(k) + \alpha_4 \sum_{k=1}^N E_{ev,soft}^{(+)}(k) \quad , \forall k \quad (4.24b)$$

$$C_{ev,soft,dep} = \alpha_5 E_{ev,dep,soft} \quad (4.24c)$$

$$C_{tot,soft} = C_{bat,soft} + C_{ev,soft} + C_{ev,soft,dep} \quad (4.24d)$$

where α_{1-5} is any arbitrary big number.

The total cost can be formulated as:

$$C_{total} = C_{grid} + C_{bat} + C_{ev} + C_{pv} + C_{tot,soft} \quad (4.25)$$

The objective function is to minimise the cost of operation. This includes the cost of Energy consumption (C_{grid}), the operational cost of individual components (C_{bat} , C_{ev} , and C_{pv}) and cost aspects for soft constraints ($C_{soft,total}$). The objective function of the top-layer of the EMS can be formulated as:

$$\begin{aligned} & \underset{P_{pv}, P_{bat}, P_{ev}}{\text{minimise}} \quad C_{total} \\ & \text{subject to} \quad (4.1 - 4.25) \end{aligned} \quad (4.26)$$

The non-linear behaviour of the battery degradation makes this a non-linear programming. Although integer values are used for EV, they are not part of the decision variables, resulting in a non linear programming (NLP) instead of a mixed integer non linear programming. The programming model is solved using the Antigone [69] algorithm in General Algebraic Modeling System (GAMS).

ADN control mechanism

As mentioned in Section 1.1, the distributed energy resources (DER) in an active distribution network (ADN) have a certain degree of responsibility for system support. This system support is coordinated by the Voltage management system (VMS), which can compute the voltage profile and, if necessary, use the DER to prevent and correct the voltage deviation. This chapter focuses on the interaction between the optimal charging algorithm of the energy management system (EMS) and the VMS. Section 5.1 considers the various possible control structures for this interaction. In Section 5.2, the implemented control techniques for correction of the voltage deviation are discussed. Section 5.3 presents the different control techniques for preventing voltage deviations. Finally, Section 5.4 discussed the possibility of reserving generation and load capacity.

5.1. Control structure

The need for proper coordination between multi-port converters has been explained in Section 2.2.2. As mentioned in Section 1.1, the power system, as a whole, has a hierarchical control structure. Here, we look at the supervisory level of the distribution network, where a control structure is still largely absent. The control structure in the distribution network can be implemented in different ways. These are centralised, distributed, decentralised and hierarchical control structures, as shown in Figure 5.1.

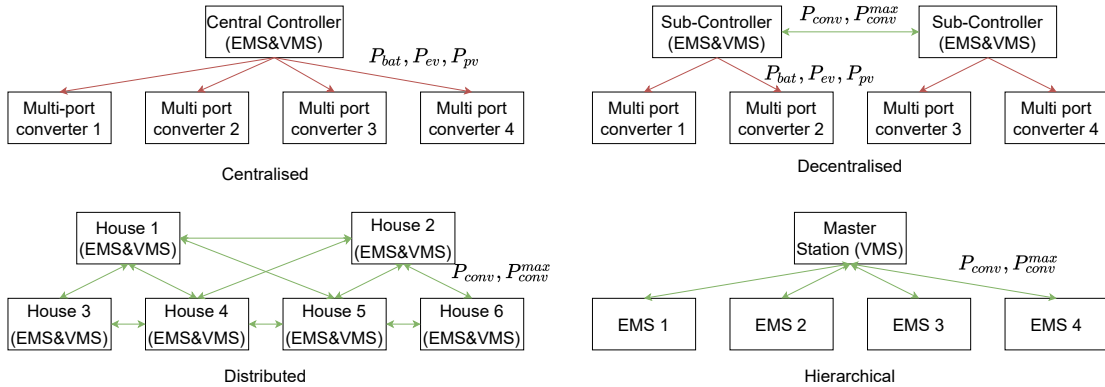


Figure 5.1: The possible control structures in a distribution network. The red lines indicate direct optimal control inputs for individual converters. The green lines indicate data exchange containing operational limits (P_{conv}^{max}) of the EMS and the required amount of active power (P_{conv}).

In a centralised solution, a single controller will compute, for all houses, the optimal (dis)charging patterns of the BESS (P_{bat}), EV (P_{ev}) and possible curtailment of the MPPT (P_{pv}). The cost function of Equation 4.26 is expanded to include all decision variables of all the multi-port converters to achieve the optimal control input. At that same moment the controller is also computing the voltage profile and the necessary steps to stay within the voltage limit. The EMS and VMS are merged into a single controller. Although this would yield the best optimisation results, resulting in the lowest cost, the computation time will render it unusable. The computational complexity causes this long computation time due to many dependable decision variables and the need to compute the voltage profile in the same controller. Furthermore,

Q_{conv} is the reactive power control input of the multi-port converter. V_{mag} and Q_{conv} go directly to the multi-port converter, as they are computed in the VMS and the EMS have no control over these variables. S_{total} is the total apparent power exchanged with the distribution network.

The data exchange between the EMS and the VMS is limited. The EMS calculates the control inputs and the corresponding required power (P_{conv}) from the distribution network. Only the necessary active power is sent to the VMS, responding with the voltage magnitude (V_{mag}) and one of the three correction techniques. These correction techniques are APC, RPC or a combination (APC and RPC). These techniques can combine the limitation of active power (P_{conv}^{max}) and a reactive power control input (Q_{conv}).

5.2. Control model for correction

After discussing the control structure and data exchange between the VMS and the EMS, this section focuses on the procedure of correcting the voltage deviation. A "correction" in this thesis means the possibility of removing the voltage deviation by limiting the amount of active power (APC), injection or absorption of reactive power (RPC) or a combination (APC & RPC). An iterative procedure has been designed. The flowchart of this procedure is depicted in Figure 5.3.

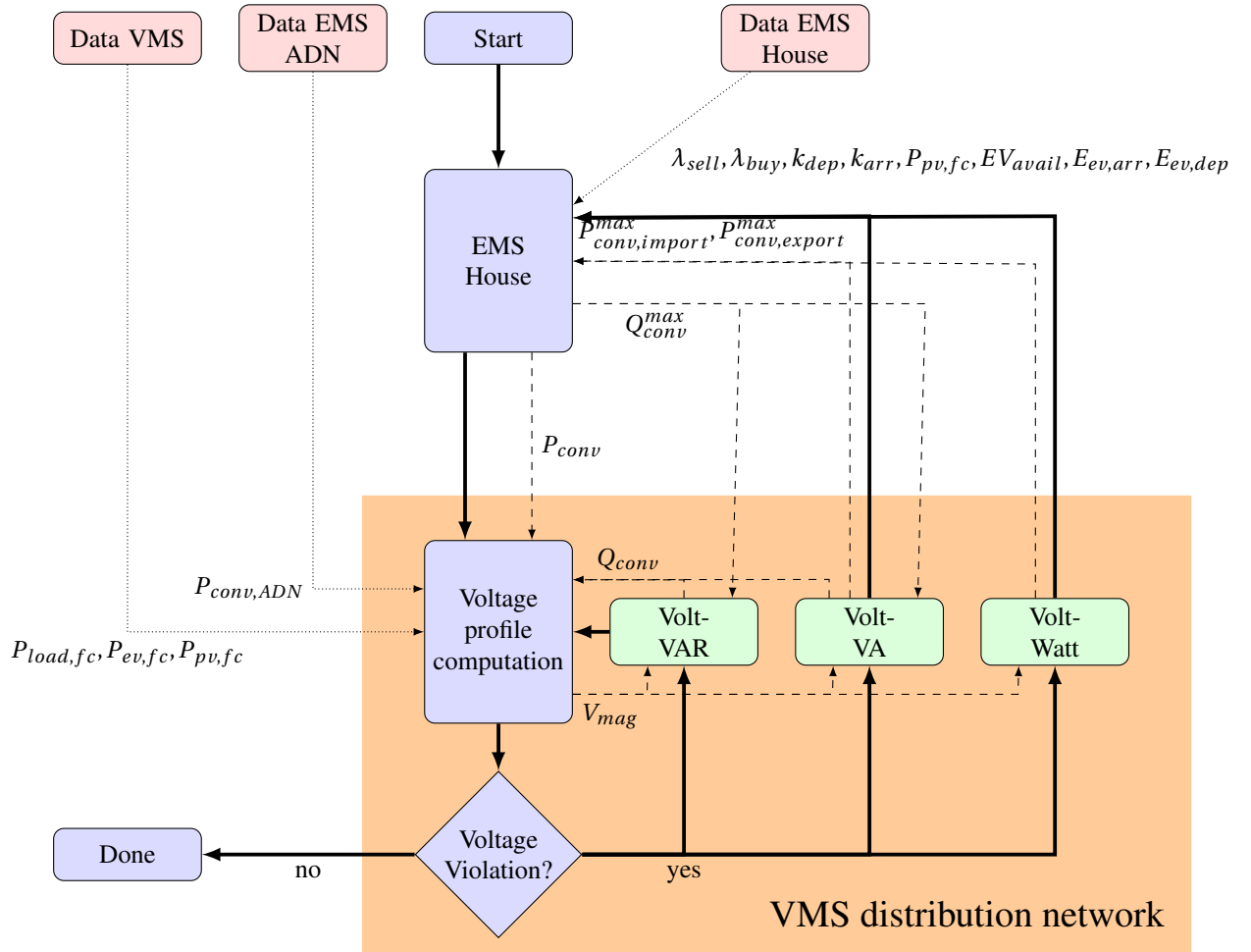


Figure 5.3: Proposed flowchart for correcting voltage violation in a distribution network. The red rectangles are data input, and the green rectangles are the control methods for correction. The system is finished when no voltage violations are found in the distribution network, or the iteration limit has been exceeded. The solid lines depict the direction of the flowchart, the dotted lines are for data inputs, and the dashed lines are data outputs of the corresponding blocks.

Starting off, the optimal control inputs are computed in the top layer of the EMS, based on the user input and forecasting data. After the optimal control inputs have been computed, the corresponding individual

active power requirement P_{conv} of all 96 time steps are determined and send to the VMS. After receiving P_{conv} from each EMS in the ADN, the VMS computes the corresponding voltage profile for each time step. The voltage profile is computed, for each step, based on the expected load profile ($P_{load,fc}$), the energy demand of each EMS ($P_{conv,ADN}$), but also on the predicted PV generation ($P_{pv,fc}$) and EV demand ($P_{ev,fc}$) from houses which do not have a multi-port converter. If no voltage limit is exceeded, the system is done. If not, three methods have been developed for the correction of the voltage deviation. These techniques are Volt-Watt (APC), Volt-VAR (RPC) and Volt-VA (APC&RPC).

5.2.1. Volt-Watt

If selected, in Figure 5.3, the Volt-Watt method limits the amount of energy the AC/DC converter can import or export. It does this by altering $P_{conv,ex}^{max}$ or $P_{conv,imp}^{max}$ from Equations 4.4a and 4.4b. In total, 96 curtailment segments are computed, one for each time step used for all multi-port converters. After computing these limitations, the flowchart in Figure 5.3 continues back to the EMS. The EMS optimises the cost function (Equation 4.26) again with adjusted constraints. This iterates until the voltage violation is resolved. In the Volt-Watt method, reactive power can be set to zero (Active power only) or a predefined power factor. As this thesis already looks at reactive power control (RPC), only a uniform power factor (no reactive power) is used.

The applied method of curtailment is given in Figure 5.4. It uses linear increments to curtail power import or export, based on the voltage level. If a voltage sag is expected, the import capacity is decreased for that time interval, and if a voltage swell is expected, the feed-in is limited.

The curtailment step in Figure 5.4 is based on the maximum value or minimum value voltage magnitude in the distribution network. If, for example, the voltage on a single bus exceeds the voltage limit at $k = 5$, all EMS are curtailed on the export at that time step. This means that each time step is checked for voltage deviations and, if necessary, corrected accordingly.

A static upper bound (C_{high}) is used to prevent large curtailments. This is necessary as the number of multi-ports may vary, resulting in an overcut if the percentage is not limited. Although this does not result in an infeasible solution, it will result in higher cost, as the capacity at this optimal point is not fully utilised. A lower bound (C_{low}) is used to prevent small increments. The trade-off has been made between computational time and accuracy. The maximum divergent for all correction methods have been set to 0.001 p.u. ($\approx 0,4V$) within the voltage limits. The effect of the curtailment can be observed in Figure 5.5.

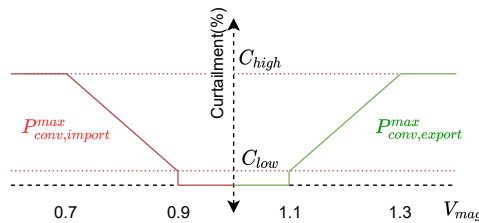


Figure 5.4: This figure shows the linear increment of curtailment based on the voltage magnitude. The highest (or lowest) voltage magnitude of all houses is taken to decide the necessary amount of curtailment for all houses. Based on this bus, $P_{conv,imp}^{max}$ or $P_{conv,ex}^{max}$ is curtailed equally in each house with a multi-port converter.

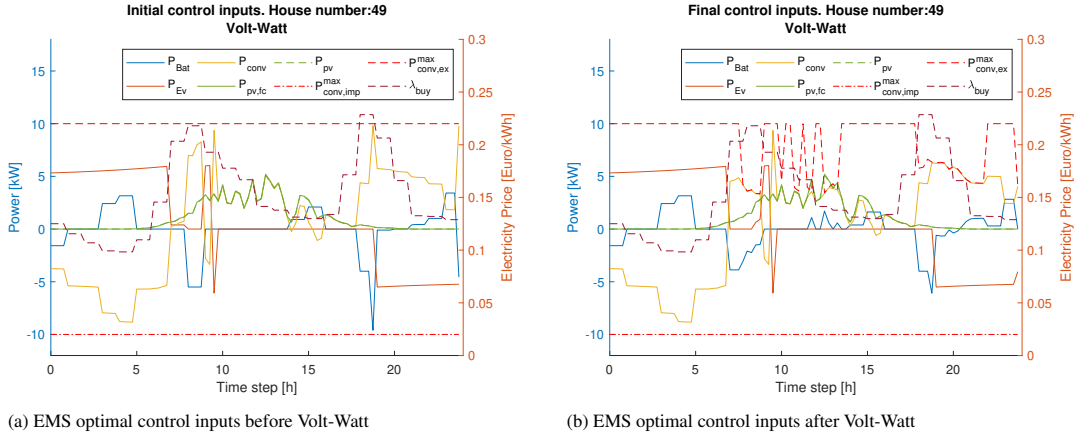


Figure 5.5: Figure 5.5a shows the original optimal control inputs computed by the EMS. After following the control procedure of Figure 5.3, with Volt-Watt as the correction technique, the curtailed result is shown in Figure 5.5b. The external variation on $P_{conv,imp}^{max}$, $P_{conv,ex}^{max}$ are the PV generation, the difference in load forecast and variation in charging patterns per house.

5.2.2. Volt-VAR

Instead of limiting the active power (P_{conv}), the Volt-VAR method corrects the voltage magnitude of the distribution network, using only reactive power (Q_{conv}). As shown in Figure 5.3, the maximum amount of reactive power (Q_{conv}^{max}) is determined by the EMS. This is because the maximum amount of reactive power is directly connected to the active power (P_{conv}), as stated in Equation 2.8 and seen in Figure 5.6b. The voltage correction, using Volt-VAR, starts by computing the voltage profile and detects any voltage violation. Suppose any voltage violation has occurred, the amount of reactive power Q_{conv} is computed for each individual house and time step, determined by the maximum reactive power available at that house (Q_{conv}^{max}) at that time step. This reactive power is then used to recompute the voltage profile. As the voltage profile can not improve after adding the max reactive power (Q_{conv}^{max}), the maximum amount of iterations for Volt-VAR in Figure 5.3, is set to one.

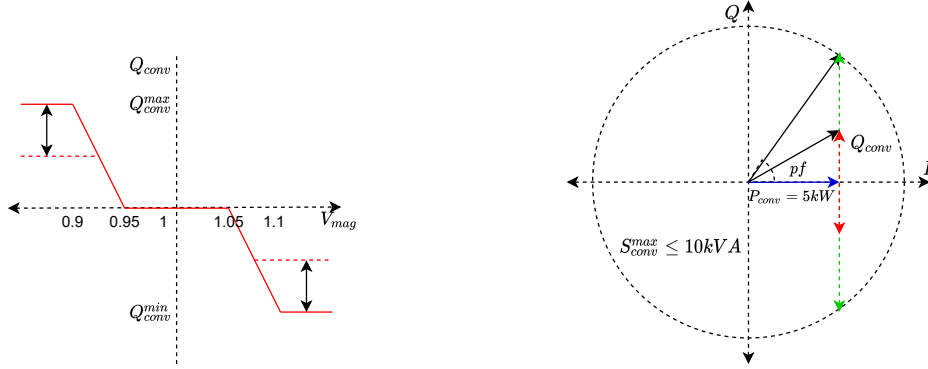
If the power factor is limited, the maximum reactive power is equal to Equation 2.7, thereby forming the maximum reactive power of:

$$Q_{conv,pf=[0-0.9]}^{max} = \min \left(P_{conv} \sqrt{\frac{1-pf^2}{pf^2}}, \sqrt{(S_{conv}^{max})^2 - P_{conv}^2} \right) \quad (5.1)$$

Here, pf is the power factor, and S_{conv}^{max} is the apparent power rating of the multi-port converter.

Three methods are developed for the determination of Q_{conv} . These are droop, sensitivity and incremental control.

Voltage droop control uses a predefined amount of reactive power (QV-curve) corresponding to the voltage magnitude, as seen in Figure 5.6a. This method uses the maximum (or minimum) voltage in the entire network to determine Q_{conv} for every multi-port converter.



(a) This figure shows the amount of reactive power each multi-port converter absorbs/injects into the system based on the magnitude of the voltage extrema computed by the VMS. The dotted red line represents a possible decrease of Q_{conv} due to inverter limitations, as shown in Figure 5.6b.

(b) This figure shows the limitation of the reactive power injection or absorption based on the amount of P_{conv} required by each house. The green line represents no power factor, while the red line shows a restricted power factor. The converter to the grid is capable of handling 10 kVA of power.

Figure 5.6: Overview of the principles needed for voltage droop control.

As P_{conv} varies, it influences the amount of Q_{conv} that can be absorbed or injected. After determining the reactive power for each house, the voltage profile is recalculated. After this step, the system is done, as the number of maximum iterations is reached.

The second method, Volt-VAR sensitivity, determines which multi-port converter should inject reactive power based on the "sensitivity" of their location in the distribution network. The sensitivity coefficient of a multi-port converter influences the amount of reactive power needed to alter the voltage magnitude. This sensitivity coefficient varies between houses. The sensitivity coefficient can be determined by taking the Jacobian of the power flow equations. The derivation of the power flow equations is stated in Appendix listing B. The power flow equations for the distribution network are:

$$P_i = \sum_{j=1}^n |Y_{ij}| |V_i| |V_j| \cos(\theta_{ij} + \delta_j - \delta_i) \quad (5.2a)$$

$$Q_i = - \sum_{j=1}^n |Y_{ij}| |V_i| |V_j| \sin(\theta_{ij} + \delta_j - \delta_i) \quad (5.2b)$$

In these equations, P_i and Q_i are the active and reactive powers of bus i , n is the number of buses in the distribution network, $Y_{ij} \angle \theta_{ij}$ is the admittance of the line running from bus i to bus j , and δ_i and δ_j are the corresponding angles of bus voltages (V_i, V_j). The corresponding Jacobian matrix for Equations 5.2a and 5.2b is: saadat1999power

$$\begin{bmatrix} \Delta P_2 \\ \vdots \\ \Delta P_n \\ \Delta Q_2 \\ \vdots \\ \Delta Q_n \end{bmatrix} = \begin{bmatrix} \frac{\partial P_2}{\partial \delta_2} & \cdots & \frac{\partial P_2}{\partial \delta_n} & \frac{\partial P_2}{\partial |V_2|} & \cdots & \frac{\partial P_2}{\partial |V_n|} \\ \vdots & \ddots & \vdots & \vdots & \ddots & \vdots \\ \frac{\partial P_n}{\partial \delta_2} & \cdots & \frac{\partial P_n}{\partial \delta_n} & \frac{\partial P_n}{\partial |V_2|} & \cdots & \frac{\partial P_n}{\partial |V_n|} \\ \frac{\partial Q_2}{\partial \delta_2} & \cdots & \frac{\partial Q_2}{\partial \delta_n} & \frac{\partial Q_2}{\partial |V_2|} & \cdots & \frac{\partial Q_2}{\partial |V_n|} \\ \vdots & \ddots & \vdots & \vdots & \ddots & \vdots \\ \frac{\partial Q_n}{\partial \delta_2} & \cdots & \frac{\partial Q_n}{\partial \delta_n} & \frac{\partial Q_n}{\partial |V_2|} & \cdots & \frac{\partial Q_n}{\partial |V_n|} \end{bmatrix} \begin{bmatrix} \Delta \delta_2 \\ \vdots \\ \Delta \delta_n \\ \Delta |V_2| \\ \vdots \\ \Delta |V_n| \end{bmatrix} \quad (5.3)$$

Here, bus 1 is assumed to be a slack bus. This bus in the IEEE European low voltage test feeder is the transformer, which is considered to have a uniform voltage magnitude and phase angle. The Jacobian matrix shows the linearised relationship between the voltage angle ($\Delta\delta$) and magnitude ($\Delta|V|$) and the change in active (ΔP) and reactive (ΔQ) power [59]. The Jacobian matrix can be reduced to:

$$\begin{bmatrix} \Delta P \\ \Delta Q \end{bmatrix} = \begin{bmatrix} \frac{\partial P}{\partial \delta} & \frac{\partial P}{\partial |V|} \\ \frac{\partial Q}{\partial \delta} & \frac{\partial Q}{\partial |V|} \end{bmatrix} \begin{bmatrix} \Delta\delta \\ \Delta|V| \end{bmatrix} \quad (5.4)$$

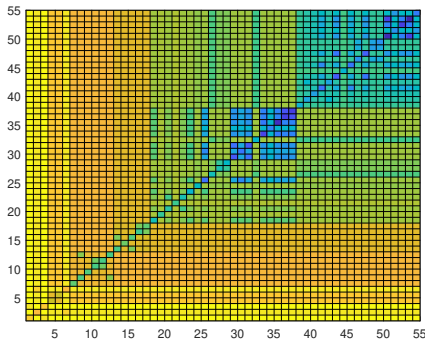
Taking the inverse, the sensitivity relationship can be described as: [35]

$$\begin{bmatrix} \Delta\delta \\ \Delta|V| \end{bmatrix} = \underbrace{\begin{bmatrix} S_{\theta P} & S_{\theta Q} \\ S_{|V|P} & S_{|V|Q} \end{bmatrix}}_{J^{-1}=S} \begin{bmatrix} \Delta P \\ \Delta Q \end{bmatrix} \quad (5.5)$$

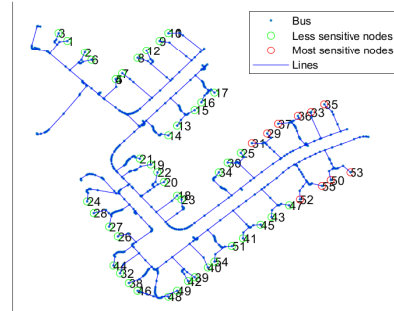
The second line of Equation 5.5 shows that the voltage has a direct correlation between the active and reactive power. This leads to:

$$\Delta|V| = S_{|V|P}\Delta P + S_{|V|Q}\Delta Q \quad (5.6)$$

In this scenario, the value of multi-port converter P_{conv} has already been determined, leaving only the variation from the reactive power ($S_{|V|Q}\Delta Q$). Figure 5.7a shows the sensitivity matrix $S_{|V|Q}$ of the IEEE European low voltage test feeder. The blue colour indicates a high sensitivity. The yellow colour indicates a low sensitivity. High sensitivity results in a higher voltage correction for the same amount of reactive power.



(a) Sensitivity Matrix of the IEEE European low voltage test feeder. The numbers in the axis are the house numbers. The locations of these houses are shown in Figure 5.7b



(b) This figure indicates the top 10 most "sensitive" houses of the IEEE European low voltage test feeder. They are all located at the end of the feeder.

Figure 5.7: These figures show the sensitivity coefficient $S_{V,Q}$ of the houses and their position in the distribution network. Figure 5.7a shows the voltage correlation on reactive power usage between the houses, and Figure 5.7b shows the location of the most sensitive houses in the low voltage feeder.

The houses with the highest sensitivity are all at the end of the distribution network, as shown in Figure 5.7b. Although less reactive power is needed, more losses are generated due to the length of the distance to the transformer, as shown in 5.8.

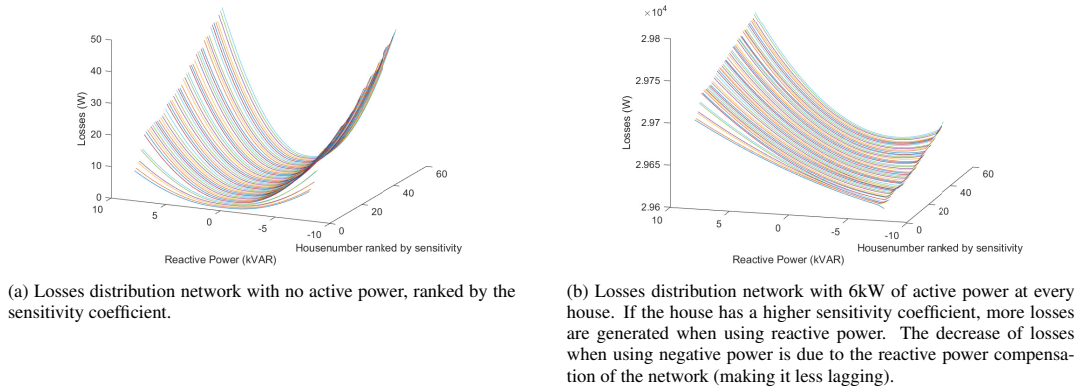


Figure 5.8: An overview of the losses in the grid compared to the sensitivity coefficient when no active power (Figure 5.8a) and 6kW active power (Figure 5.8b) is used at each house. In this Figure, house 55 has the highest sensitivity coefficient, and house 1 has the lowest. The reactive power is only used at that specific house. At all the other houses, the reactive power is zero. The figure indicates that the houses which have the highest sensitivity coefficient thus can more easily control the voltage using reactive power yields the highest losses.

The procedure to compute the reactive power (Q_{conv}) is different from voltage droop control. In this case, instead of the amount of reactive power needed, the number of houses that use reactive power is computed. The picked houses have the highest sensitivity coefficient and use all the available reactive power. To decrease the amount of reactive power, an iterative procedure has been created to increase or decrease the number of houses based on the acquired voltage profile, as shown in Figure 5.9.

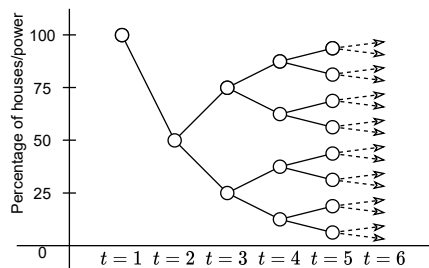


Figure 5.9: Progression of the number of houses that inject/absorb 100% of the reactive power (sensitivity) or percentage of Q_{conv}^{max} that is injected/absorbed (incremental) in computation iteration t . Based on the calculated voltage profile, the number of houses can be increased or decreased (sensitivity), or the amount of reactive power can be increased or decreased (incremental).

At the start, if a voltage violation happens at time step k , all houses use their maximum amount of reactive power. As the voltage profile is updated, it can be checked whether or not the voltage deviation has been solved. If not, the voltage deviation can not be solved using Volt-VAR. If the voltage deviation is removed, the number of houses decreases. Based on the voltage profile, the number of houses is either increased or decreased.

Figure 5.10 demonstrates the iteration procedure of Figure 5.9. It shows the iteration procedure and increased accuracy. Within 8 iterations the whole active power (P_{conv}) range of the multi-port converter can be corrected. Furthermore, the iteration procedure can be sped up. Only the first iteration has to check all 96 data frames. All the values which are already within limits or after iteration are with the 1% range, are removed from the computation.

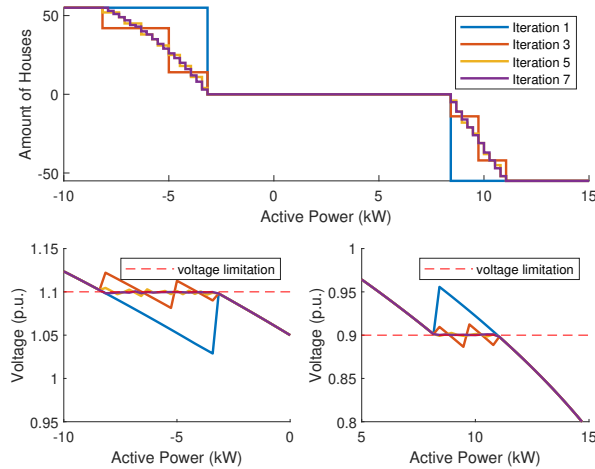


Figure 5.10: The top figure shows the results of the iterative procedure, tested on a varying active power scale. It shows the number of houses used for reactive power support. The bottom figures show the corresponding voltage profile. In this figure, it is assumed that all houses have 10 kVAR of reactive power available for demonstrative purposes. As this capacity is not always available, a sharper increase in houses is expected. The negative value is the injection of reactive power, while the positive values are the absorption of reactive power.

The third method is incremental Volt-VAR. In this method, every house injects the same amount of reactive power, similar to voltage droop control. However, voltage droop control injects or absorbs a predefined amount of reactive power, while the incremental Volt-VAR minimises reactive power output. It does this similar to Volt-VAR sensitivity using the procedure of Figure 5.9. An overview of the iterations is shown in Figure 5.11.

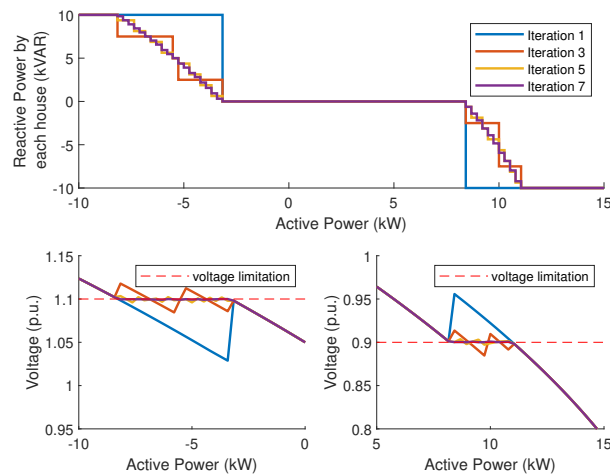


Figure 5.11: The top figure shows the results of the iterative procedure, tested on a varying active power scale. It shows the amount of reactive power each house uses for reactive power support. The bottom figures show the corresponding voltage profile. In the figure, for demonstrative purposes, it is assumed that all houses have 10 kVAR of reactive power available. As this is not always achievable, a varying pattern of reactive power support is expected as some houses reach their possible support Q_{conv}^{max} earlier. The negative value is the injection of reactive power, while the positive value corresponds to the absorption of reactive power.

Compared to Volt-VA sensitivity, it can be seen that the Volt-VAR incremental indeed uses more reactive power to compensate minor deviations, as shown in the straight purple line in Figure 5.11, compared to the more curved line in Figure 5.10. This difference in reactive power usage diminishes when the deviation becomes more prominent.

5.2.3. Volt-VA

The Volt-VA method is a combination of the Volt-Watt and Volt-VAR methods. This technique combines the curtailment of active power and sets control inputs for reactive power control.

In Figure 5.3, after the computation of the voltage profile, the procedure of Volt-VAR is followed. The required amount of reactive power Q_{conv} is computed for each house and time step, using either Volt-VAR incremental or sensitivity. Only these two are used as they use less reactive power and are more accurate. If the reactive power compensation is not enough to remove the voltage deviation, additional curtailment for P_{conv}^{max} is computed using the Volt-Watt procedure.

The first iteration in the Volt-VAR procedure is set to 100% to decrease computation time, as shown in Figure 5.9. Namely, if the maximum amount of reactive power is not enough to correct the voltage violation, all other options will neither. If, after the first computation, the voltage can not be corrected at any of the time steps, the computation stops. All the computed Q_{conv} will be used, and the procedure continues to the Volt-Watt. This is done to prevent additional curtailment of P_{conv} . As in this showcase, only these time steps still have voltage deviations after reactive power compensation.

5.2.4. Volt-VA optimisation problem

The next possible step would include an optimisation problem. This optimisation problem can be used to find the optimal reactive power setpoints while minimising distribution losses and replacing the Volt-VAR step. To decrease computation time, parts of the IEEE European low voltage test feeder distribution lines have been merged, as seen in Figure 5.12. The number of buses has been reduced from 906 to 110.

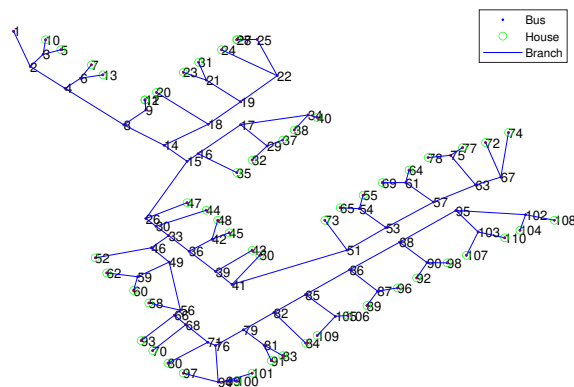


Figure 5.12: A reduced version of the single line diagram of the IEEE European LV Test Feeder.

This optimisation aims to minimise the power losses caused by the distribution line while staying within the voltage limit. This optimisation problem can be formulated as:[40]

$$\min_{Q_{conv,i}, V_i^{itc}} \sum_{ij \in B} P_{ij}^{loss} \quad (5.7a)$$

$$Q_{conv,i} = -\frac{\omega}{s_i}(V_i - V_i^{itc}) \quad \forall i \quad (5.7b)$$

$$Q_{conv,i}^{max} \leq Q_{conv,i} \leq Q_{conv,i}^{min} \quad \forall i \quad (5.7c)$$

$$\sum_{j \in J(i)} P_{ij} = \sum_{h \in H(i)} P_{hi} + P_{conv,i} \quad \forall i \quad (5.7d)$$

$$\sum_{j \in J(i)} Q_{ij} = \sum_{h \in H(i)} Q_{hi} + Q_{conv,i} \quad \forall i \quad (5.7e)$$

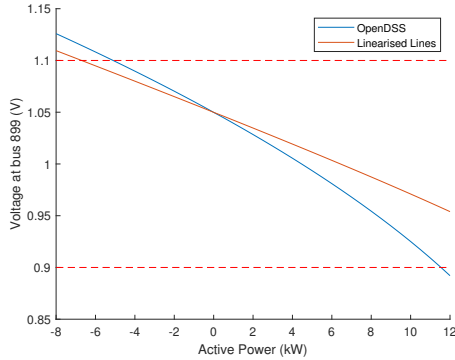
$$V_j = V_i - \frac{(R_{ij}P_{ij} + X_{ij}Q_{ij})}{V_0} \quad \forall ij \quad (5.7f)$$

$$P_{ij}^{loss} = R_{ij} \frac{P_{ij}^2 + Q_{ij}^2}{V_0^2} \quad \forall ij \quad (5.7g)$$

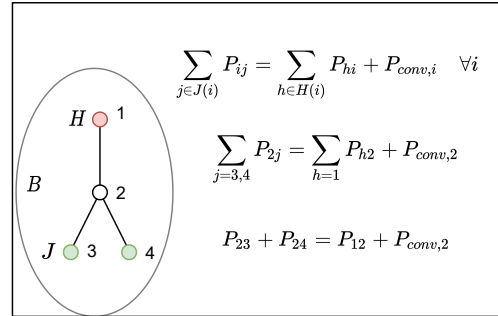
$$V_i^{min} \leq V_i \leq V_i^{max} \quad \forall i \quad (5.7h)$$

Here, J, H and B are the child buses, parent buses and the edge set, as shown in Figure 5.13b. V^{itc} is the voltage magnitude at which the droop curve cuts the x-axis, R_{ij} and X_{ij} are the resistance and reactance of the line from bus i to j , P_{ij}^{loss} is the line losses from bus i to j , ω is the control gain of droop control function, V_0 is the voltage at the transformer and V_i is the voltage magnitude at bus i and s_i the sensitivity of bus reactive power injection to the bus voltage magnitude.

The linearisation of the lines ($V_j = V_i - \frac{(R_{ij}P_{ij} + X_{ij}Q_{ij})}{V_0} \quad \forall ij$) does not work for this feeder. It gives a distinct deviation from the voltage computed by OpenDSS, as seen in Figure 5.13.



(a) The difference in voltage using linearised line of Equation 5.7f and the VMS (computed in OpenDSS).



(b) An explanation of the function of child buses (J), parent buses (H) and the edge set (B) using Equation 5.7d

Figure 5.13: Explanation of the limited use of optimisation, caused by linearised lines (Figure 5.13a) and the description of child and parent buses (Figure 5.13b)

5.2.5. Summary

The three methods, Volt-Watt, Volt-VAR, and Volt-VA, to correct the voltage deviation are explained. In the Volt-VAR, three techniques have been discussed. The overview of performance and losses by using the Volt-VAR method in the distribution network is shown in Figure 5.14.

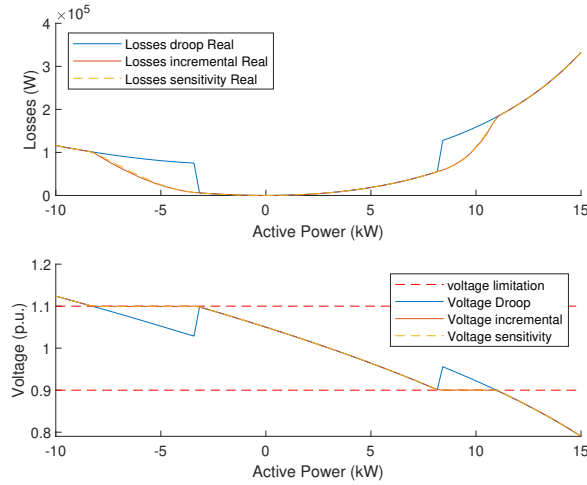


Figure 5.14: Losses and corresponding voltage level with different Volt-VAR techniques. The figure assumes all 55 houses have a multi-port converter, and the P_{conv} of all multi-port converters is set to zero. This means every multi-port converter has all its available reactive power Q_{conv}^{max} .

It shows that both the incremental and sensitivity approach outperforms the droop on losses and voltage regulation. The only benefit of voltage droop is the faster computation time. However, the optimisation procedures partly diminish the computation benefit. Besides higher losses and worse accuracy, the gradual deployment of multi-port converter needs recalibration of the linear curve for voltage droop control.

In most cases, Volt-VAR cannot prevent voltage deviations and is a less favourable option for voltage correction. However, the Volt-VAR is used as part of the Volt-VA procedure. Both Volt-Watt and Volt-VA are able to correct the voltage deviation.

5.3. Prevention measures

The VMS has demonstrated how a voltage violation can be corrected in the forecast. Figure 5.15 demonstrates a problem that can not be corrected but instead should be prevented. The figure shows a situation in which the voltage violation already has occurred, even without the added demand or generation from the multi-port converter. This can happen if a large part of the network has no multi-port converter due to the uncontrolled energy exchange of the EV and PV. The left plot of Figure 5.15 shows a voltage profile before the addition of the multi-port converter.

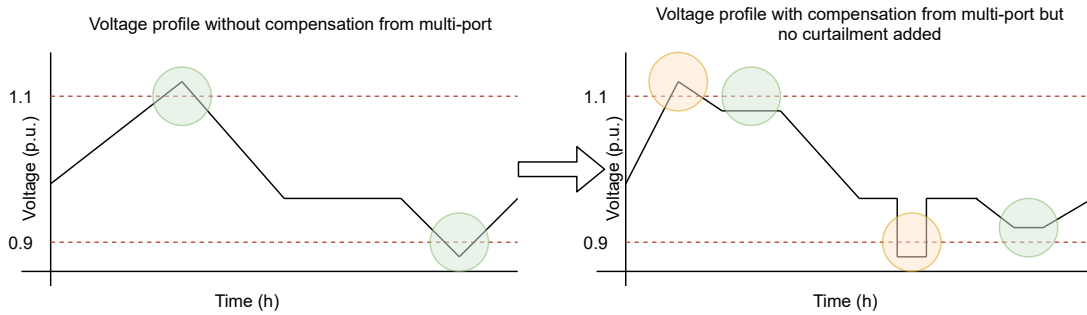


Figure 5.15: Voltage profile problems before compensation (left) and after compensation (right). The initial violations (green) have been resolved due to price changes, and the remaining violations (yellow) can be resolved using Volt-Watt and Volt-VA.

The green part has no guarantee to be resolved, as the optimisation of Chapter 4 wants to minimise cost, and these time steps might not be optimal to do so. To prevent this, the price is adjusted, as shown in Figure 5.16. This means that the buying and selling prices ($\lambda_{buy/sell}$) are increased when the voltage gets too low (to amplify export) or decreased when the voltage exceeds the limit (to increase import). The prices are set 1 cent above the maxima for stimulating export and 1 cent below the minima for promoting the importation of energy.

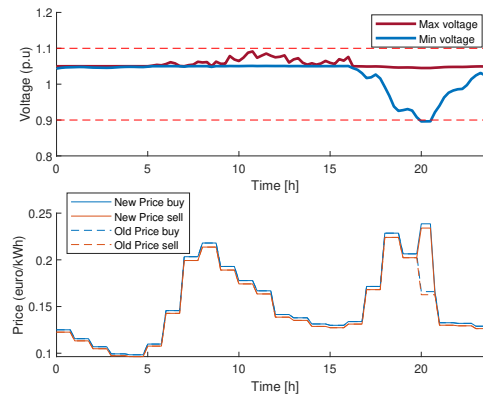


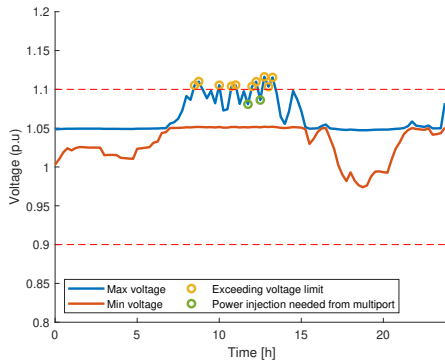
Figure 5.16: Price alterations based on exceeding voltage levels. At 8 PM the export and import prices are increased to encourage the export of energy by the multi-port converter.

In Figure 5.16 the max voltage and min voltage are the maximum voltage and minimum voltage in the entire distribution network. The voltage violation occurs before the flowchart procedure in Figure 5.3 starts. Therefore a part is added on top of Figure 5.3, resulting in Figure 5.19. Before the iteration procedure starts, the voltage profile is checked, and the prices are adjusted accordingly. This has to be done only once per moving horizon step.

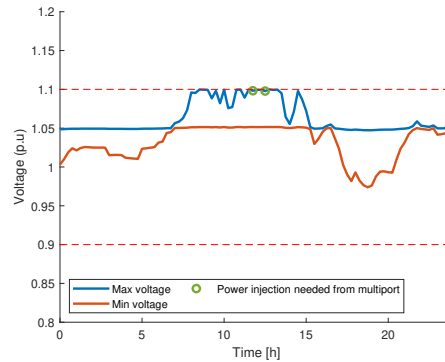
To prevent extra cost for the DSO, the amount of power used at these beneficial prices are reduced by the correction methods, as presented in Figures 5.17 and 5.18.

Here, in Figure 5.17a the green circles indicate that a price alteration is needed, and they also show that too much cheap energy is imported as the voltage is far below the maximum operational point. Figure 5.17b shows that the green circles have been corrected to the voltage limit. Furthermore, the other voltage violations (yellow circles) have been resolved using either active or reactive power.

The result of the Volt-Watt/Volt-VA (APC part) method is shown in Figure 5.18. When price alterations occur, not only is the system encouraged to import energy, it will curtail its PV power, as shown in Figures 5.18a and 5.18b (green dashed line). This helps to keep capacity for real-time control, which will be further discussed in Section 6.3.

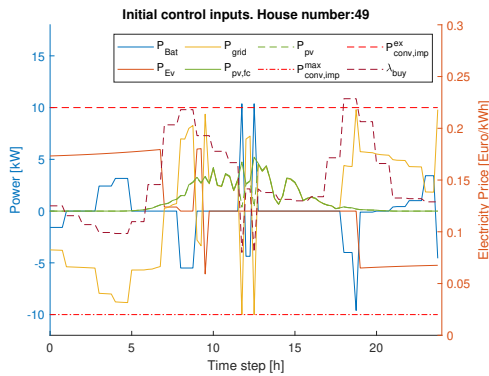


(a) The voltage profile after the voltage calculation step for price alterations and before the first computation of the EMS.

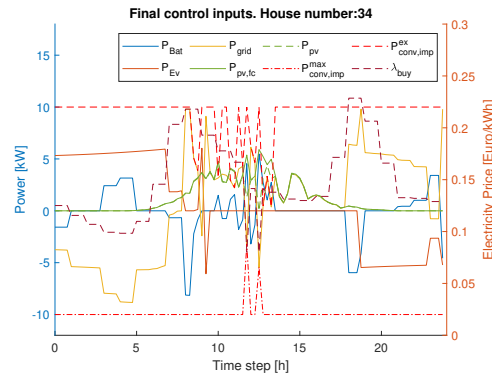


(b) The voltage profile after the final iteration, using the flowchart in Figure 5.19.

Figure 5.17: The change in voltage profile before and after the implementation of Volt-Watt or Volt-VA using the flowchart from Figure 5.19.



(a) EMS initial optimal control inputs using Volt-Watt/Volt-VA, with price adjustments at 11-12 AM.



(b) EMS final optimal control inputs using Volt-Watt/Volt-VA, with price adjustments at 11-12 AM.

Figure 5.18: Figure 5.18a shows the original optimal control inputs computed by the EMS. After following the control procedure of Figure 5.19, the curtailed result is shown in Figure 5.18b. The change in $P_{conv,imp}^{max}$ is to prevent the multi-port converter from importing additional cheap energy.

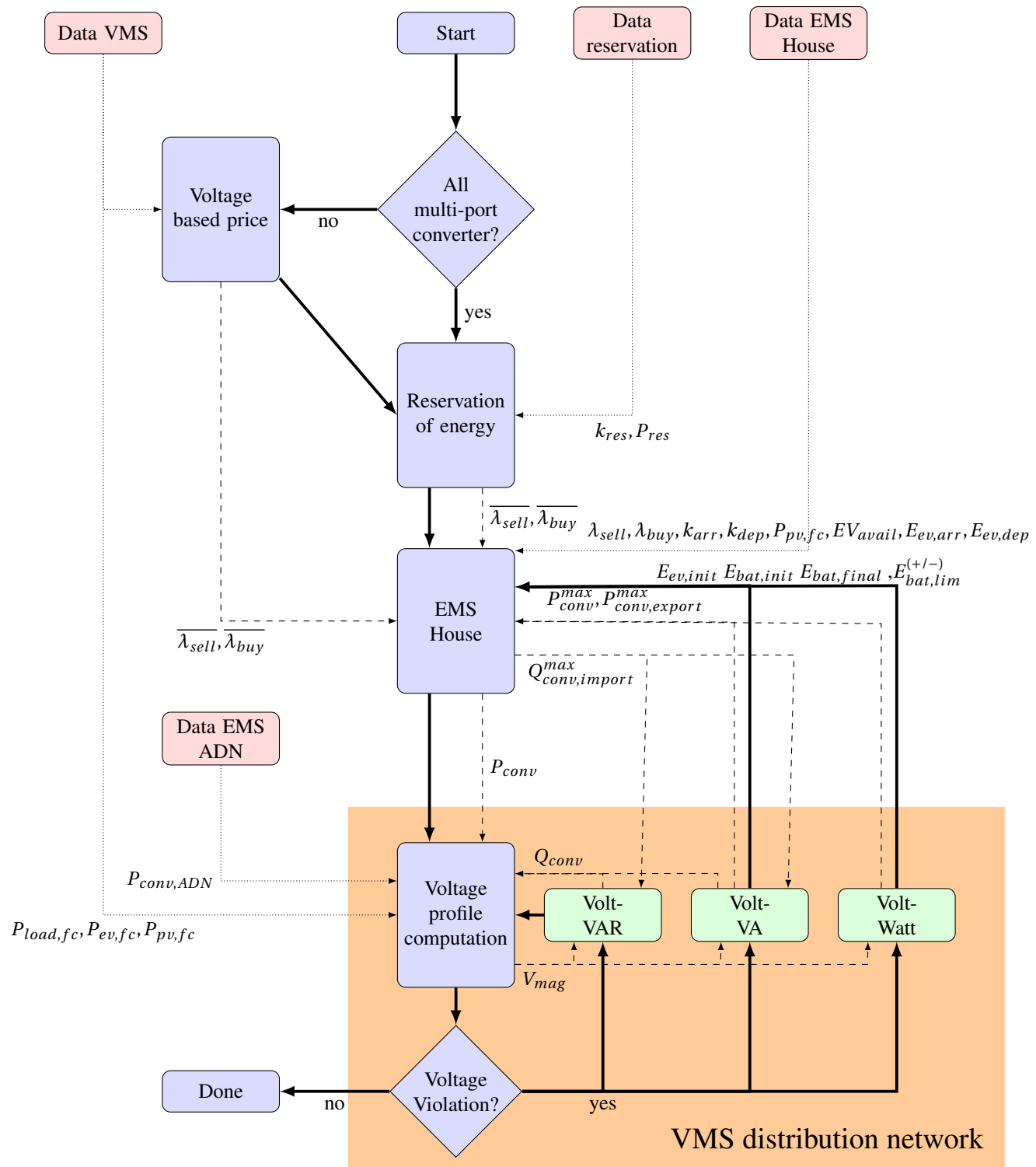


Figure 5.19: Proposed flowchart for correcting and prevention of voltage violation in a distribution network. The red rectangles are data input, and the green rectangles are the control methods for correction. The system is finished when no voltage violations are found in the distribution network, or the iteration limit has been exceeded. The solid lines depict the direction of the flowchart, the dotted lines are for data inputs, and the dashed lines are data outputs of the corresponding blocks.

The second prevention method implemented is the reservation of BESS capacity to withstand real-time forecasting errors. When the EV is unavailable for (dis)charging, the BESS is responsible for system response. This system response includes the additional import of energy when too much energy is generated in the distribution network and the export of energy when too much energy is consumed in the distribution network. This reservation is needed to prevent the battery from reaching its capacity limits, as this results in a decrease of (dis)charging power. This decrease of (dis)charging power is shown in Figure 5.20.

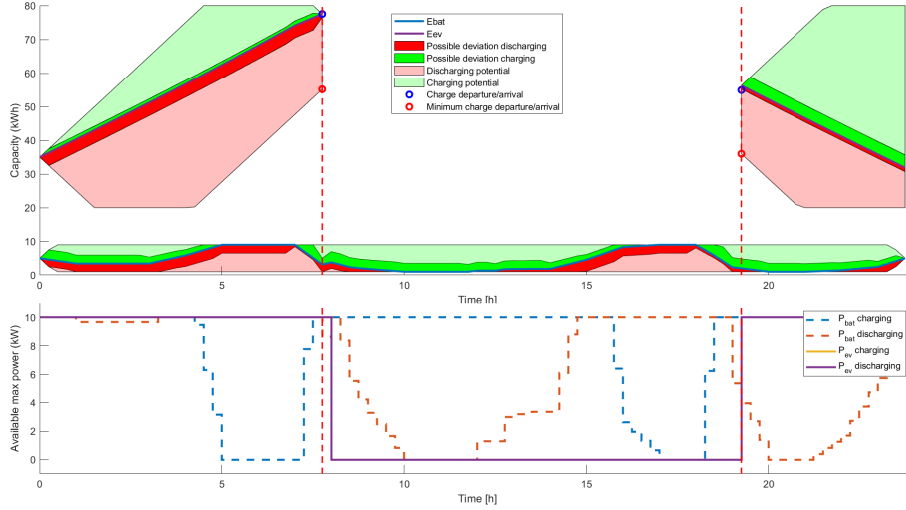


Figure 5.20: This figure shows the lack of import and export power capabilities at specific time frames when the EV has left the house. The top figure shows the optimisation range of both the EV (E_{ev}) and BESS (E_{bat}). The bottom figure shows the corresponding maximum (dis)charging capabilities of the EV and BESS.

By reserving capacity, it is possible to guarantee that the multi-port converter is capable of importing/exporting an additional amount of power. This reservation of energy by the BESS can be achieved by adding $E_{bat,lim}^{(+)}$ and $E_{bat,lim}^{(-)}$ parameters to state constraints of E_{bat} , as used in Equations 4.10a and 4.10b. The constraints for the charge level of the battery become:

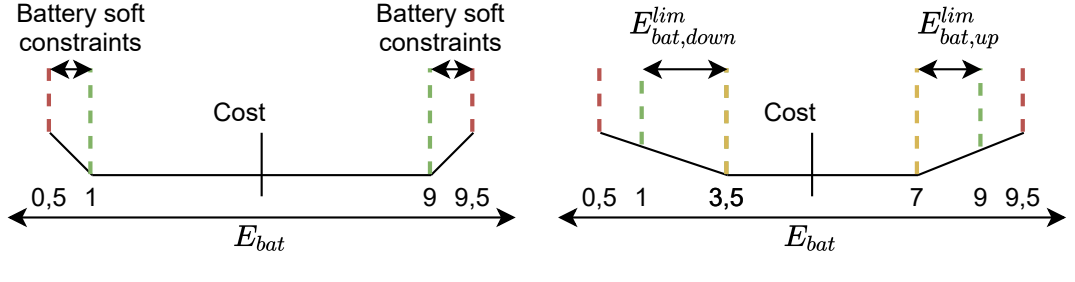
$$E_{bat}(k) \leq 9 - E_{bat,lim}^{(+)}(k) + E_{bat,soft}^{(+)}(k) \quad , \forall k \quad (5.8a)$$

$$E_{bat}(k) \geq 1 + E_{bat,lim}^{(-)}(k) - E_{bat,soft}^{(-)}(k) \quad , \forall k \quad (5.8b)$$

$$0 \leq E_{bat,soft}^{(+)}(k) \leq 0.5 + E_{bat,lim}^{(+)}(k) \quad , \forall k \quad (5.8c)$$

$$0 \leq E_{bat,soft}^{(-)}(k) \leq 0.5 + E_{bat,lim}^{(-)}(k) \quad , \forall k \quad (5.8d)$$

The explanation of how the added $E_{bat,lim}^{(+/-)}$ change the cost function on the state of E_{bat} is shown in Figure 5.21.



).pdf

Figure 5.21: The figure on the left shows the representation of Equation 4.10. Additional costs are only made when the state exceeds one of the green lines. Only if the red line is exceeded the model becomes infeasible. The figure on the right represents Equation 5.8, using the added $E_{bat,lim}^{(+/-)}$. Adding $E_{bat,lim}^{(+/-)}$ to Equations 5.8a and 5.8b narrows the bandwidth of E_{bat} with zero cost. Equations 5.8c and 5.8d are added to prevent the operational range from decreasing. The battery state is still feasible between 5% and 95% of its capacity.

The capacity of $E_{bat,lim}^{(+/-)}$ is set to 2,5. This number is picked as this is the maximum charging/discharging rate in 15 minutes. After replacing the old constraints, the increase in (dis)charging capacity is shown in Figure 5.22.

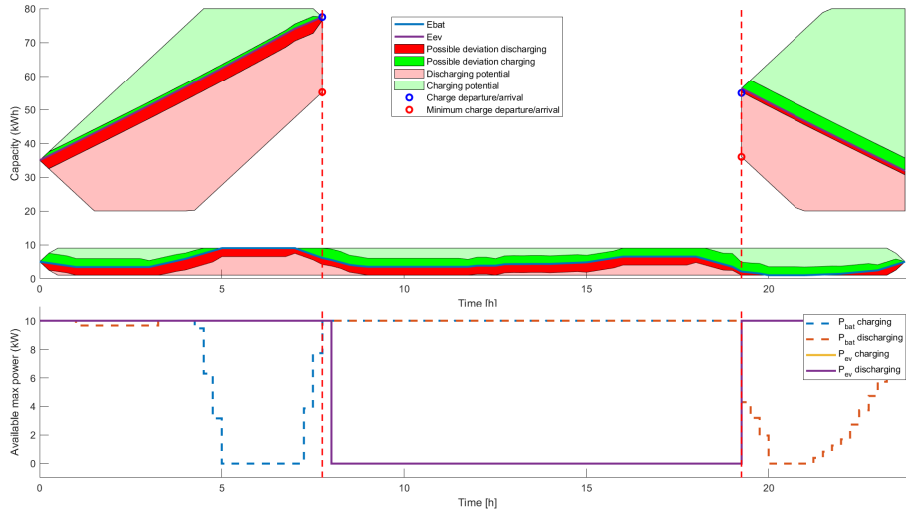


Figure 5.22: Using the $E_{bat,lim}^{(+/-)}$ constraint, the EMS has reserved battery capacity in E_{bat} , resulting in the maximal (dis)charging potential.

The new variables of $E_{bat,lim}^{(+/-)}$ are added to the cost. The new cost function is:

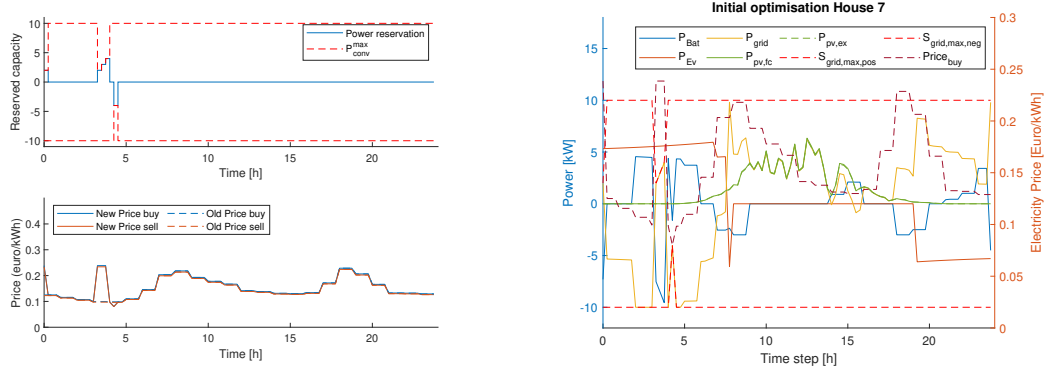
$$C_{bat,lim} = \alpha_6 \sum_{k=1}^N E_{bat,lim}^{(+)} + \alpha_7 \sum_{k=1}^N E_{bat,lim}^{(-)} \quad (5.9a)$$

$$C_{total} = C_{grid} + C_{bat} + C_{ev} + C_{pv} + C_{tot,soft} + C_{bat,lim} \quad (5.9b)$$

where α_6 and α_7 is an arbitrarily large number.

5.4. Power Reservation

Besides prevention and correction, the DSO might use the distribution network for load balancing and tertiary frequency control. This can be achieved by enabling requests for power exchange between the DSO and EMS. To promote this exchange, the same price mechanism is used as in the previous section. As time slot k_{res} can be reserved, all houses, with the corresponding wanted power exchange P_{res} , as shown in Figure 5.19. The voltage profile is checked whether or not it is feasible. If it is possible, the capacity is reserved. Figure 5.23 shows the price alterations and the corresponding influence on the optimal control inputs.



(a) The top figure shows the reservation of energy P_{res} and the corresponding constraints necessary to prevent additional energy export or import. The bottom figure shows the adjusted prices.

(b) The corresponding impact of the power reservation on the optimal control inputs.

Figure 5.23: The power reservation and price correction (left) and the resulting optimal power control inputs (right).

6

Reference tracking and real-time control

In the previous chapters, the focus is primarily on preventing and correcting voltage deviations based on user inputs, forecasts and record data. However, due to the intermittent nature of the load demand and PV generation, voltage deviations are still possible. These deviations caused by random influences have to be corrected in real-time. Firstly, in Section 6.1, the control structure, the type of errors and the need for a real-time controller are explained. Secondly, in Section 6.2, the reference tracker is presented. Lastly, In Section 6.3, the real-time controller is discussed.

6.1. Need for real-time control

In Chapter 4, the EMS of the multi-port converter is introduced, and the top-layer optimal charging algorithm is discussed. The two lower controllers of the EMS are briefly mentioned and consists of a reference tracker and real-time controller. They are positioned between the optimal charging algorithm and the multi-port converter, as shown in Figure 6.1.

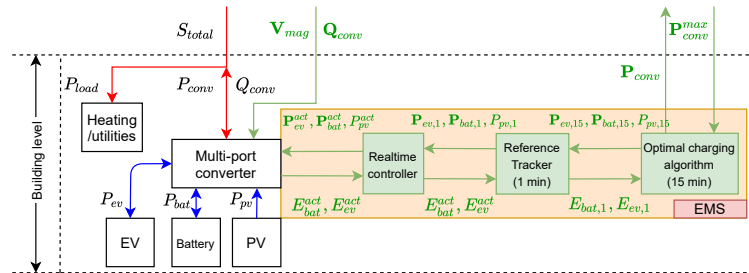


Figure 6.1: The EMS structure and the corresponding data exchange between the EMS layers. The red lines show the AC power flow while the blue is DC. Lines with arrows at both ends are a bidirectional electricity flow, and a single arrow represents uni-directional flow. The green blocks are the controllers, and the green lines are the corresponding data outputs/inputs.

These controllers have the task to control the multi-port controller on a small time scale (1 min to real-time). They are needed to prevent the negative effect of forecast errors.

In this distribution network, two types of error influence the voltage profile. These are the error in load and the error in PV generation. Their influence on voltage sway and voltage sag are shown in Figure 6.2

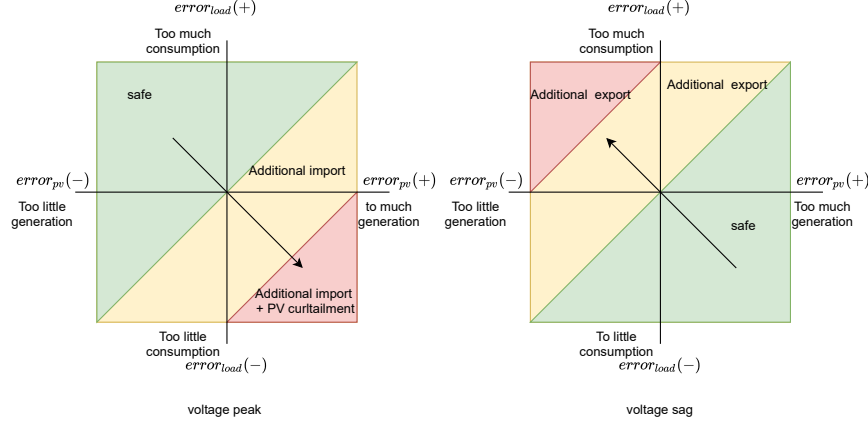


Figure 6.2: This figure shows the potential problem areas for an overvoltage (voltage peak) and a undervoltage (voltage sag) and the corresponding action needed by the multi-port converter.

A difference between the PV and load is that the error of the PV only occurs during a limited time (from sunrise to sunset) and varying error range (during peak hour, a significant error can occur, during the evening, only a small one). A second difference is that the PV can be regulated in the multi-port converter by changing the efficiency in the maximum power point tracker or storing energy in the BESS. A variation in load can only be compensated by limiting the amount of power the multi-port converter imports or exports.

The real-time controller plays a vital role in keeping the distribution network controllable and safe. These are especially important when only a part of the distribution network has a multi-port converter.

6.2. Reference tracker

The reference tracker keeps the battery state $E_{bat,1min}$ close to the value of the optimal charging algorithm $E_{bat,15min}$. This is needed because the battery can quickly drain or fill up during high forecast errors. If this happens, the battery can no longer be used for system support and will lead to possible voltage violations.

The Reference tracker is almost identical to the optimal charge algorithm. It has the same PV, EV, energy balance, and battery degradation models, but it does have a different prediction horizon. The prediction horizon of the reference tracker is set to 120 (2 hours) to have a large horizon but a computation time of less than a second. All the limitations (e.g. $P_{conv,impl}^{max}$) are still upheld but now span 15-time steps instead of 1. To cope with the shorter time interval, the capacity constraints (Equations 4.8, 4.9, and 4.15) and the departure charge (Equation 4.14e) are removed. The final value $E_{bat,1min,final}$ and $E_{ev,1min,final}$ are set equal to the expected value of $E_{bat,15min}$ and $E_{ev,15min}$ at that time step.

The main goal of the reference tracker is to stay close to the original state charge $E_{bat,15min}$. The reference tracker of the state variable is implemented as:

$$E_{bat,1min}(k) \geq E_{bat,15min}(k) - E_{bat,np}^{(-)}(k) - E_{bat,dev}^{(-)}(k) \quad , \forall k \quad (6.1a)$$

$$E_{bat,1min}(k) \leq E_{bat,15min}(k) + E_{bat,np}^{(+)}(k) + E_{bat,dev}^{(+)}(k) \quad , \forall k \quad (6.1b)$$

$$E_{bat,dev}^{(-)}(k) \leq E_{bat,15min}(k) - 1 - E_{bat,np}^{(-)}(k) \quad , \forall k \quad (6.1c)$$

$$E_{bat,dev}^{(+)}(k) \leq 10 - E_{bat,15min}(k) - E_{bat,np}^{(+)}(k) \quad , \forall k \quad (6.1d)$$

$$E_{bat,dev}^{(-)}(k) \geq 0 \quad , \forall k \quad (6.1e)$$

$$E_{bat,dev}^{(+)}(k) \geq 0 \quad , \forall k \quad (6.1f)$$

$E_{bat,15min}$ is the state value computed by the optimal charging algorithm, $E_{bat,1min}$ is the state value of the reference tracker. $E_{bat,np}^{(+/-)}$ is the value which $E_{bat,1min}$ may deviate from $E_{bat,15min}$ with no additional cost. $E_{bat,dev}^{(+/-)}$ is the added cost for deviation from $E_{bat,15min}$. The difference between $E_{bat,np}^{(+/-)}$ and $E_{bat,dev}^{(+/-)}$ is shown in Figure 6.3.

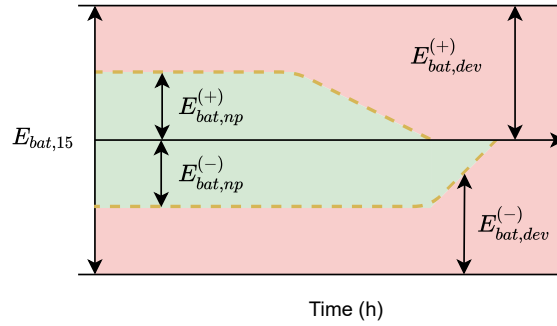


Figure 6.3: The figure represents Equation 6.1 and shows the cost for deviation of $E_{bat,15min}$ over time. When $E_{bat,1min}$ stays within the green area $E_{bat,np}^{(+)}$, no penalty is attached to the reference tracker.

$E_{bat,dev}^{(+/-)}$ is added to the cost function and formulated as:

$$C_{dev} = \sum_{k=1}^{N_{1min}} \alpha_8 E_{bat,dev}^{(+)}(k) + \sum_{k=1}^{N_{1min}} \alpha_9 E_{bat,dev}^{(-)}(k) + \sum_{k=1}^{N_{1min}} \alpha_{10} E_{ev,dev}^{(+)}(k) + \sum_{k=1}^{N_{1min}} \alpha_{11} E_{ev,dev}^{(-)}(k) \quad , \forall k \quad (6.2)$$

where α_{8-11} is an arbitrary big number, C_{dev} is the cost for deviating of $E_{bat,15min}$, and N_{1min} is the prediction horizon of the reference tracker. Although $E_{np}^{(+/-)}$ can be set to a high value, this could lead to strong deviation of $E_{bat,1min}$ and may cause harm in the long run.

Figure 6.4 shows an example of the moving horizon window with the reference tracker. It shows that even though P_{bat} varies to remove the forecast error, the battery charge is hardly impacted due to the reference tracker.

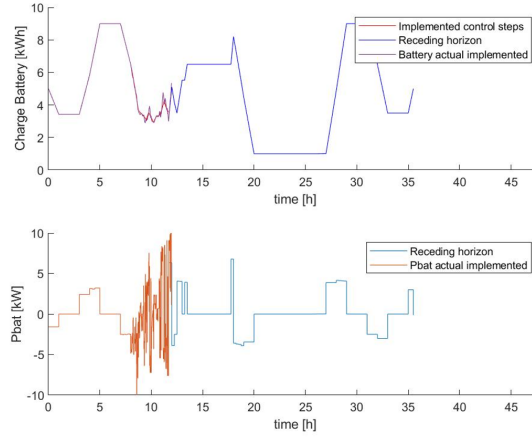


Figure 6.4: This figure shows the performance of the reference tracking. Even if the P_{bat} deviates strong, only a minimal deviation of E_{bat} has occurred.

6.3. Real-time controller

The real-time controller is the controller closest to the multi-port converter. It is responsible for the energy balance in the multi-port converter and the removal of load and PV errors. The DC and AC energy balance of the multi-port converter are:

$$P_{conv}(k) = P_{pv} - P_{bat}(k) - P_{ev}(k) \quad , \forall k \quad (6.3a)$$

$$P_{grid}(k) = P_{conv}(k) - P_{load}(k) \quad , \forall k \quad (6.3b)$$

There are two possible ways these balances in Equation 6.3 can be disrupted. These are a variation in load (ΔP_{load}) and PV generation (ΔP_{pv}). Both are expected in a residential area. To accommodate these errors, the equations change to:

$$P_{conv}(k) + \Delta P_{conv}(k) = P_{pv}(k) + \Delta P_{pv}(k) - P_{bat}(k) + \Delta P_{bat}(k) - P_{ev}(k) + \Delta P_{ev}(k) \quad , \forall k \quad (6.4a)$$

$$P_{grid}(k) = P_{conv}(k) + \Delta P_{conv}(k) - P_{load}(k) + \Delta P_{load}(k) \quad , \forall k \quad (6.4b)$$

The operation of the real-time controller has been divided into three sectors. These are normal operation (sector 1), a possible overvoltage (Sector 2) or a possible undervoltage (sector 3). The operational conditions are shown in Table 6.1.

Table 6.1: An overview of the Hazards that the real-time controller can face and the conditions needed for a particular sector.

Sector	Threat	Operational condition
1	None	-
2	Overvoltage	$\max(V^{mag}(k)) \geq 1.07$ p.u. or $P_{pv}^{max}(k) - P_{pv,fc}(k) > P_{cap,imp}(k)$
3	Undervoltage	$\min(V^{mag}(k)) \leq 0.92$ p.u.

$P_{pv}^{max}(k)$ is the maximum PV generation over the last 15 day period. $P_{cap,ex}(k)$ and $P_{cap,imp}(k)$ are the maximum power capacities that every multi-port converter additionally can export or import at time step k to reach one of the voltage limits, as shown in Figure 6.5.

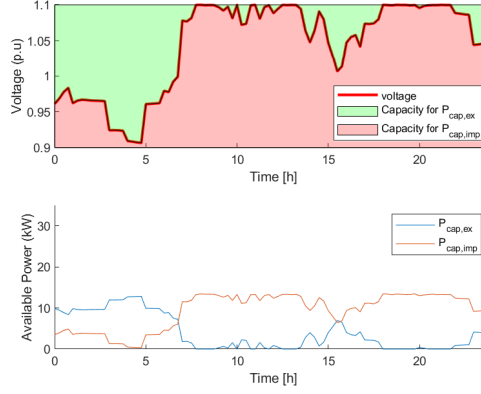
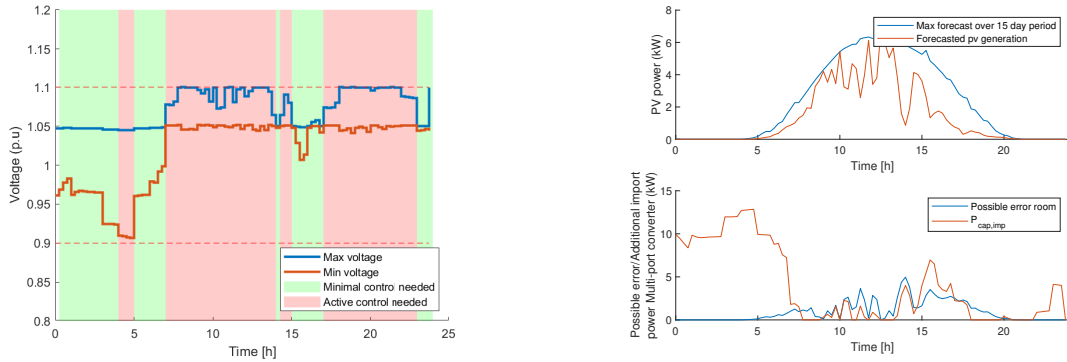


Figure 6.5: This figure shows the reserve capacity available in the network. The top figure shows that if the voltage is high, no energy can be exported, and if the voltage is at a minimum, no additional energy can be imported. The bottom figure shows the amount of power each multi-port converter can import or feed in at that time step. The amount of available power is dependant on the amount of multi-port converters in the distribution network.

Figure 6.6a shows when real-time control is needed, based on Table 6.1. Sector 2 is determined if the maximum voltage is above 1.07 p.u. when no PV occurs. When PV occurs, the forecast is compared with the maximum generation possibility and the possible import capability of the converter, as shown in Figure 6.6b.



(a) This figure shows when active control is needed in the real-time controller to prevent hazards. Based on the operational conditions in Table 6.1 and the PV generation and possible generation compared to the available capacity of the multi-port converter P_{conv} from Figure 6.6b. It can be determined whether or not minimal control actions are needed

(b) This figure shows the possible change in the operational condition of Sector 2 in Table 6.1. It can be seen that at 15:00 hours, no active control is needed due to having a larger capacity available, resulting in the green part in Figure 6.6a.

Figure 6.6: Figure 6.6a shows when the real-time controller is in either Sector 1 or a potential hazard has occurred. Figure 6.6b shows one of the operational conditions for Sector 2 from Table 6.1.

If there are fewer multi-port converters in the network, it has to compensate by importing additional energy from the distribution network if there is an overproduction of energy ($\Delta P_{pv} > 0$).

Assuming that the multi-port converters are spread at random, this ratio can be determined as:

$$r_{pv} = \frac{\sum P_{pvfc,mult}}{\sum P_{pvfc,houses}} \quad (6.5)$$

where $P_{pvfc,mult}$ is the expected generation of PV by multi-port converters, and $P_{pvfc,houses}$ is the total generation of PV in the distribution network.

To compensate for the people who do not have a multi-port, the error in the network, caused by PV is:

$$\Delta P_{pv,error}(k) = r_{pv}(P_{pvfc}(k) - P_{pv,act}(k)) \quad (6.6)$$

The generation of PV has a high correlation: if the error is positive at the house, it is assumed to be positive at the neighbours house due to the limit size of the distribution network. Unfortunately, the load error can not be compensated, as you do not know the energy consumption of the neighbours. This means that the error for the load remains at:

$$\Delta P_{load,error}(k) = P_{load,fc}(k) - P_{load,act}(k) \quad (6.7)$$

To remove the total error from the distribution network and keep a stable voltage profile, Equation 6.6 and 6.7 are combined to:

$$\Delta P_{total,error}(k) = \Delta P_{pv,error}(k) - \Delta P_{load,error}(k) \quad (6.8)$$

6.3.1. Capacity availability

To be able to correct errors, (dis)charging capacity is needed in the multi-port converter. This capacity in the converters of the system is determined as:

$$P_{conv,bat,dis}^{max} = \max(0, \min(P_{bat}^{max}, P_{bat,dis}^{max}, P_{conv}^{max} - P_{pv} + \Delta P_{pv} + P_{ev})) \quad (6.9a)$$

$$P_{conv,bat,ch}^{max} = \max(0, \min(P_{bat}^{max}, P_{bat,ch}^{max}, P_{conv}^{max} + P_{pv} + \Delta P_{pv} - P_{ev})) \quad (6.9b)$$

$$P_{conv,ev,dis}^{max} = \max(0, \min(P_{ev}^{max}, P_{ev,dis}^{max}, P_{conv}^{max} - P_{pv} + \Delta P_{pv} + P_{bat})) \quad (6.9c)$$

$$P_{conv,ev,ch}^{max} = \max(0, \min(P_{ev}^{max}, P_{ev,ch}^{max}, P_{conv}^{max} + P_{pv} + \Delta P_{pv} - P_{bat})) \quad (6.9d)$$

$$P_{conv,conv,ex}^{max} = \min(P_{cap,ex}, P_{conv}^{max} - P_{conv}) \quad (6.9e)$$

$$P_{conv,conv,imp}^{max} = \min(P_{cap,imp}, P_{conv}^{max} + P_{conv}) \quad (6.9f)$$

$$P_{conv,pv,res} = P_{pv,fc} + \Delta P_{pv} \quad (6.9g)$$

Here, ΔP_{pv} is the error of the generated PV in the multi-port converter. $P_{conv,bat,ch/dis}^{max}$, $P_{conv,ev,ch/dis}^{max}$ and $P_{conv,conv,ex/imp}^{max}$ are the remaining capacities of the converters. If e.g. $P_{ev} = 4\text{ kW}$ and no PV generation occurs, $P_{conv,bat,ch}^{max}$ can only be 6 kW as it is limited by the maximum amount of energy the multi-port converter can import. $P_{bat,dis}^{max}$, $P_{bat,ch}^{max}$, $P_{ev,dis}^{max}$ and $P_{ev,ch}^{max}$ are computed as:

$$P_{bat,dis}^{max} = \max(0, \min(10, E_{bat} - E_{bat}^{min} / \Delta t)) \quad (6.10a)$$

$$P_{bat,ch}^{max} = \max(0, \min(10, E_{bat}^{max} - E_{bat} / \Delta t)) \quad (6.10b)$$

$$P_{ev,dis}^{max} = \max(0, \min(10, E_{ev} - E_{ev}^{min} / \Delta t)) \quad (6.10c)$$

$$P_{ev,ch}^{max} = \max(0, \min(10, E_{ev}^{max} - E_{ev} / \Delta t)) \quad (6.10d)$$

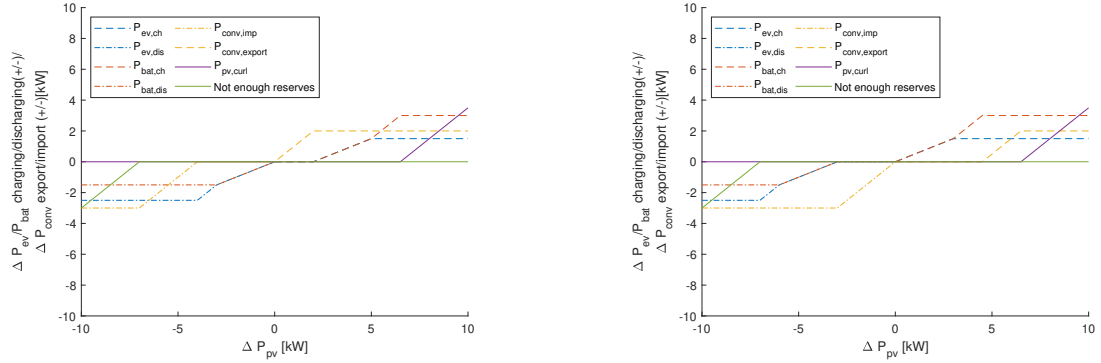
Here, the values of $E_{bat}^{max/min}$ and $E_{ev}^{max/min}$ are described in Sections 4.3.2 and 4.3.3. Due to the capacity reservation in Section 5.3, the value of $P_{bat,dis}^{max}$ and $P_{bat,ch}^{max}$ is always 10 kW if the EV is not available.

6.3.2. Sector 1 (no hazard)

Sector 1 is the scenario where no disruption of load or PV could cause significant harm to the voltage level. In this scenario, ΔP_{load} is not compensated (Equation 6.7), and the sole purpose of the real-time controller is to provide the energy balance (Equation 6.3a). Furthermore, the ratio determined in Equation 6.5 is set to 1 to limit buying and selling of energy. Although the real-time controller only provides an energy balance in this scenario, economic benefits can be obtained. If energy is expensive, the real-time controller prefers selling additional PV power ($\Delta P_{pv} > 0$) over storing it in the battery. Similar when too little is

generated ($\Delta P_{pv} < 0$) and the price is high, the battery can be discharged (or reduce charging) instead of importing additional energy. An overview of the buying strategy and its equations are shown in Figure 6.7 and Equation 6.12. The decision-making process is based on the average price of the time interval:

$$\lambda_{avg} = \frac{\sum_{k=1}^N \lambda_{buy}(k)}{N} \quad (6.11)$$



(a) Control outputs if $\lambda_{buy} > \lambda_{avg}$. The real-time controller wants to sell its additional generated energy by PV as the price is high. If $\Delta P_{pv,error}$ is negative, it tries to decrease charging of the EV and BESS instead of buying the energy.

(b) Control outputs if $\lambda_{buy} < \lambda_{avg}$. The real-time controller stores a surplus of PV energy, as selling it is less profitable. If too little is generated, buying additional power from the network is cheaper.

Figure 6.7: The corresponding control inputs based on $\Delta P_{pv,error}$ and the energy price are shown. The limitations on the y-axis are to demonstrate the possible limitations as set by equation 6.9. Furthermore, in both situations, the EV is assumed to be connected.

Figure 6.7a shows the situation when it is expensive to buy electricity and profitable to sell energy. The real-time controller acts accordingly by preferring selling energy at an energy surplus instead of storing it. It only starts storing energy when $P_{conv,conv,ex}^{max}$ is exceeded. If no adequate storage capacity is available or is already full, the system results in its final resort by curtailing the amount of PV generated. In the situation that there is less generated energy, the real-time controller prefers (dis)charging (or reduced charging) the BESS before importing additional power. Figure 6.7b shows the situation when it is cheap to buy electricity. As shown in the figure, it is precisely the opposite of Figure 6.7a.

The left part of Figure 6.7a ($\Delta P_{pv} < 0$) and the right part of Figure 6.7b ($\Delta P_{pv} > 0$) can be described by the following equations:

$$\Delta P_{ev} = \text{sign}(\Delta P_{total,error}) \max(\min(|\alpha \Delta P_{total,error}|, P_{conv,ev,res}), \min(|\Delta P_{total,error}| - \min(|\beta \Delta P_{total,error}|), P_{conv,bat,res}), P_{conv,ev,res}) \quad (6.12a)$$

$$\Delta P_{bat} = \text{sign}(\Delta P_{total,error}) \max(\min(|\beta \Delta P_{total,error}|, P_{conv,bat,res}), \min(|\Delta P_{total,error}| - \min(|\alpha \Delta P_{total,error}|, P_{conv,ev,res}), P_{conv,bat,res}) \quad (6.12b)$$

$$\Delta P_{conv} = \min(\max(\Delta P_{total,error} - \Delta P_{ev} - \Delta P_{bat}, -P_{conv,conv,res}), P_{conv,conv,res}) \quad (6.12c)$$

$$P_{pv,curt} = \min(\max(\Delta P_{total,error} - \Delta P_{conv} - \Delta P_{bat} - \Delta P_{ev}, 0), P_{conv,pv,res}) \quad (6.12d)$$

Here, sign is defined as:

$$\text{sign}(x) \begin{cases} 1, & \text{if } x > 0 \\ 0, & \text{if } x = 0 \\ -1, & \text{if } x < 0 \end{cases} \quad (6.13)$$

α and β values are determined by the availability of the EV for charging/discharging. α and β are formulated as:

$$\alpha = \begin{cases} 0.5 & , EV_{availability} = 1 \\ 1 & , EV_{availability} = 0 \end{cases} \quad (6.14)$$

$$\beta = 1 - \alpha$$

Furthermore, when the EV is not available ($\beta = 0$) ΔP_{ev} is automatically set to zero, and lastly:

$$P_{conv,ev,res} = \begin{cases} P_{conv,ev,ch}^{max} & , \text{if } P_{total,error} > 0 \text{ and } Sector \neq 3 \\ P_{conv,ev,dis}^{max} & , \text{otherwise} \end{cases} \quad (6.15a)$$

$$P_{conv,bat,res} = \begin{cases} P_{conv,bat,ch}^{max} & , \text{if } P_{total,error} > 0 \text{ and } Sector \neq 3 \\ P_{conv,bat,dis}^{max} & , \text{otherwise} \end{cases} \quad (6.15b)$$

$$P_{conv,conv,res} = \begin{cases} P_{conv,conv,imp}^{max} & , \text{if } P_{total,error} > 0 \text{ and } Sector \neq 3 \\ P_{conv,conv,ex}^{max} & , \text{if } \Delta P_{load,error} > 0 \\ P_{conv,conv,ex}^{max} + \Delta P_{load,error} & , \text{otherwise} \end{cases} \quad (6.15c)$$

These are added to provide the correct maximum charging and keeping the formulas compact.

The left part of Figure 6.7a ($\Delta P_{pv} < 0$) and the right part of Figure 6.7b ($\Delta P_{pv} > 0$) is defined as:

$$\Delta P_{conv} = \text{sign}(\Delta P_{total,error}) \max(\min(|\Delta P_{total,error}|, P_{conv,conv,res}), \min(|\Delta P_{total,error}| - \min(|\Delta P_{total,error}|, P_{conv,conv,res}), P_{conv,conv,res})) \quad (6.16a)$$

Now the remaining part of the function can be split into two modes. The first where the capacity of $P_{conv,ev,res} < P_{conv,bat,res}$:

$$\Delta P_{ev} = \text{sign}(\Delta P_{total,error}) \min(|\alpha(\Delta P_{total,error} - \Delta P_{conv})|, P_{conv,ev,res}) \quad (6.16b)$$

$$\Delta P_{bat} = \begin{cases} \text{sign}(\Delta P_{total,error}) \min(|\beta(\Delta P_{total,error} - \Delta P_{conv})|, P_{conv,bat,res}) & , \text{if } \Delta P_{ev} \neq \text{sign}(\Delta P_{total,error}) P_{conv,ev,res} \\ \text{sign}(\Delta P_{total,error}) \min(|(\Delta P_{total,error} - \Delta P_{conv}) - \Delta P_{ev}|, P_{conv,bat,res}) & , \text{if } \Delta P_{ev} = \text{sign}(\Delta P_{total,error}) P_{conv,ev,res} \end{cases} \quad (6.16c)$$

and the second when $P_{conv,ev,res} \geq P_{conv,bat,res}$:

$$\Delta P_{bat} = \text{sign}(\Delta P_{total,error}) \min(|\beta(\Delta P_{total,error} - \Delta P_{conv})|, P_{conv,bat,res}) \quad (6.16d)$$

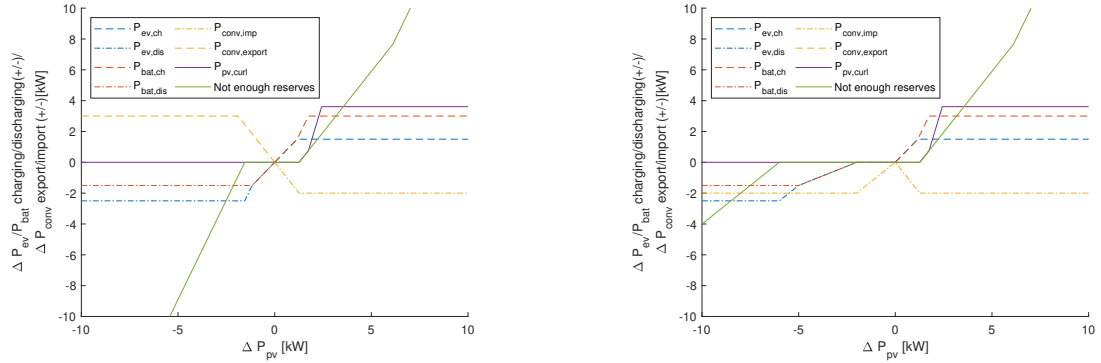
$$\Delta P_{ev} = \begin{cases} \text{sign}(\Delta P_{total,error}) \min(|\alpha(\Delta P_{total,error} - \Delta P_{conv})|, P_{conv,ev,res}) & , \text{if } \Delta P_{bat} \neq \text{sign}(\Delta P_{total,error}) P_{conv,bat,res} \\ \text{sign}(\Delta P_{total,error}) \min(|(\Delta P_{total,error} - \Delta P_{conv}) - \Delta P_{bat}|, P_{conv,ev,res}) & , \text{if } \Delta P_{bat} = \text{sign}(\Delta P_{total,error}) P_{conv,bat,res} \end{cases} \quad (6.16e)$$

And the $P_{pv,cur1}$ can be defined as:

$$P_{pv,cur1} = \min(\max(\Delta P_{total,error} - \Delta P_{conv} - \Delta P_{ev} - \Delta P_{bat}, 0), P_{conv,pv,res}) \quad (6.16f)$$

6.3.3. Sector 2 (Overvoltage hazard)

In Sector 2, the real-time controller has to prevent a possible overvoltage. The $\Delta P_{total,error}$ from Equation 6.8 is used, taking in the ΔP_{load} from Equation 6.7 and ΔP_{pv} with ratio from Equation 6.6. This means the real-time controller in an overvoltage situation has to compensate for their own load and for the generation of PV without a multi-port converter. Figure 6.8 shows the control inputs in the situation where an overvoltage can occur.



(a) Control outputs if $\lambda_{buy} > \lambda_{avg}$ and $\Delta P_{load} = 0$. Additional power is imported to prevent voltage violations caused by uncontrolled PV systems in the distribution network.

(b) Control outputs if $\lambda_{buy} < \lambda_{avg}$ and $\Delta P_{load} = 0$. If a positive error occurs ($\Delta P_{pv} > 0$) additional power is still imported. However due to the low price, if the PV error is negative, additional energy can be bought.

Figure 6.8: These figures show the control outputs of Sector 2 based on the difference between the forecast and actual generation. The limitations on the y-axis are to demonstrate the possible limitations as set by equation 6.9. Furthermore, in both situations, the EV is assumed to be connected. In this case, the chosen ratio is 2.58

Figure 6.8a shows the situation where buying energy is expensive. In contrast to Sector 1, the real-time controller has to purchase power when an error occurs to remove the additional energy from PV panels without a multi-port converter. An illustrative example is given in Figure 6.9. The amount needed for this import is:

$$\Delta P_{conv} = \Delta P_{total,error} - \Delta P_{pv} \quad (6.17)$$

Figure 6.8b shows the situation when the energy is cheaper than average. When a surplus of PV occurs, the control inputs behave the same as in Figure 6.8a. When the PV error is negative the real-time controller will buy power. This would lead, in reality, to a decrease in discharging of batteries. As a protective measure, if the battery is near the limits, the situation returns to Figure 6.8a.

To obtain Figure 6.8, the following equations have been made for Figure 6.8a and the right part ($\Delta P_{pv} > 0$) of Figure 6.8b. The dynamics can be written as:

$$\Delta P_{ev} = \text{sign}(\Delta P_{total,error}) \max(\min(|\alpha \Delta P_{total,error}|, P_{conv,ev,res}), \min(|\Delta P_{total,error}| - \min(|\beta \Delta P_{total,error}|), P_{conv,bat,res}), P_{conv,ev,res}) \quad (6.18a)$$

$$\Delta P_{bat} = \text{sign}(\Delta P_{total,error}) \max(\min(|\beta \Delta P_{total,error}|, P_{conv,bat,res}), \min(|\Delta P_{total,error}| - \min(|\alpha \Delta P_{total,error}|, P_{conv,ev,res}), P_{conv,bat,res}) \quad (6.18b)$$

$$\Delta P_{conv} = \min(\max(\Delta P_{pv} - \Delta P_{total,error}, -P_{conv,conv,res}) P_{conv,conv,res}) \quad (6.18c)$$

$$P_{pv,curl} = \max(\min(\Delta P_{total,error} - \Delta P_{ev} - \Delta P_{bat} + (\Delta P_{total,error} - \Delta P_{pv} + \Delta P_{conv}), P_{conv,pv,res}), 0) \quad (6.18d)$$

Equations 6.18a and 6.18b are the same as Equations 6.12a and 6.12b in Sector 1. Equations 6.18c till 6.18d are altered to buy and sell additional power to prevent voltage violations in the distribution network.

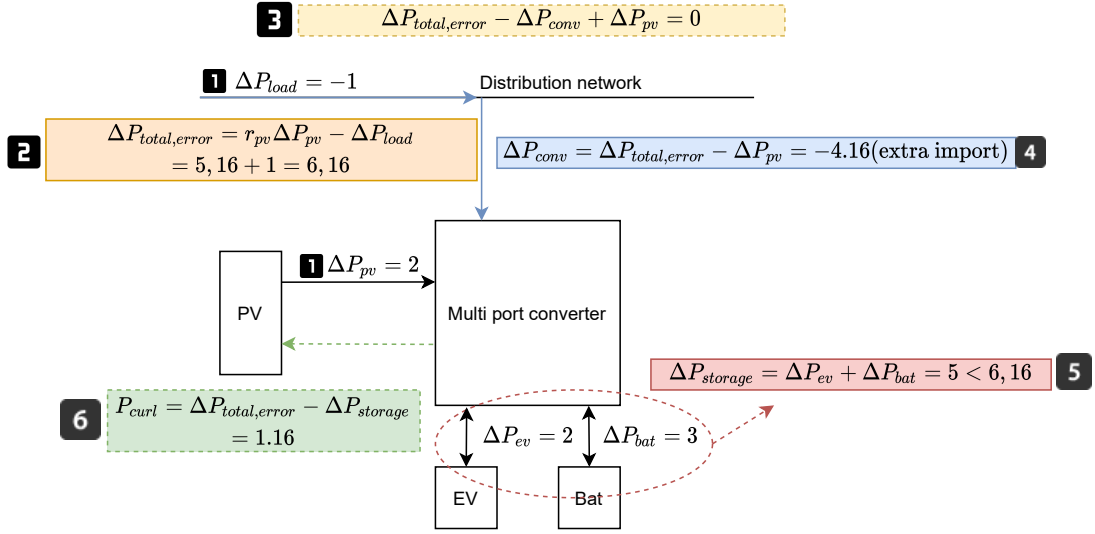


Figure 6.9: This figure shows which actions are taken to prevent voltage violations. Based on the surplus generated by the PV, measures have to be considered. Based on the ratio of 2.58 a total of 5.16 kW PV power needs to be compensated. Combined with the load error a total of 6.16 kW needs to be compensated. A part of the 6.16 kW is the surplus generated by the PV in the multi-port converter. This generation does not require additional import of power. The remaining capacity can be calculated using Equation 6.17. The energy is stored in BESS and (if possible) EV. In the figure, their capacity limit is reached. Therefore, the additional power needs to be curtailed by the PV.

To obtain the left part of Figure 6.8b ($\lambda_{buy} < \lambda_{avg}, \Delta P_{total,error} < 0$), the following equations have been used:

$$\Delta P_{conv} = \text{sign}(\Delta P_{total,error}) \max(\min(|\Delta P_{pv}|, P_{conv,max,imp}), \min(|\Delta P_{pv}| - \min(|\Delta P_{pv}|, P_{conv,max,imp}), P_{conv,max,imp})) \quad (6.19a)$$

where in this case, the edge cases $P_{conv,max,imp}$ are already filled in (instead of Equation 6.15).

Similar as in Equation 6.16 there are two sections. The first where the capacity of $P_{conv,ev,res} < P_{conv,bat,res}$:

$$\begin{aligned} \Delta P_{ev} &= \text{sign}(\Delta P_{pv}) \min(|\alpha(\Delta P_{pv} - \Delta P_{conv})|, P_{conv,ev,res}) \quad (6.19b) \\ \Delta P_{bat} &= \begin{cases} \text{sign}(\Delta P_{pv}) \min(|\beta(\Delta P_{pv} - \Delta P_{conv})|, P_{conv,bat,res}), & \text{if } \Delta P_{ev} \neq \text{sign}(\Delta P_{pv}) P_{conv,ev,res} \\ \text{sign}(\Delta P_{pv}) \min(|(\Delta P_{pv} - \Delta P_{conv}) - \Delta P_{ev}|, P_{conv,bat,res}), & \text{if } \Delta P_{ev} = \text{sign}(\Delta P_{pv}) P_{conv,ev,res} \end{cases} \quad (6.19c) \end{aligned}$$

and the second when $P_{conv,ev,res} \geq P_{conv,bat,res}$:

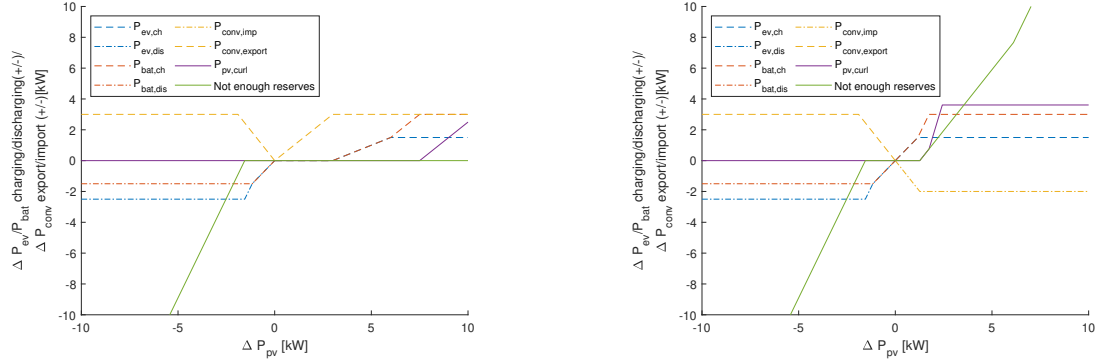
$$\begin{aligned} \Delta P_{bat} &= \text{sign}(\Delta P_{pv}) \min(|\beta(\Delta P_{pv} - \Delta P_{conv})|, P_{conv,bat,res}) \quad (6.19d) \\ \Delta P_{ev} &= \begin{cases} \text{sign}(\Delta P_{pv}) \min(|\alpha(\Delta P_{pv} - \Delta P_{conv})|, P_{conv,ev,res}), & \text{if } \Delta P_{bat} \neq \text{sign}(\Delta P_{pv}) P_{conv,bat,res} \\ \text{sign}(\Delta P_{pv}) \min(|(\Delta P_{pv} - \Delta P_{conv}) - \Delta P_{bat}|, P_{conv,ev,res}), & \text{if } \Delta P_{bat} = \text{sign}(\Delta P_{pv}) P_{conv,bat,res} \end{cases} \quad (6.19e) \end{aligned}$$

And the $P_{pv,curt}$ can be defined as:

$$P_{pv,curt} = \min(\max(\Delta P_{pv}, -\Delta P_{conv} - \Delta P_{ev} - \Delta P_{bat}, 0), P_{conv,pv,res}) \quad (6.19f)$$

6.3.4. Sector 3 (Undervoltage hazard)

If Sector 3 is needed, an undervoltage situation has occurred, caused by a high load or a lack of PV generation.



(a) Control outputs if $\lambda_{buy} > \lambda_{avg}$ and $\Delta P_{load} = 0$. In this particular case, additional PV energy ($\Delta P_{pv} > 0$) is sold if generation is higher than expected.

(b) Control outputs if $\lambda_{buy} > \lambda_{avg}$ and $\Delta P_{load} = 0$. Additional power is exported ($\Delta P_{pv} < 0$) to prevent voltage violations.

Figure 6.10: These figures show the control outputs of Sector 3 based on the difference between the forecast and actual generation. The limitations on the y-axis are to demonstrate the possible limitations as set by equation 6.9. Furthermore, in both situations, the EV is assumed to be connected. In this case, the chosen ratio is 2.58

The left part of Figure 6.10a and Figure 6.10b are a copy of Sector 2. The corresponding equations are Equations 6.18a till 6.18d. The special case with undervoltage is shown as the right part in Figure 6.10a. As $\Delta P_{pv} > 0$ there is more generation in the network, therefore additional energy can be exported for a higher price. This is achieved by:

$$\Delta P_{conv} = \text{sign}(\Delta P_{total, error}) \max(\min(|\Delta P_{pv}|, P_{conv, max, exp}), \min(|\Delta P_{pv}| - \min(|\Delta P_{pv}|, P_{conv, max, exp}), P_{conv, max, exp}), \quad (6.20a)$$

where in this case the edge cases are already filled in instead of Equation 6.15. Similar as in Equation 6.16 there are two sections. the first where the capacity of $P_{conv, ev, res} < P_{conv, bat, res}$:

$$\Delta P_{ev} = \text{sign}(\Delta P_{pv}) \min(|\alpha(\Delta P_{pv} - \Delta P_{conv})|, P_{conv, ev, res}) \quad (6.20b)$$

$$\Delta P_{bat} = \begin{cases} \text{sign}(\Delta P_{pv}) \min(|\beta(\Delta P_{pv} - \Delta P_{conv})|, P_{conv, bat, res}), & \text{if } \Delta P_{ev} \neq \text{sign}(\Delta P_{pv}) P_{conv, ev, res} \\ \text{sign}(\Delta P_{pv}) \min(|(\Delta P_{pv} - \Delta P_{conv}) - \Delta P_{ev}|, P_{conv, bat, res}), & \text{if } \Delta P_{ev} = \text{sign}(\Delta P_{pv}) P_{conv, ev, res} \end{cases} \quad (6.20c)$$

or option two when $P_{conv, ev, res} \geq P_{conv, bat, res}$:

$$\Delta P_{bat} = \text{sign}(\Delta P_{pv}) \min(|\beta(\Delta P_{pv} - \Delta P_{conv})|, P_{conv, bat, res}) \quad (6.20d)$$

$$\Delta P_{ev} = \begin{cases} \text{sign}(\Delta P_{pv}) \min(|\alpha(\Delta P_{pv} - \Delta P_{conv})|, P_{conv, ev, res}), & \text{if } \Delta P_{bat} \neq \text{sign}(\Delta P_{pv}) P_{conv, bat, res} \\ \text{sign}(\Delta P_{pv}) \min(|(\Delta P_{pv} - \Delta P_{conv}) - \Delta P_{bat}|, P_{conv, ev, res}), & \text{if } \Delta P_{bat} = \text{sign}(\Delta P_{pv}) P_{conv, bat, res} \end{cases} \quad (6.20e)$$

And the $P_{pv, curl}$ can be defined as:

$$P_{pv, curl} = \min(\max(\Delta P_{pv}, -\Delta P_{conv} - \Delta P_{ev} - \Delta P_{bat}, 0), P_{conv, pv, res}) \quad (6.20f)$$

7

Results

In this chapter, the simulation of the correction methods Volt-Watt, Volt-VA incremental and Volt-VA sensitivity are shown. The Volt-VA method is simulated with and without power factor restriction to simulate possible future use. The simulations focus on the interaction of the EMS (optimal control inputs) and VMS (voltage deviation correction), and real-time control. The interaction between EMS and VMS uses the proposed flowchart to correct and prevent voltage violation in a distribution network, as shown in Figure 5.19. To evaluate the performance of the control scheme, varying scenarios have been picked.

This chapter starts, in Section 7.1, by explaining the selection procedure of the multi-port converters. In Sections 7.2 and 7.3, a summer and winter day with varying numbers of multi-port converters are shown. In Section 7.4, the moving horizon window results are presented.

7.1. Selection procedure

To use the ratio of Equation 6.5 the houses can not be randomly removed if the number of multi-port converters decreases. Furthermore, to repeat this experiment, a strategy for selecting the houses has been made. The houses are selected based on their sensitivity coefficient computed by the Jacobian matrix as discussed in Section 5.2.2. The selection procedure is as follow: first, the two houses with the lowest sensitivity coefficient are removed from the selection and then the house with the highest sensitivity is removed. This removal repeats until no multi-port converters are left.

7.2. Summer day

In the summer, voltage violations may occur due to the increase of PV generation. Two scenarios are picked: scenario one, where the majority (45) of the houses in the distribution network have a multi-port converter and scenario two, where the minority (20) of the houses in the distribution network have a multi-port converter. The numbers 45 and 20 have been randomly picked.

Day 185 has been chosen as a lot of PV energy is generated this day and shows a clear intermittent pattern, as shown in Figure 7.1 The forecasted amount of energy generation over a period is within 10% of the actual generation. Figure 7.2 shows the benchmark of the day. As shown, the network without a multi-port converter is insufficient to cope with the generation caused by the PV.

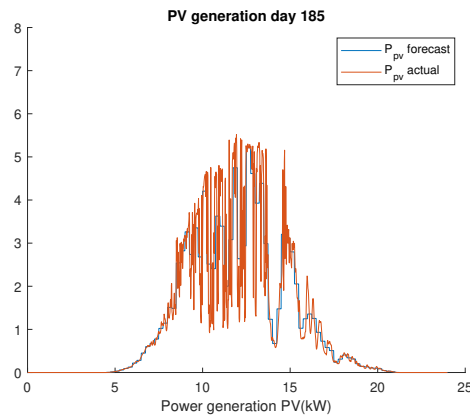


Figure 7.1: The average forecasted and actual PV profile of day 185 (summer).

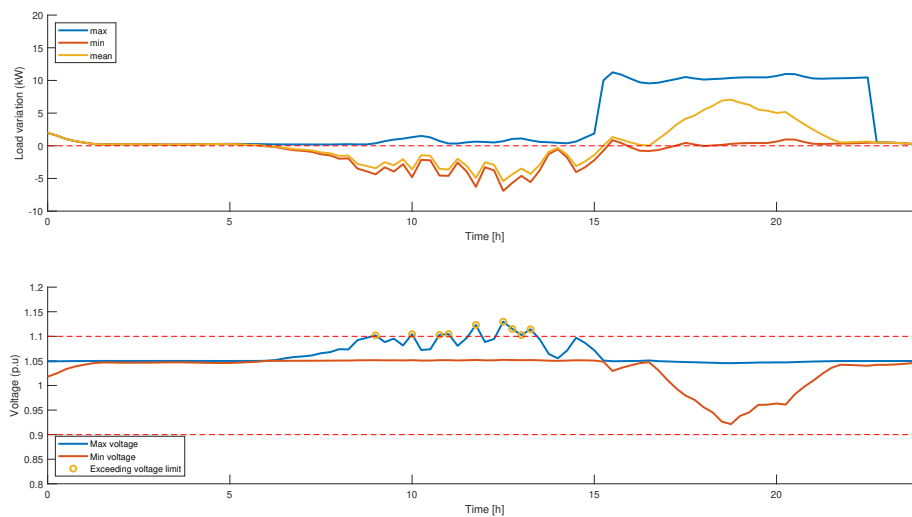


Figure 7.2: Load variation (top) and voltage profile (bottom). The load variation show a large feed-in of power between 9 AM and 3 PM, caused by PV generation, creating voltage violations.

7.2.1. Summer day with many multi-port converters (45)

Figure 7.3 shows the load variation, voltage profile and price alterations of the VMS before adding P_{conv} of the multi-port converter. This is done, as stated in Section 5.3, to prevent voltage violations in the network. The step is the "Voltage based price" in Figure 5.19. An evident decline in energy generation from 9 AM till 3 PM can be shown (PV generation) and a reduction in energy demand from 6 PM till 10 PM (EV charging). There are no voltage violations, and therefore the price does not have to change. In the remainder of the chapter, the max and min voltage of the voltage profile correspond to the maximum and minimum voltage in the entire distribution network.

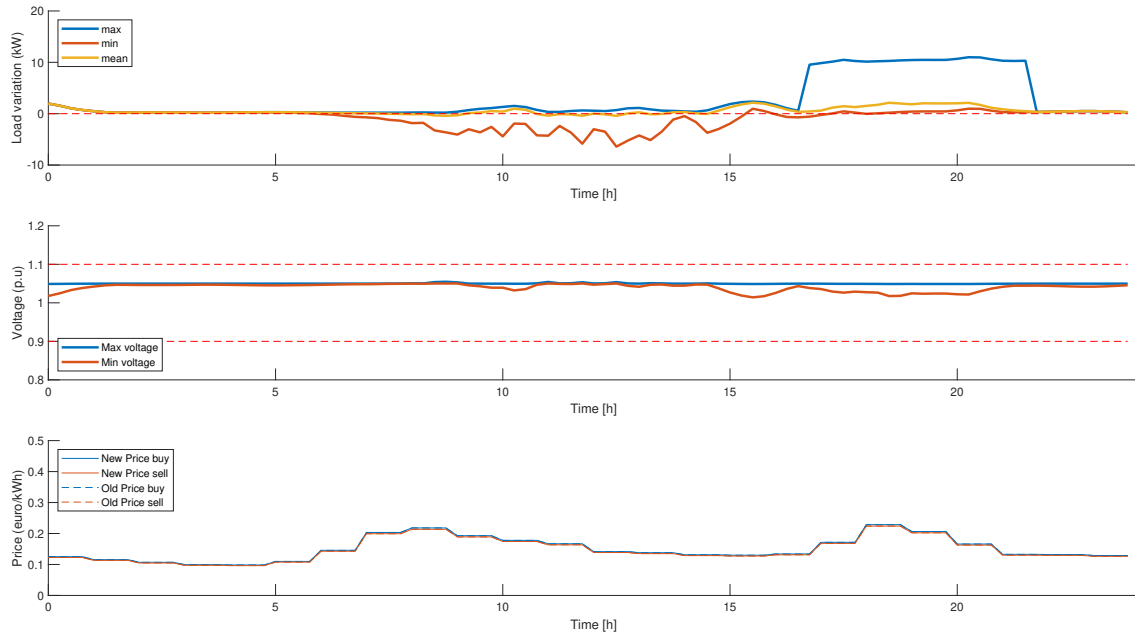


Figure 7.3: Load variation (top), voltage profile (middle), and price correction mechanism (bottom) before the multi-port converter energy demand P_{conv} is added.

Figure 7.4, shows the first iteration of the optimal charging algorithm of house number 49. This is step "EMS House" in Figure 5.19. This house has been randomly selected. No correction has taken place, therefore no variation between the correction methods are obtained.

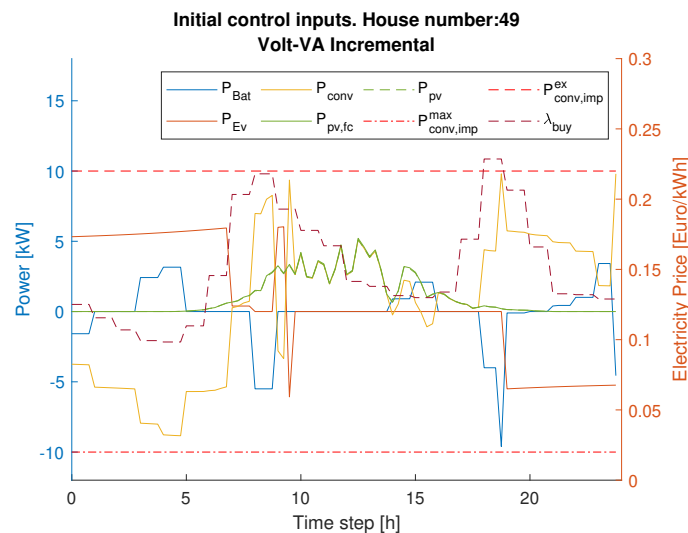


Figure 7.4: The optimal control inputs of the EMS before the correction methods are used.

The Figures 7.5 (Volt-Watt), 7.6 (Volt-VAR Incr (no pf)), 7.7 (Volt-VAR Incr (pf=0.9)), 7.8 (Volt-VAR Sens (no pf)) and 7.9 (Volt-VAR Sens (pf=0.9)) show the initial voltage violations caused by the demand of the multi-port converter. In the remainder of this chapter Volt-VA (no pf) means that no power factor restrictions have been set. If Volt-VA (pf=0.9) is mentioned, the maximum power factor is 0.9.

These figures combine the step "Voltage profile computation" and the correction method step from Figure 5.19. These figures show that by using reactive power, many of the voltage violations can be corrected. Figures 7.6 and 7.8 show an improved voltage profile over Figures 7.7 and 7.9 due to the availability of more reactive power.

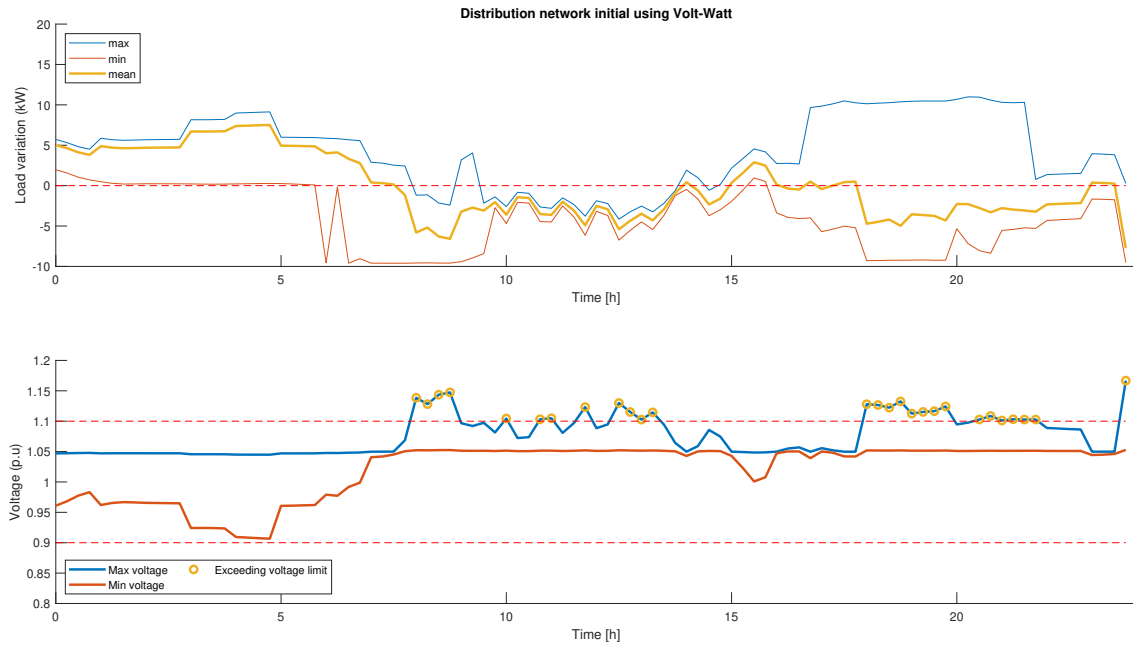


Figure 7.5: Load variation (top) and voltage profile (bottom). Initial voltage profile after adding the multi-port converter energy demand P_{conv} using the Volt-Watt method on day 185 with 45 multi-port converters.

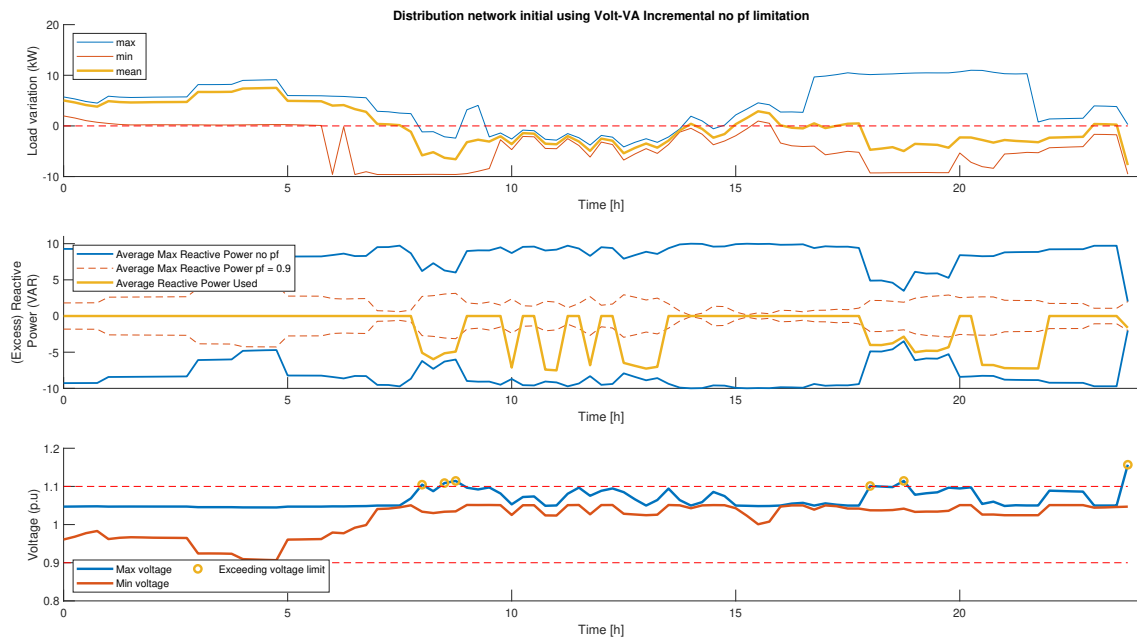


Figure 7.6: Load variation (top), reactive power usage Q_{conv} and availability Q_{conv}^{max} (middle), and voltage profile (bottom). Initial voltage profile after adding the multi-port converter energy demand P_{conv} using the Volt-VAR incremental method on day 185 with 45 multi-port converters. Reactive power compensation, with no restriction, has already been added.

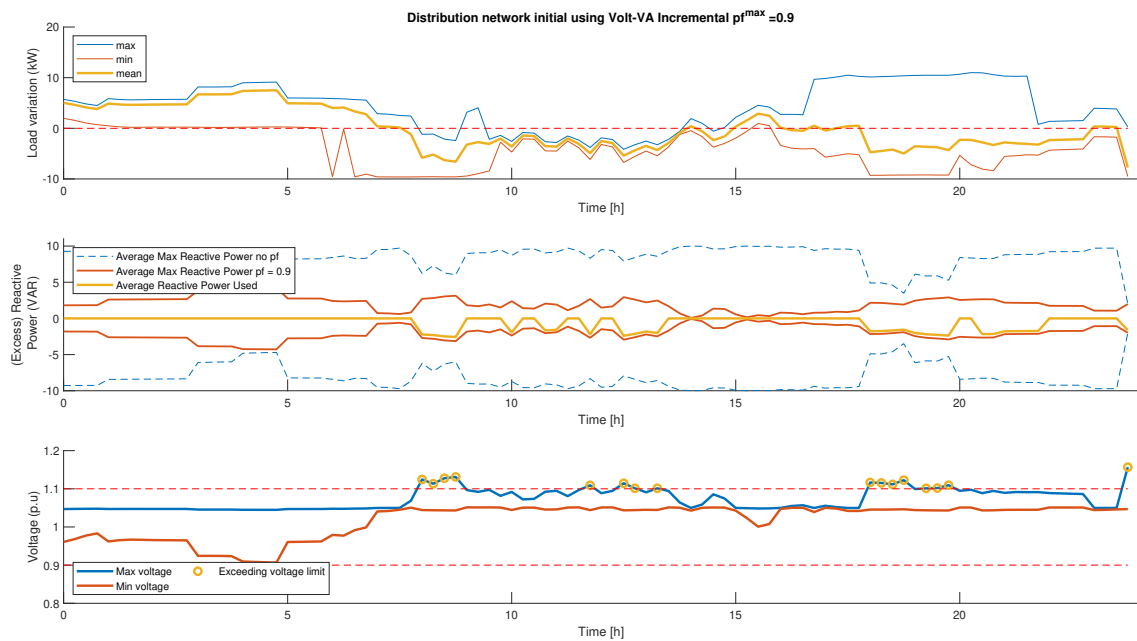


Figure 7.7: Load variation (top), reactive power usage Q_{conv} and availability Q_{conv}^{max} (middle), and voltage profile (bottom). Initial voltage profile after adding the multi-port converter energy demand P_{conv} using the Volt-VAR incremental method on day 185 with 45 multi-port converters. Reactive power compensation, with power factor restriction, has already been added.

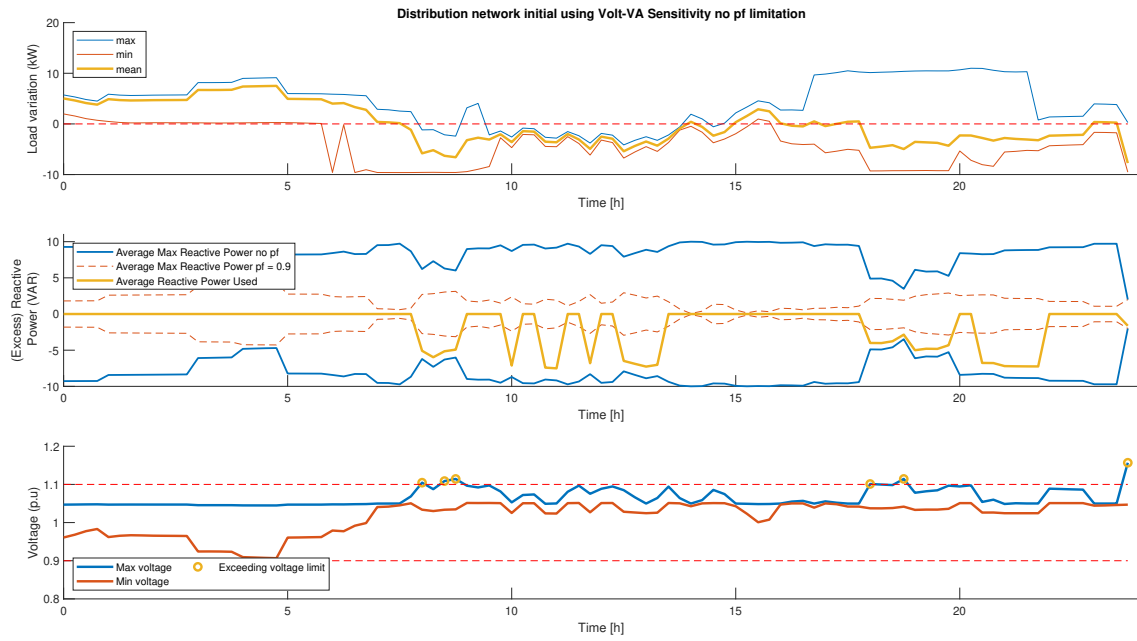


Figure 7.8: Load variation (top), reactive power usage Q_{conv} and availability Q_{conv}^{max} (middle), and voltage profile (bottom). Initial voltage profile after adding the multi-port converter energy demand P_{conv} using the Volt-VAR sensitivity method on day 185 with 45 multi-port converters. Reactive power compensation, with no restriction, has already been added.

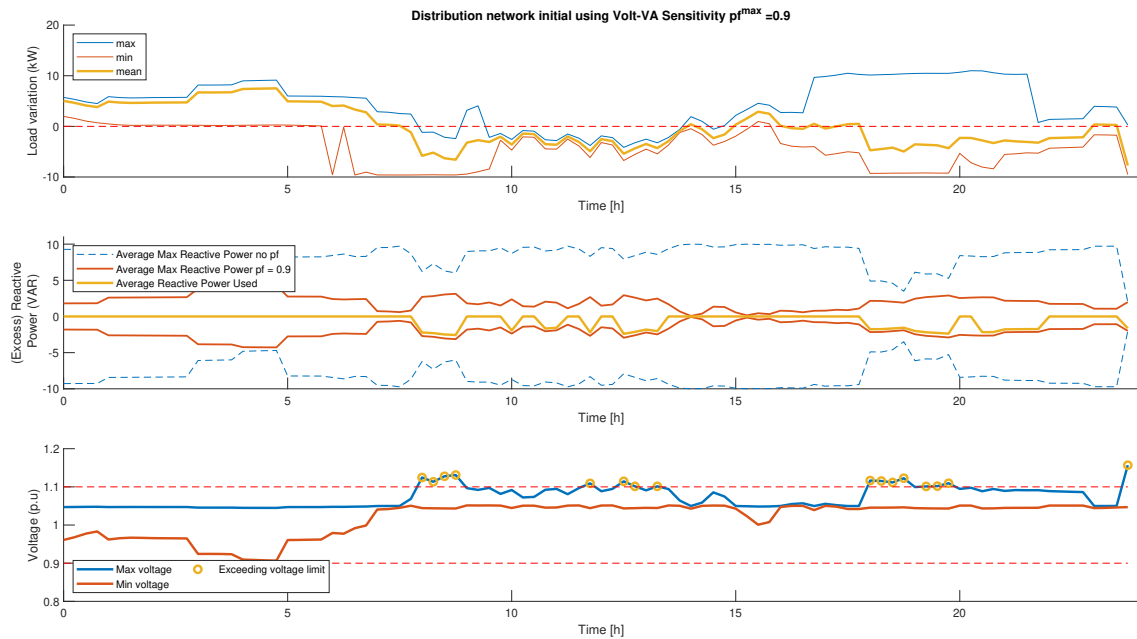


Figure 7.9: Load variation (top), reactive power usage Q_{conv} and availability Q_{conv}^{max} (middle), and voltage profile (bottom). Initial voltage profile after adding the multi-port converter energy demand P_{conv} using the Volt-VAR sensitivity method on day 185 with 45 multi-port converters. Reactive power compensation, with power factor restriction, has already been added.

The Figures 7.10 (Volt-Watt), 7.11a (Volt-VAR Incr (no pf)), 7.11b (Volt-VAR Incr (pf=0.9)), 7.12a (Volt-VAR Sens (no pf)) and 7.12b (Volt-VAR Sens (pf=0.9)), show the final iteration of the optimal charging algorithm of house number 49.

Differences can be spotted between Figure 7.10 (Volt-Watt) and the Volt-VA methods shown in Figure 7.11 and 7.12. Between the houses using power factor restrictions in Figures 7.11b and 7.12b, and the ones without in Figures 7.11a and 7.12a a clear difference in APC is shown.

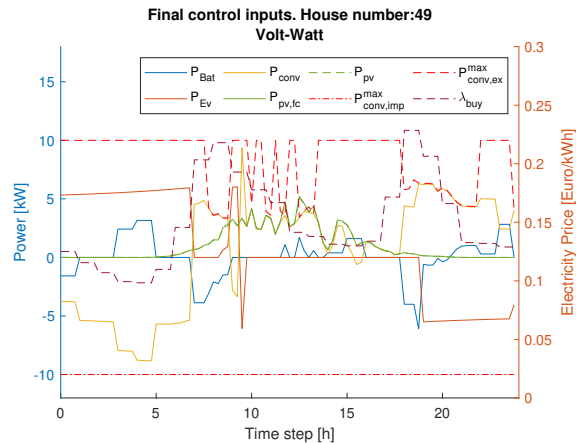
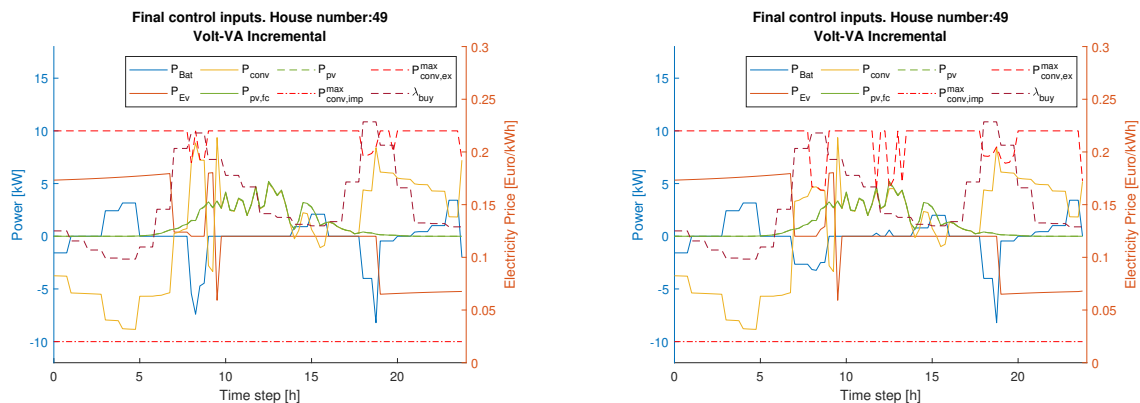


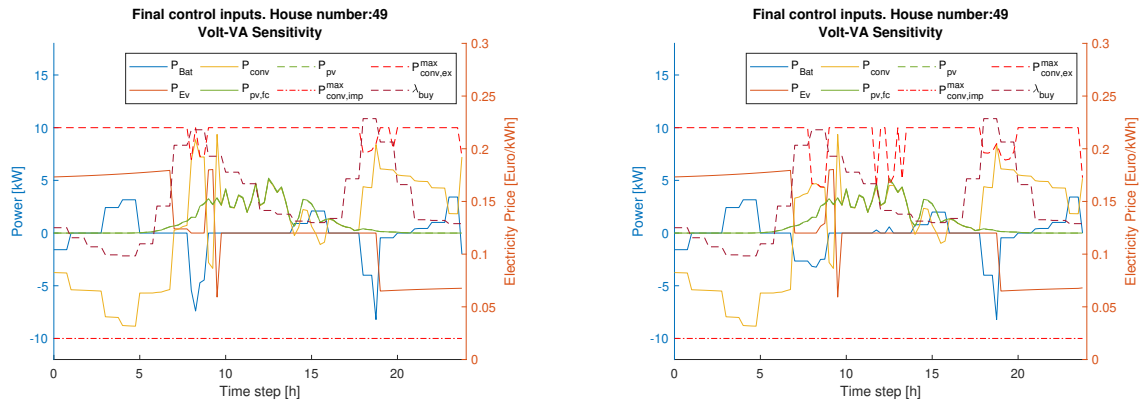
Figure 7.10: The final optimal control inputs using the Volt-Watt correction method.



(a) The final optimal control inputs using the Volt-VA incremental correction method with no power factor restriction.

(b) The final optimal control inputs using the Volt-VA incremental correction method with power factor restriction.

Figure 7.11: The final optimal control inputs using the Volt-VA incremental correction method without (Figure 7.11a) and with (Figure 7.11b) power factor restriction.



(a) The final optimal control inputs using the Volt-VA sensitivity correction method with no power factor restriction.

(b) The final optimal control inputs using the Volt-VA sensitivity correction method with power factor restriction.

Figure 7.12: The final optimal control inputs using the Volt-VA sensitivity correction method without (Figure 7.12a) and with (Figure 7.12b) power factor restriction.

The Figures 7.13 (Volt-Watt), 7.14 (Volt-VAR Incr (no pf)), 7.15 (Volt-VAR Incr (pf=0.9)), 7.16 (Volt-VAR Sens (no pf)) and 7.17 (Volt-VAR Sens (pf=0.9)) show the forecasted load demands and corrected voltage profile. As all the voltage violations have been corrected, the VMS procedure in Figure 5.19 is done.

Both Volt-VA sensitivity (no pf) and Volt-VA incremental (no pf) are capable of using more active power compared to the other methods.

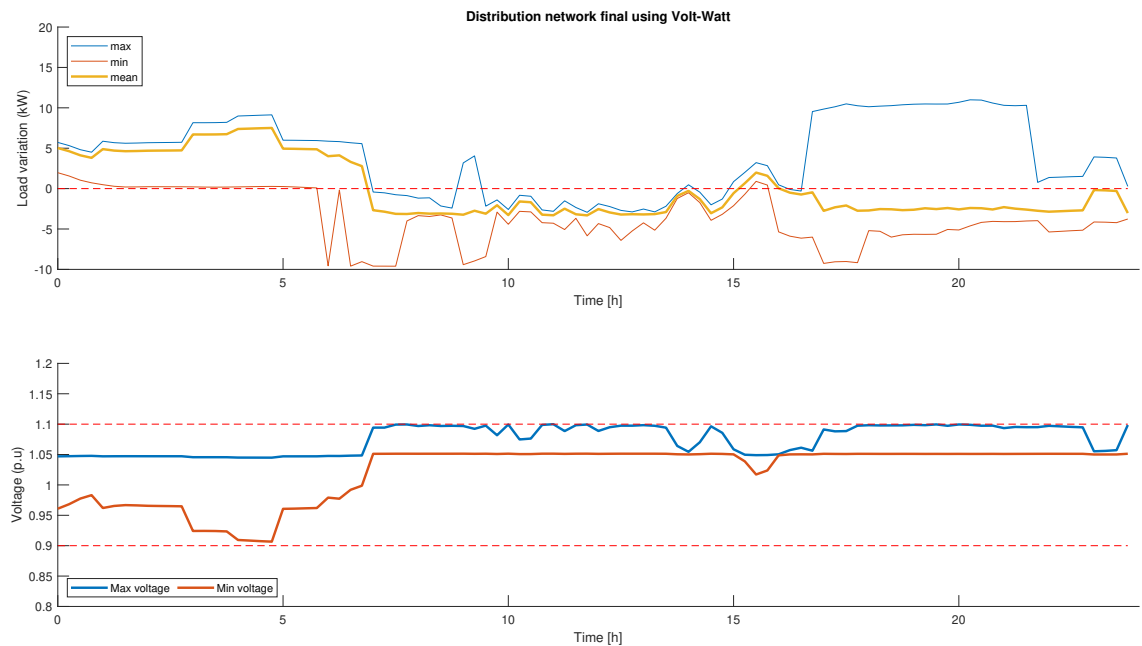


Figure 7.13: Final voltage profile after the correction iterative procedure. All voltage violations in the forecast have been removed by using the Volt-Watt method on day 185 with 45 multi-port converter.

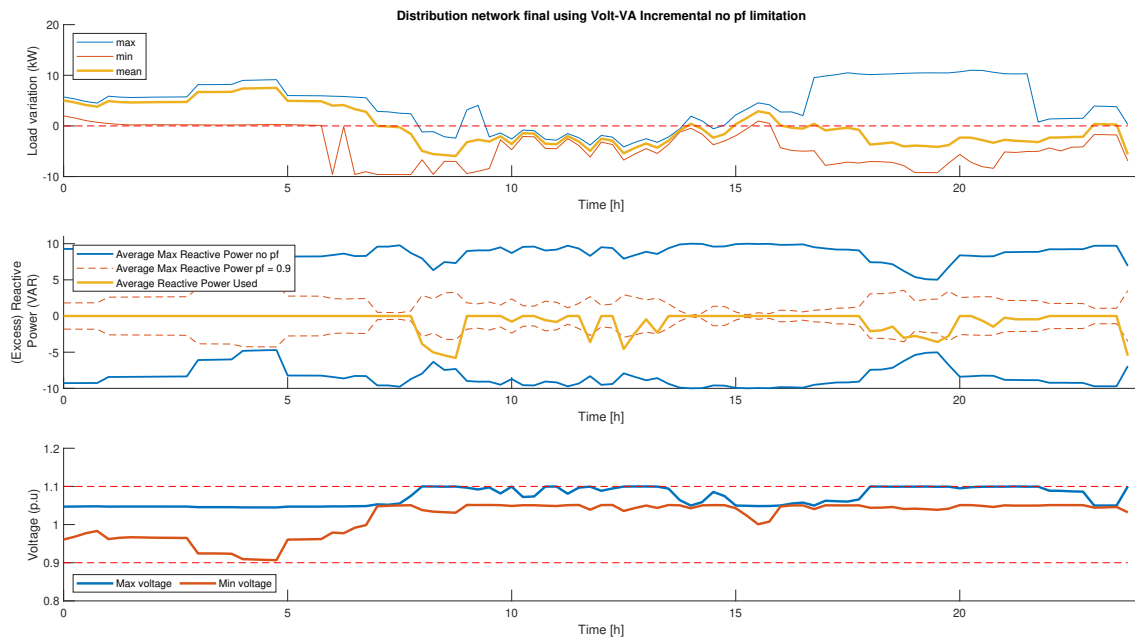


Figure 7.14: Final voltage profile after the correction iterative procedure. All voltage violations in the forecast have been removed by using the Volt-VA incremental method with no power factor restrictions, on day 185 with 45 multi-port converter.

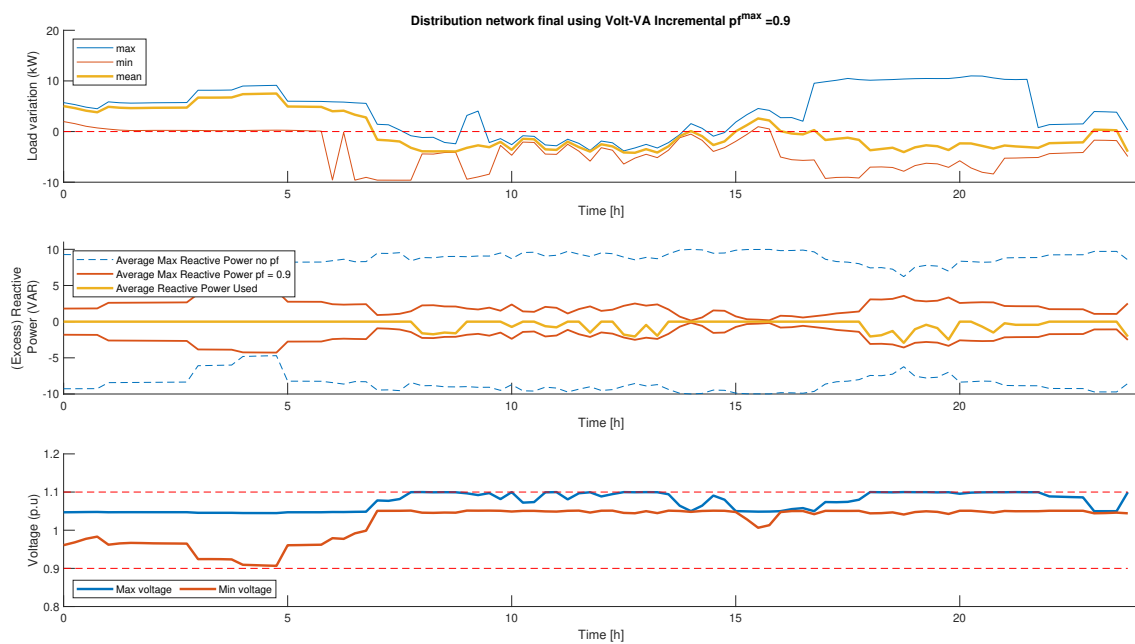


Figure 7.15: Final voltage profile after the correction iterative procedure. All voltage violations in the forecast have been removed by using the Volt-VA incremental method with power factor restrictions, on day 185 with 45 multi-port converter.

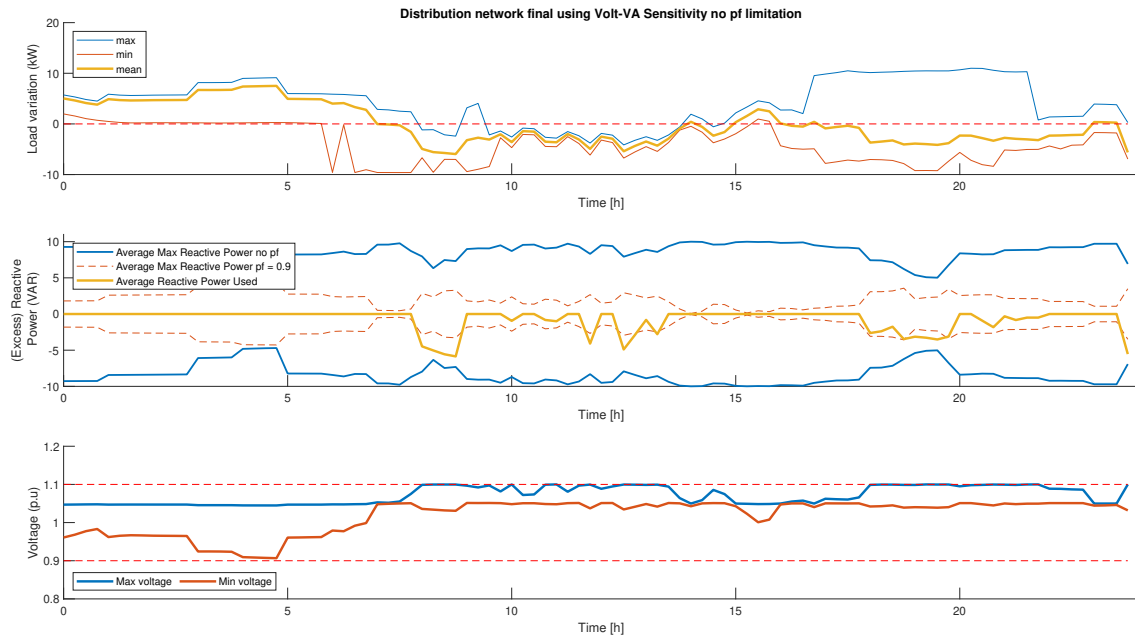


Figure 7.16: Final voltage profile after the correction iterative procedure. All voltage violations in the forecast have been removed by using the Volt-VA sensitivity method with no power factor restrictions, on day 185 with 45 multi-port converter.

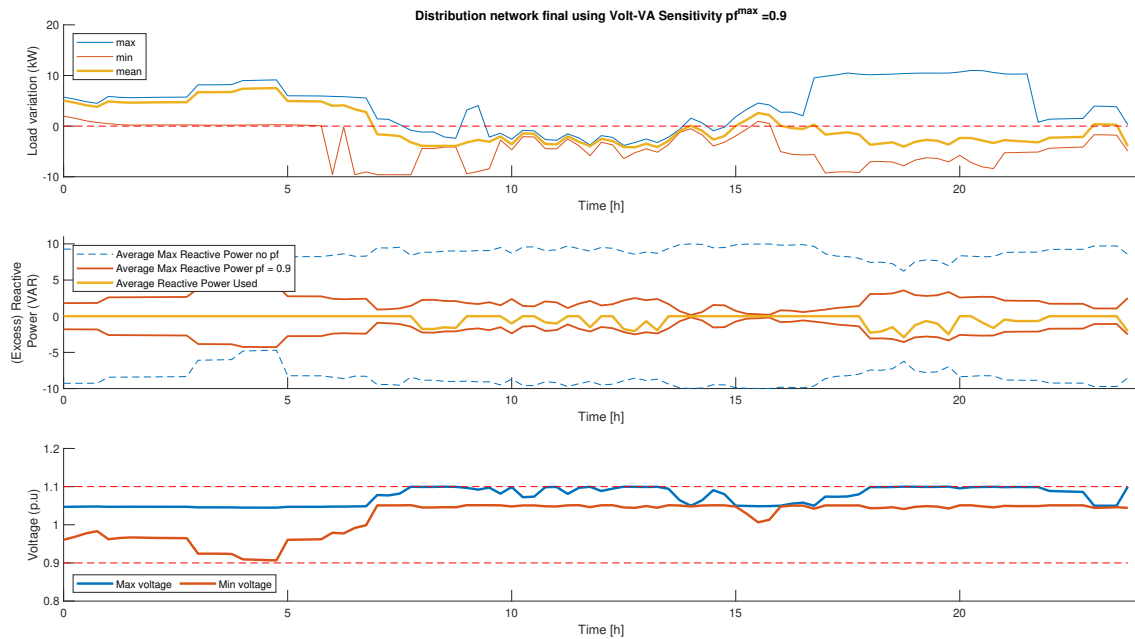


Figure 7.17: Final voltage profile after the correction iterative procedure. All voltage violations in the forecast have been removed by using the Volt-VA sensitivity method with power factor restrictions, on day 185 with 45 multi-port converter.

The Figures 7.18 (Volt-Watt), 7.19 (Volt-VAR Incr (no pf)), 7.20 (Volt-VAR Incr (pf=0.9)), 7.21 (Volt-VAR Sens (no pf)) and 7.22 (Volt-VAR Sens (pf=0.9)) show the final result after the real-time controller. Volt-Watt, Volt-VA incremental (no pf) and Volt-VA sensitivity (no pf) can remove the voltage violation using the real-time controller. Volt-VA incremental (pf=0.9) and Volt-VA sensitivity (pf=0.9) remove the real-time error if they keep their original reactive power setpoint. If they obey the power factor, a voltage violation occurs (blue dots). This is as the real-time controller does not consider the decrease of reactive power during real-time control.

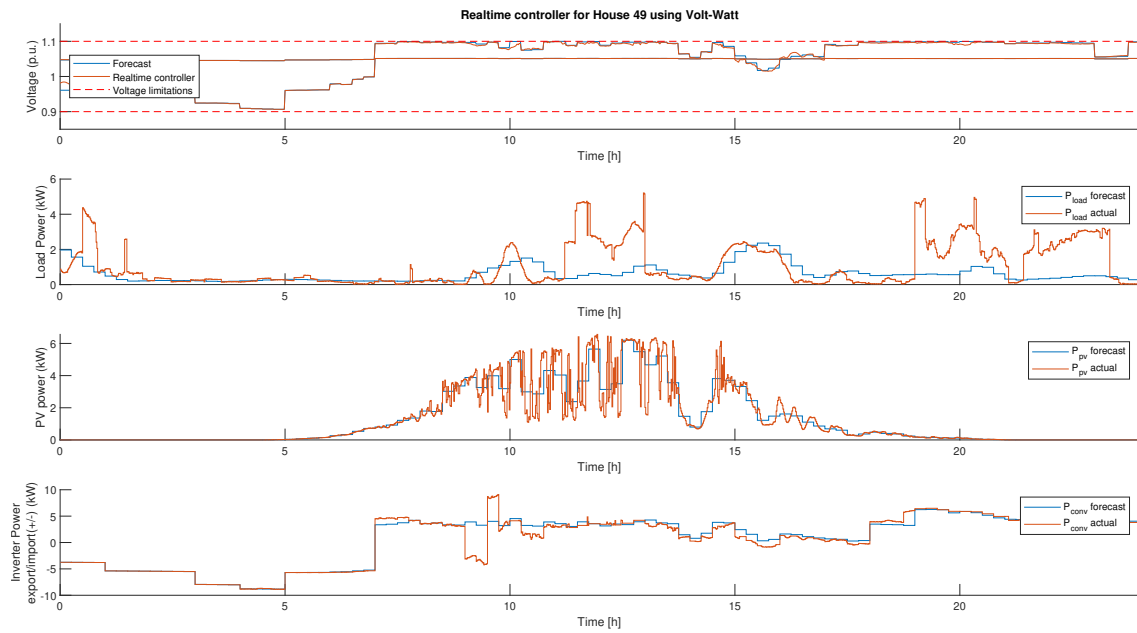


Figure 7.18: Forecasted and real-time voltage profile (top), forecasted and actual load demand at the house (middle top), forecasted and actual PV generation at the house (middle bottom), and forecasted and actual import and export of energy by the multi-port converter (bottom) on day 185 with 45 multi-port converter, using the Volt-Watt correction method for the forecast.

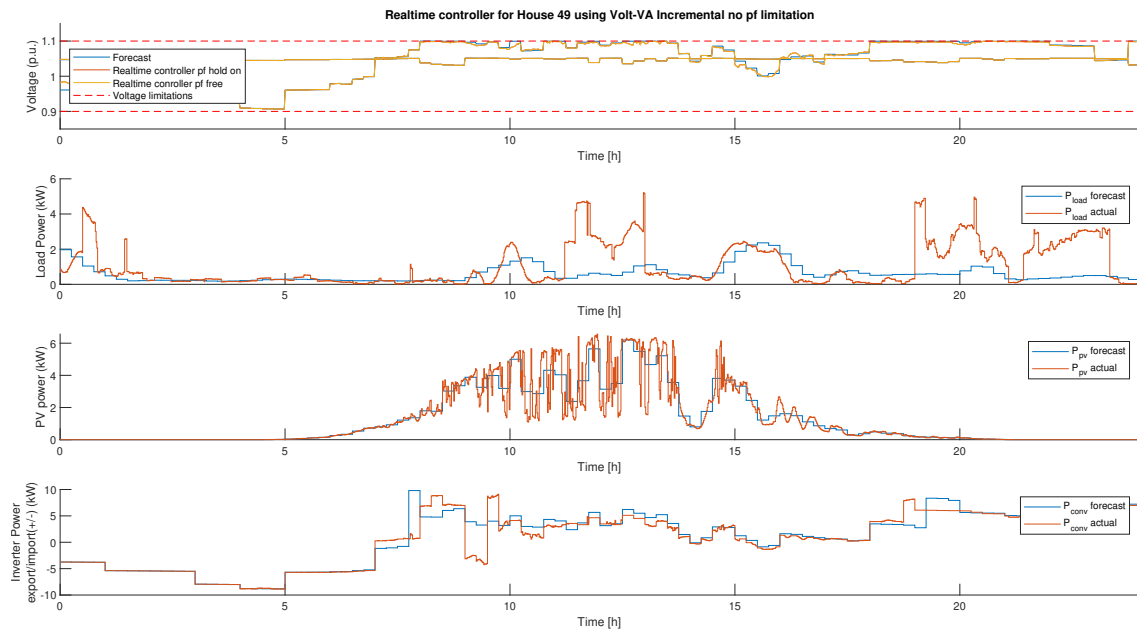


Figure 7.19: Forecasted and real-time voltage profile (top), forecasted and actual load demand at the house (middle top), forecasted and actual PV generation at the house (middle bottom), and forecasted and actual import and export of energy by the multi-port converter (bottom) on day 185 with 45 multi-port converter, using the Volt-VA incremental correction method with no power factor restrictions for the forecast.

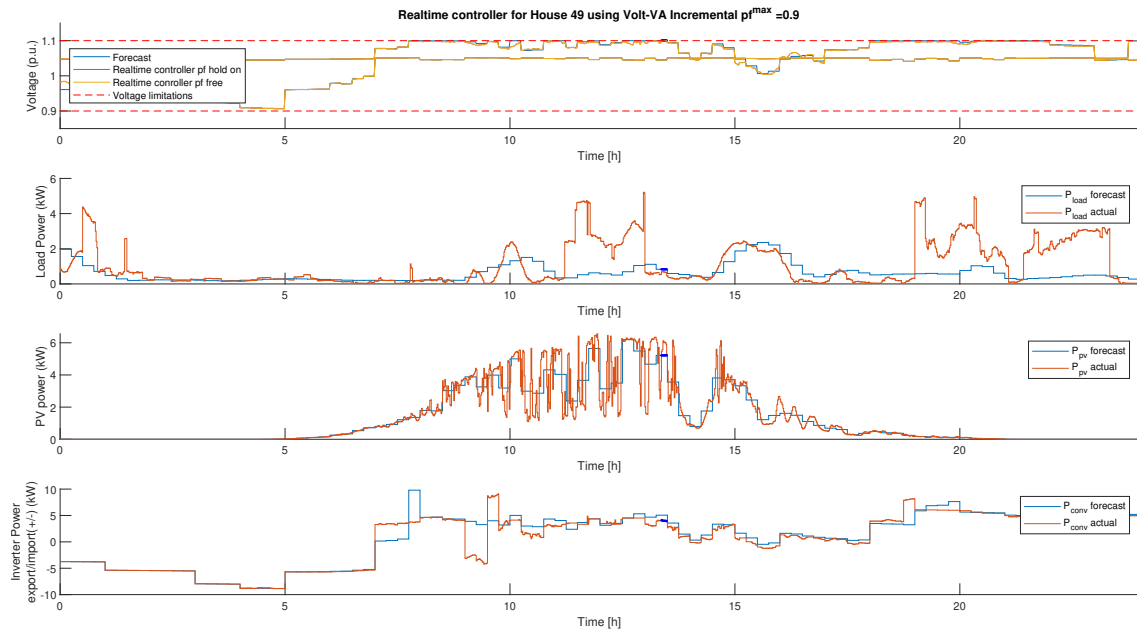


Figure 7.20: Forecasted and real-time voltage profile (top), forecasted and actual load demand at the house (middle top), forecasted and actual PV generation at the house (middle bottom), and forecasted and actual import and export of energy by the multi-port converter (bottom) on day 185 with 45 multi-port converter, using the Volt-VA incremental correction method with power factor restrictions for the forecast. Removal of the voltage violation is only possible if the original reactive power setpoint is used. If the real-time controller obey the power factor, a voltage violation occurs (blue dots).

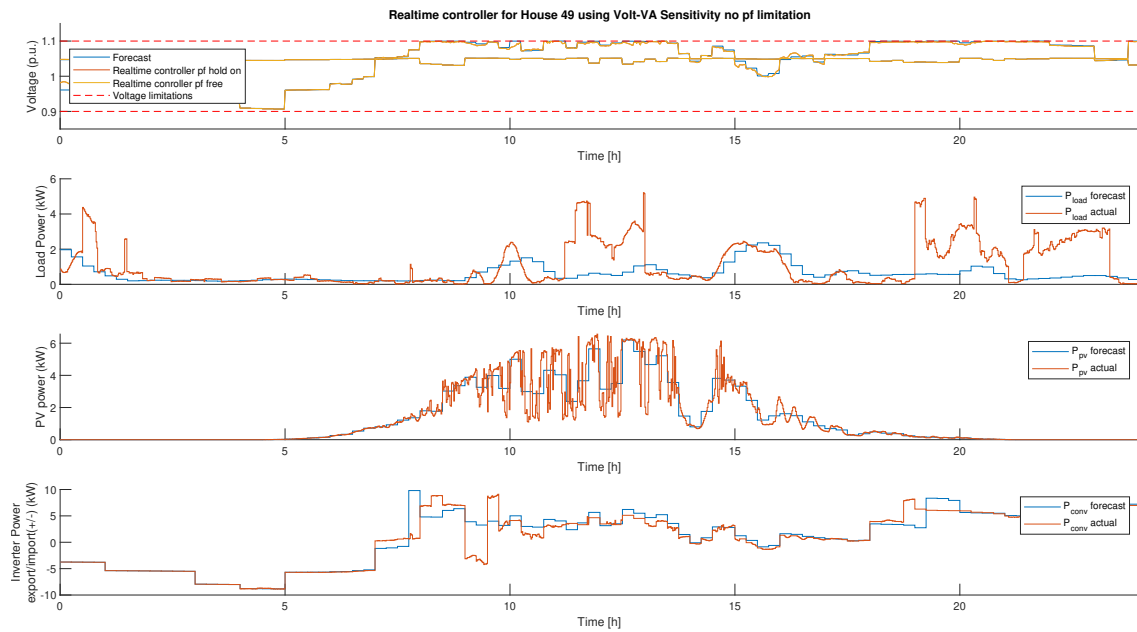


Figure 7.21: Forecasted and real-time voltage profile (top), forecasted and actual load demand at the house (middle top), forecasted and actual PV generation at the house (middle bottom), and forecasted and actual import and export of energy by the multi-port converter (bottom) on day 185 with 45 multi-port converter, using the Volt-VA sensitivity correction method with no power factor restrictions for the forecast.

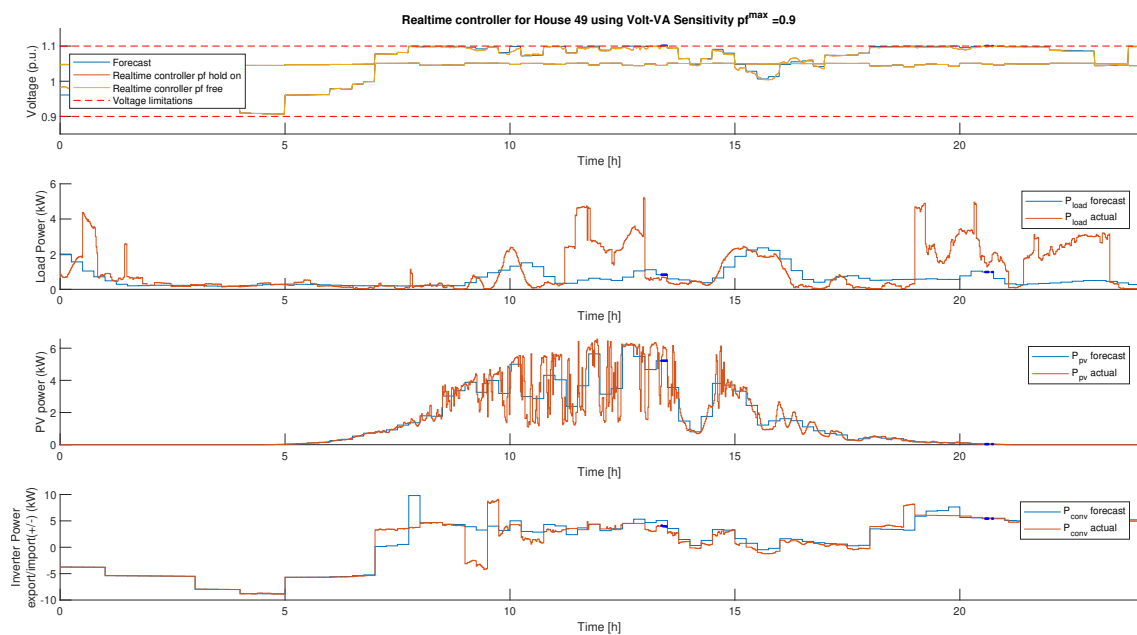


Figure 7.22: Forecasted and real-time voltage profile (top), forecasted and actual load demand at the house (middle top), forecasted and actual PV generation at the house (middle bottom), and forecasted and actual import and export of energy by the multi-port converter (bottom) using the Volt-VA sensitivity correction method with power factor restrictions for the forecast. Removal of the voltage violation is only possible if the original reactive power setpoint is used. If the real-time controller obey the power factor, a voltage violation occurs (blue dots).

7.2.2. Summer day with few multi-port converters(20)

Figure 7.23 shows the load variation, voltage profile and price alterations of the VMS before adding P_{conv} of the multi-port converter. This is done, as stated in Section 5.3, to prevent voltage violations in the network. The step is the "Voltage based price" in Figure 5.19. Less decline is shown compared to Section 7.2.1, as less PV and EV are removed and replaced with multi-port converters.

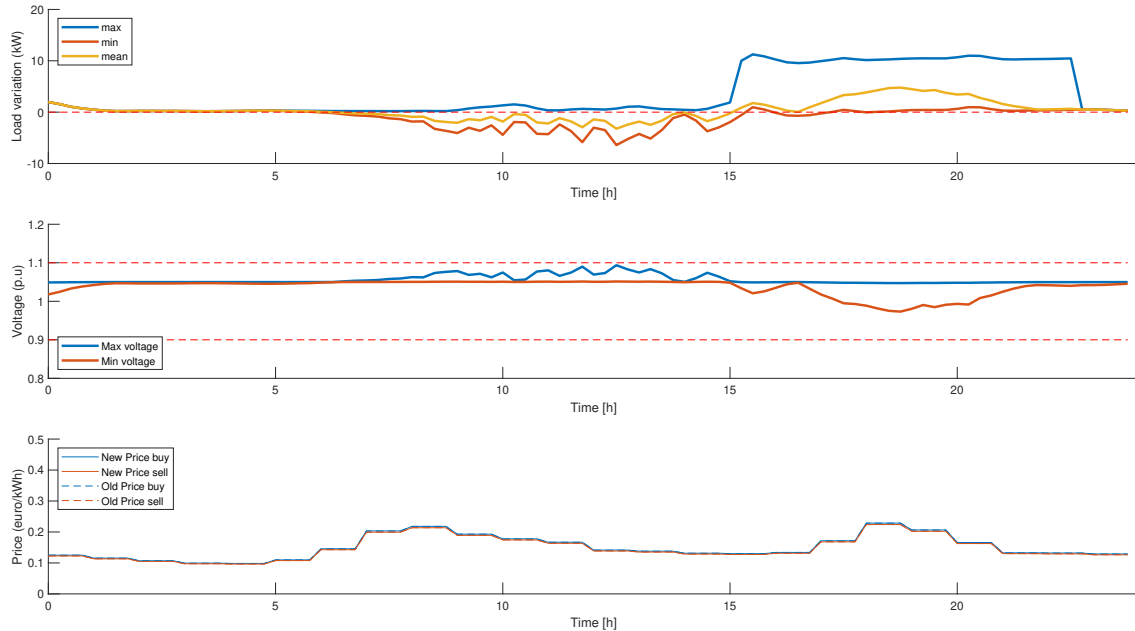


Figure 7.23: Load variation (top), voltage profile (middle), and price correction mechanism (bottom) before the multi-port converter energy demand P_{conv} is added.

Figure 7.24, shows the first iteration of the optimal charging algorithm of house number 49. The result is identical to Figure 7.4.

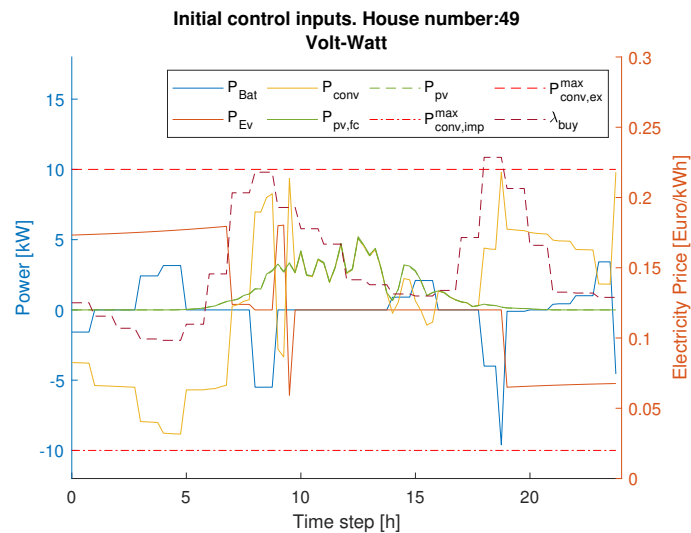


Figure 7.24: The optimal control inputs of the EMS before the correction methods are used.

The Figures 7.25 (Volt-Watt), 7.26 (Volt-VAR Incr (no pf)), 7.27 (Volt-VAR Incr (pf=0.9)), 7.28 (Volt-VAR Sens (no pf)) and 7.29 (Volt-VAR Sens (pf=0.9)) show the initial voltage violations caused by the demand of the multi-port converter.

Compared to 7.2.1 less energy is used and fewer voltage violations have to be corrected.

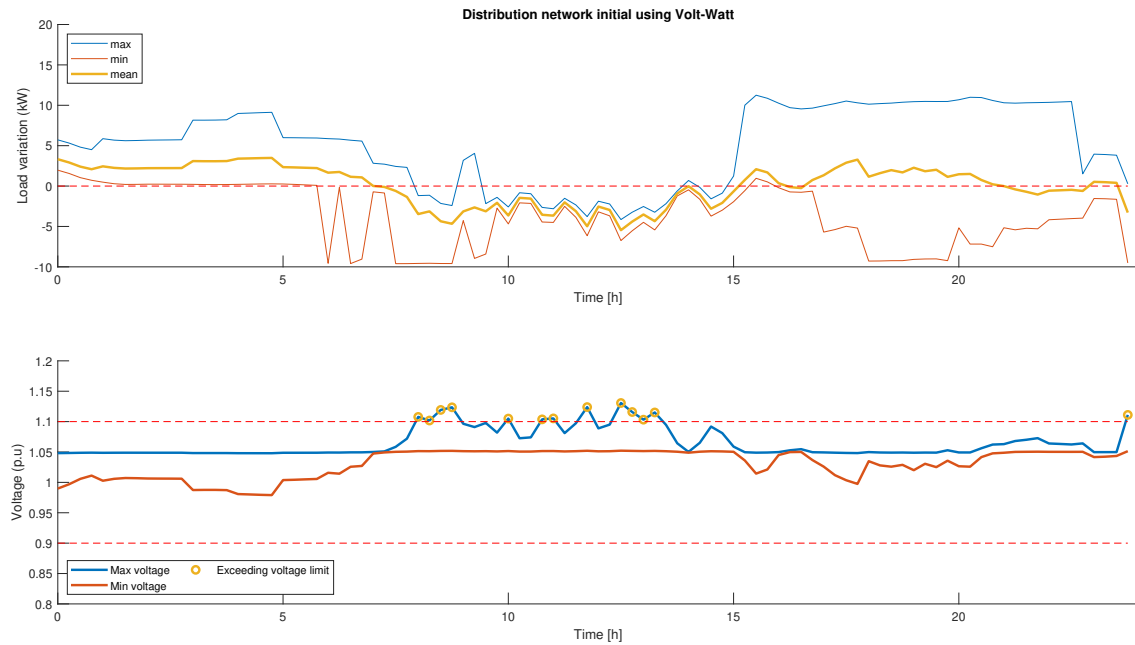


Figure 7.25: Load variation (top) and voltage profile (bottom). Initial voltage profile after adding the multi-port converter energy demand P_{conv} using the Volt-Watt method on day 185 with 20 multi-port converters.

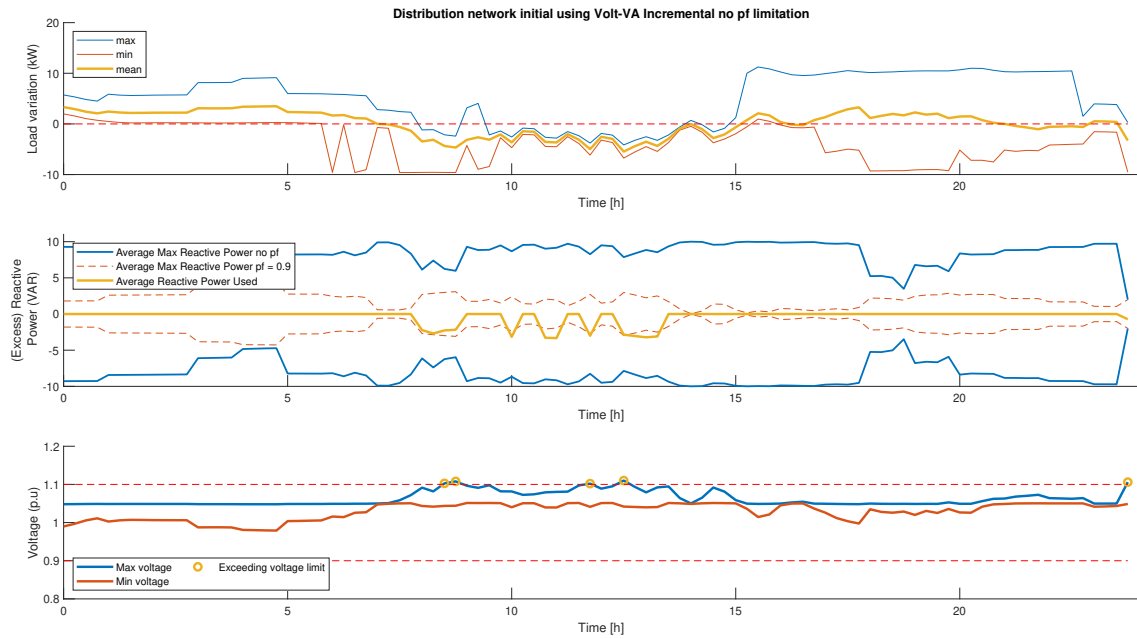


Figure 7.26: Load variation (top), reactive power usage Q_{conv} and availability Q_{conv}^{max} (middle), and voltage profile (bottom). Initial voltage profile after adding the multi-port converter energy demand P_{conv} using the Volt-VAR incremental method on day 185 with 20 multi-port converters. Reactive power compensation, with no restriction, has already been added.

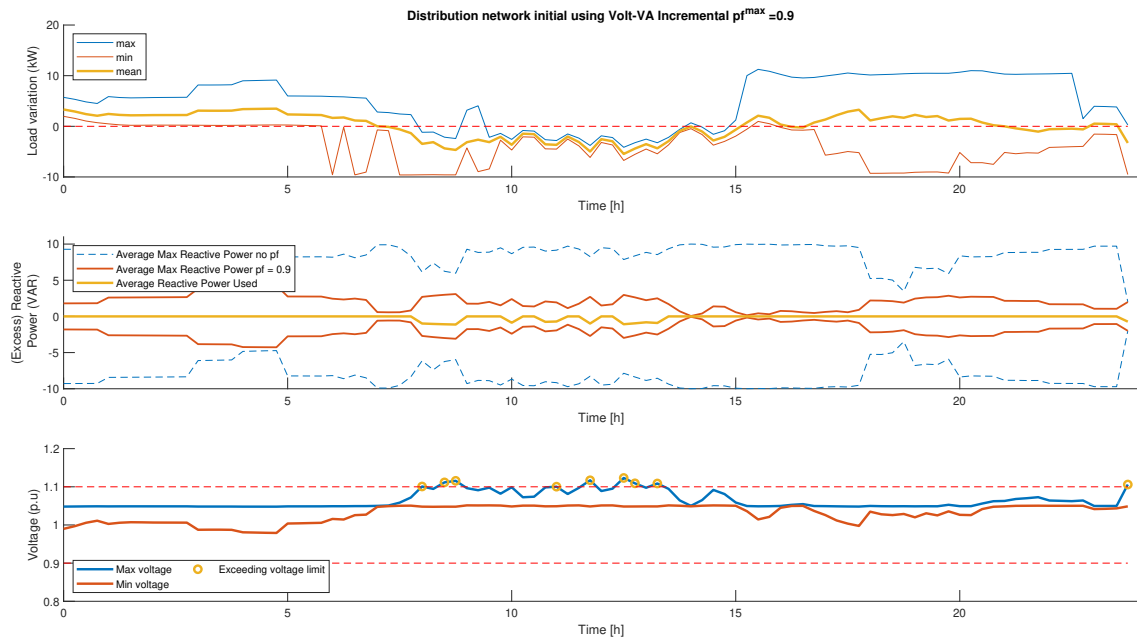


Figure 7.27: Load variation (top), reactive power usage Q_{conv} and availability Q_{conv}^{max} (middle), and voltage profile (bottom). Initial voltage profile after adding the multi-port converter energy demand P_{conv} using the Volt-VAR incremental method on day 185 with 20 multi-port converters. Reactive power compensation, with power factor restriction, has already been added.

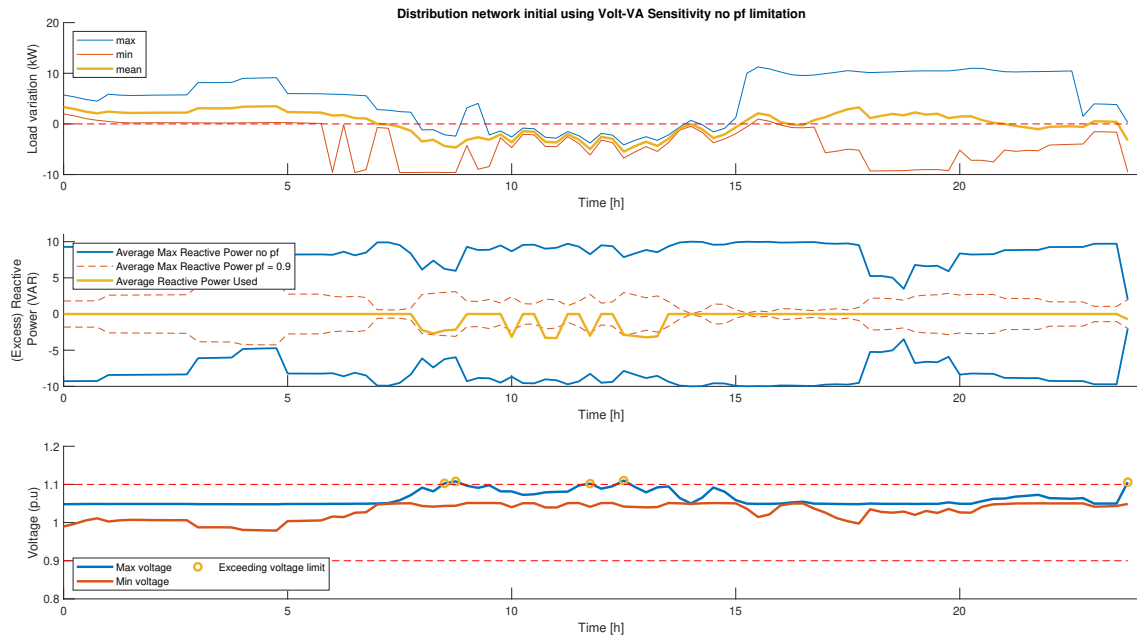


Figure 7.28: Load variation (top), reactive power usage Q_{conv} and availability Q_{conv}^{max} (middle), and voltage profile (bottom). Initial voltage profile after adding the multi-port converter energy demand P_{conv} using the Volt-VAR sensitivity method on day 185 with 20 multi-port converters. Reactive power compensation, with no restriction, has already been added.

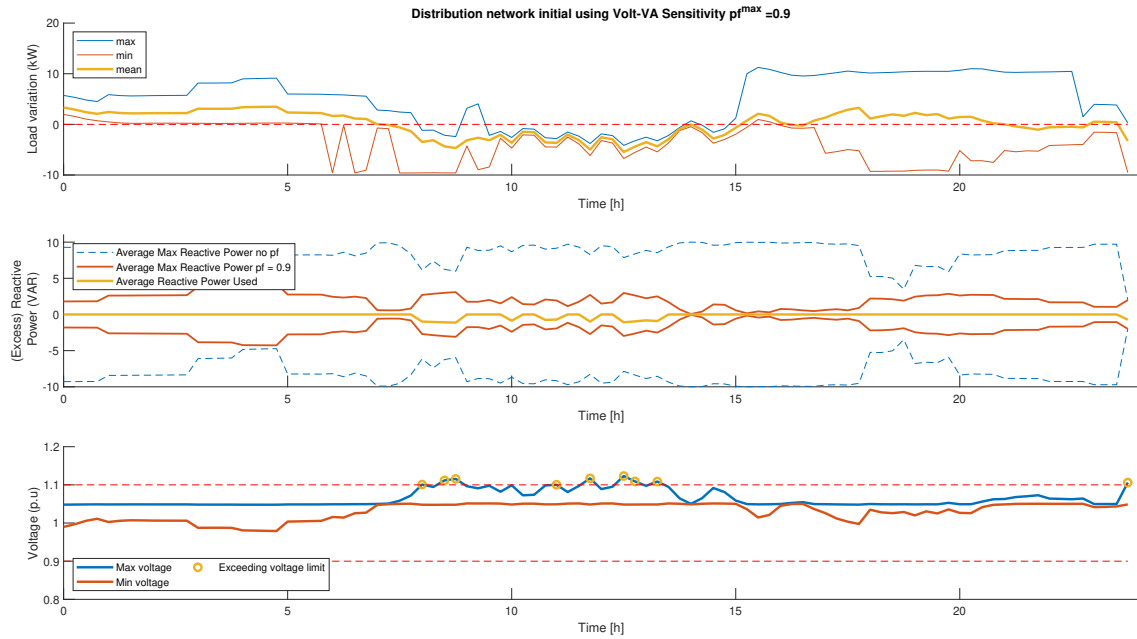


Figure 7.29: Load variation (top), reactive power usage Q_{conv} and availability Q_{conv}^{max} (middle), and voltage profile (bottom). Initial voltage profile after adding the multi-port converter energy demand P_{conv} using the Volt-VAR sensitivity method on day 185 with 20 multi-port converters. Reactive power compensation, with power factor restriction, has already been added.

The Figures 7.30 (Volt-Watt), 7.31a (Volt-VAR Incr (no pf)), 7.31b (Volt-VAR Incr (pf=0.9)), 7.32a (Volt-VAR Sens (no pf)) and 7.32b (Volt-VAR Sens (pf=0.9)), show the final iteration of the optimal charging algorithm of house number 49. This is the step "EMS House" in Figure 5.19.

Compared to 7.2.1 less curtailment is necessary from 4 PM till 9 PM, as more uncontrolled EV are using energy and less multi-port converters are competing with each other for a spot with a high buying or selling price.

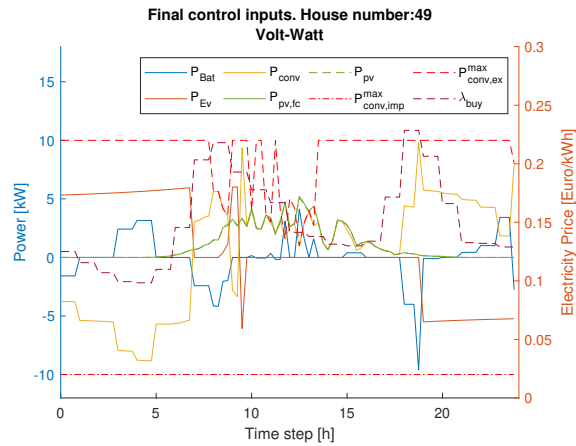
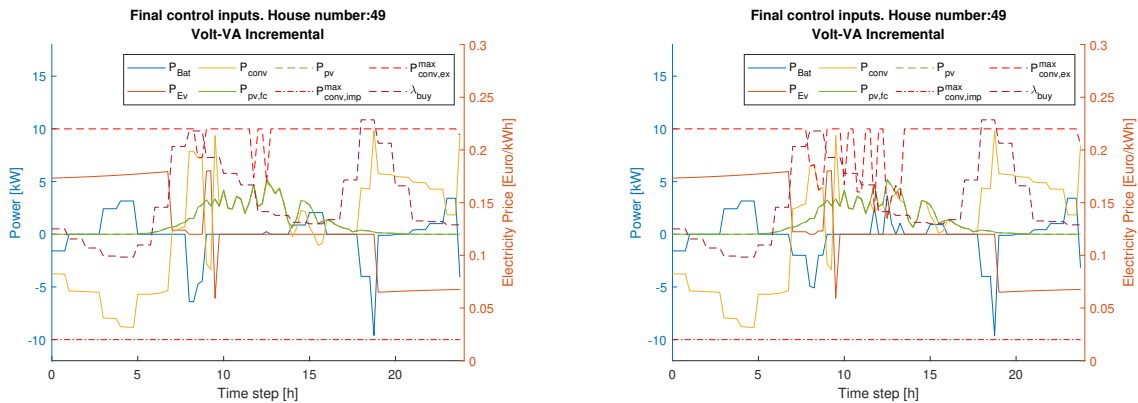


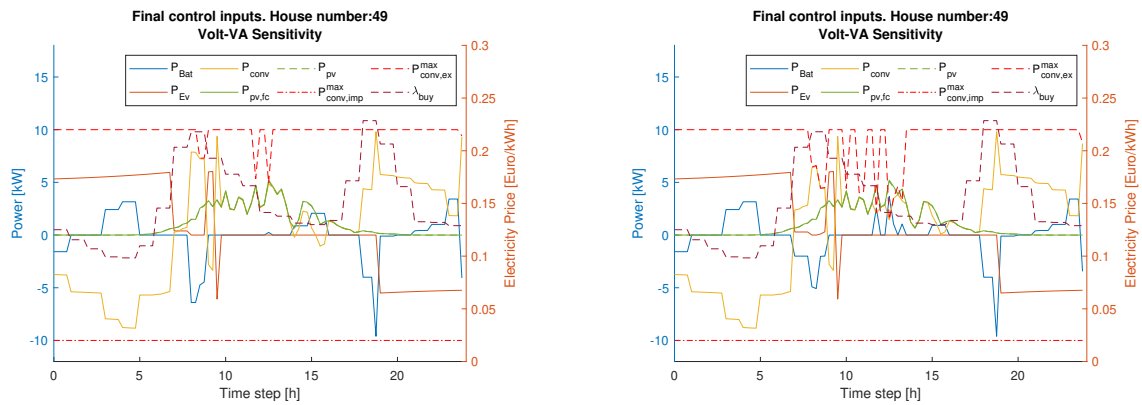
Figure 7.30: The final optimal control inputs using the Volt-Watt correction method.



(a) The final optimal control inputs using the Volt-VA incremental correction method with no power factor restriction.

(b) The final optimal control inputs using the Volt-VA incremental correction method with power factor restriction.

Figure 7.31: The final optimal control inputs using the Volt-VA incremental correction method without (Figure 7.31a) and with (Figure 7.31b) power factor restriction.



(a) The final optimal control inputs using the Volt-VA sensitivity correction method with no power factor restriction.

(b) The final optimal control inputs using the Volt-VA sensitivity correction method with power factor restriction.

Figure 7.32: The final optimal control inputs using the Volt-VA sensitivity correction method without (Figure 7.32a) and with (Figure 7.32b) power factor restriction.

The Figures 7.33 (Volt-Watt), 7.34 (Volt-VAR Incr (no pf)), 7.35 (Volt-VAR Incr (pf=0.9)), 7.36 (Volt-VAR Sens (no pf)) and 7.37 (Volt-VAR Sens (pf=0.9)) show the forecasted load demands and corrected voltage profile. As all the voltage violations have been corrected, the VMS procedure in Figure 5.19 is done.

Compared to Section 7.2.1, less energy is used in the network.

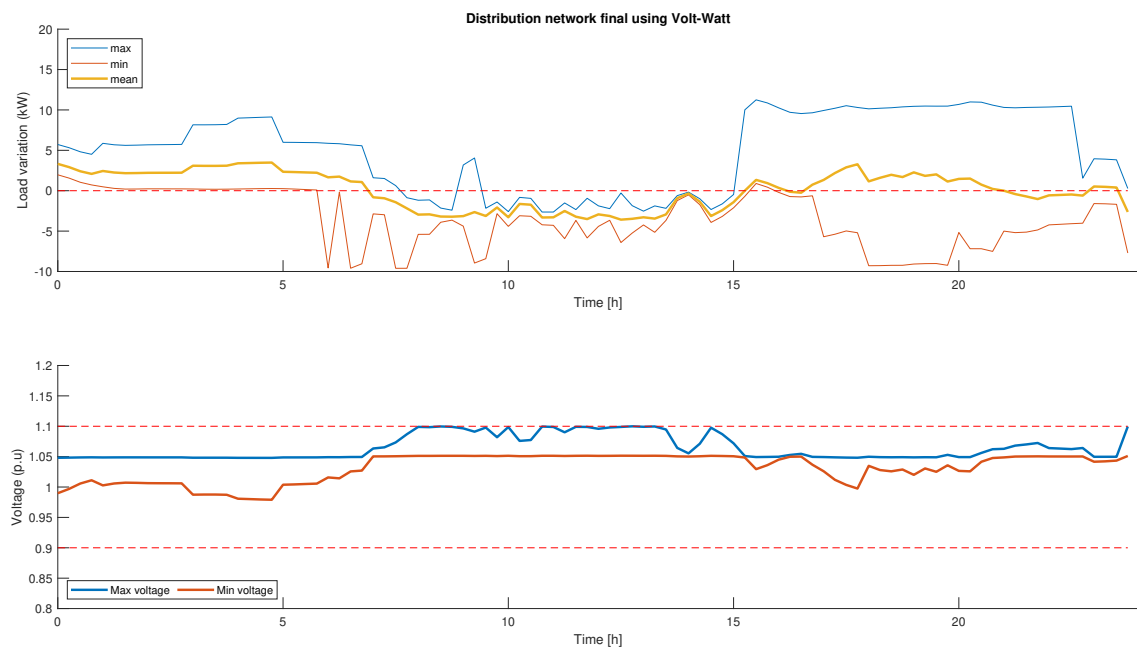


Figure 7.33: Final voltage profile after the correction iterative procedure. All voltage violations in the forecast have been removed by using the Volt-Watt method on day 185 with 20 multi-port converter.

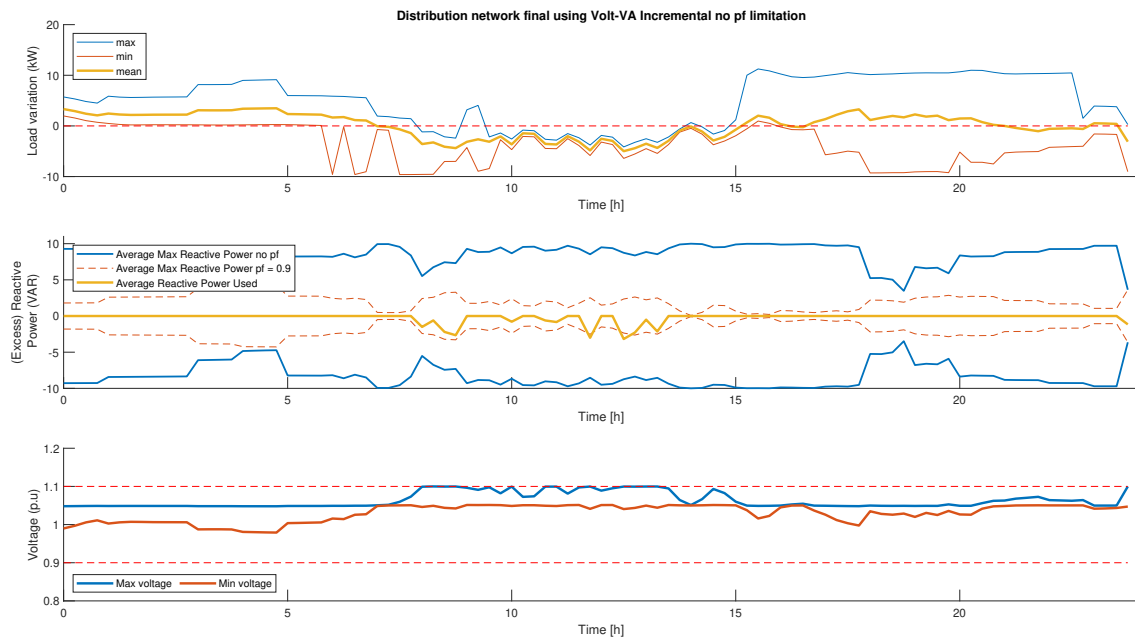


Figure 7.34: Final voltage profile after the correction iterative procedure. All voltage violations in the forecast have been removed by using the Volt-VA incremental method with no power factor restrictions, on day 185 with 20 multi-port converter.

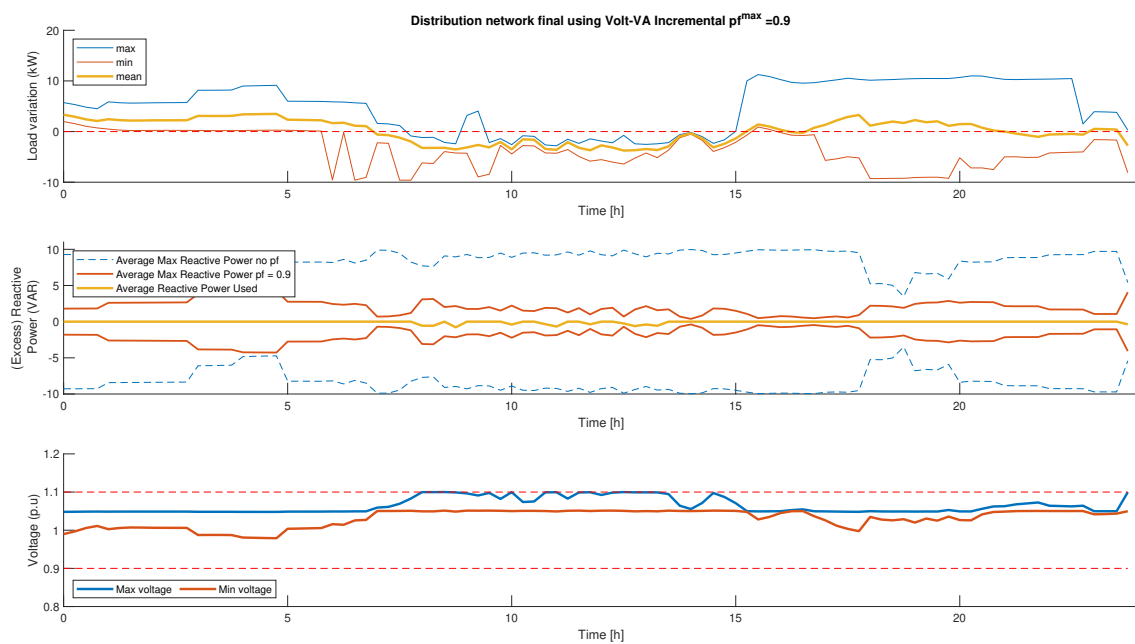


Figure 7.35: Final voltage profile after the correction iterative procedure. All voltage violations in the forecast have been removed by using the Volt-VA incremental method with power factor restrictions, on day 185 with 20 multi-port converter.

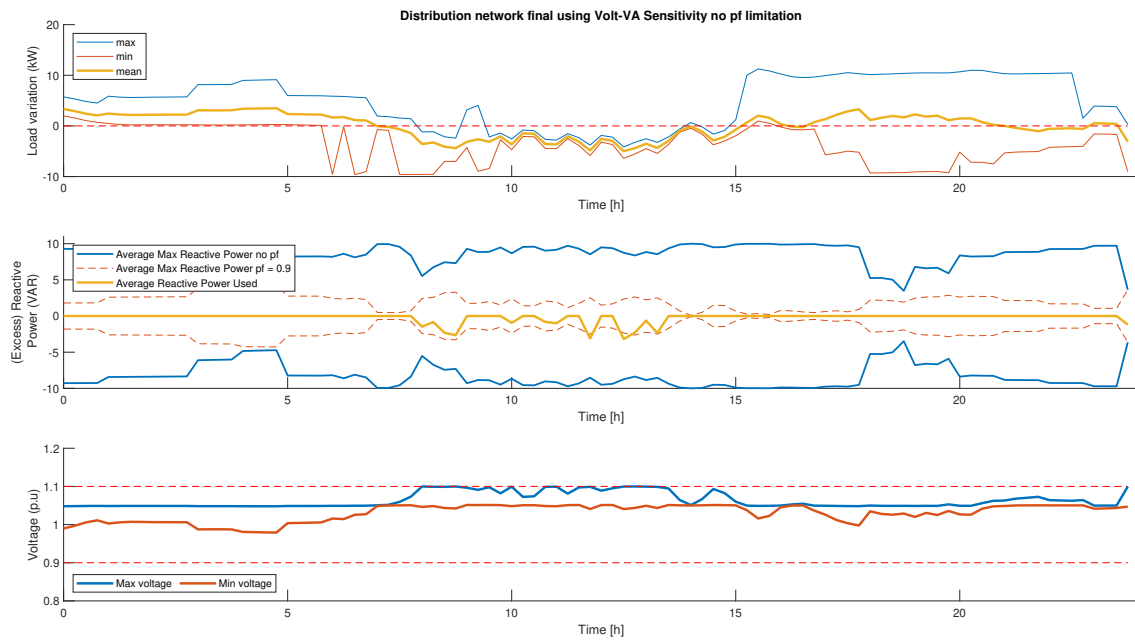


Figure 7.36: Final voltage profile after the correction iterative procedure. All voltage violations in the forecast have been removed by using the Volt-VA sensitivity method with no power factor restrictions, on day 185 with 20 multi-port converter.

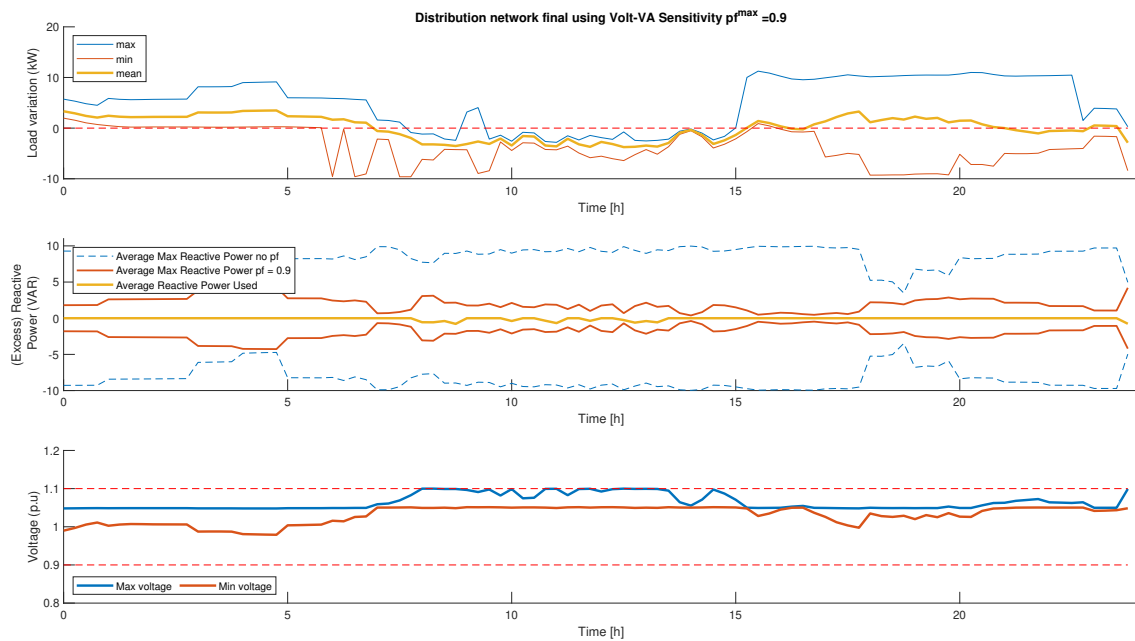


Figure 7.37: Final voltage profile after the correction iterative procedure. All voltage violations in the forecast have been removed by using the Volt-VA sensitivity method with power factor restrictions, on day 185 with 20 multi-port converter.

The Figures 7.38 (Volt-Watt), 7.39 (Volt-VAR Incr (no pf)), 7.40(Volt-VAR Incr (pf=0.9)), 7.41 (Volt-VAR Sens (no pf)) and 7.42 (Volt-VAR Sens (pf=0.9)) show the final result after the real-time controller. Volt-Watt, Volt-VA incremental (no pf) and Volt-VA sensitivity (no pf) can remove the voltage violation using the real-time controller. Volt-VA incremental (pf=0.9) and Volt-VA sensitivity (pf=0.9) remove the real-time error if they keep their original reactive power setpoint. If they obey the power factor, a voltage violation occurs (blue dots). This is as the real-time controller does not consider the decrease of reactive power during real-time control.

Compared to Section 7.2.1 some small voltage violations occur in the Volt-Watt (blue dots), Volt VA incremental (red dots), and Volt VA sensitivity (red dots) method. If the ratio of Equation 6.5 is increased by 0.1 all problems will be removed.

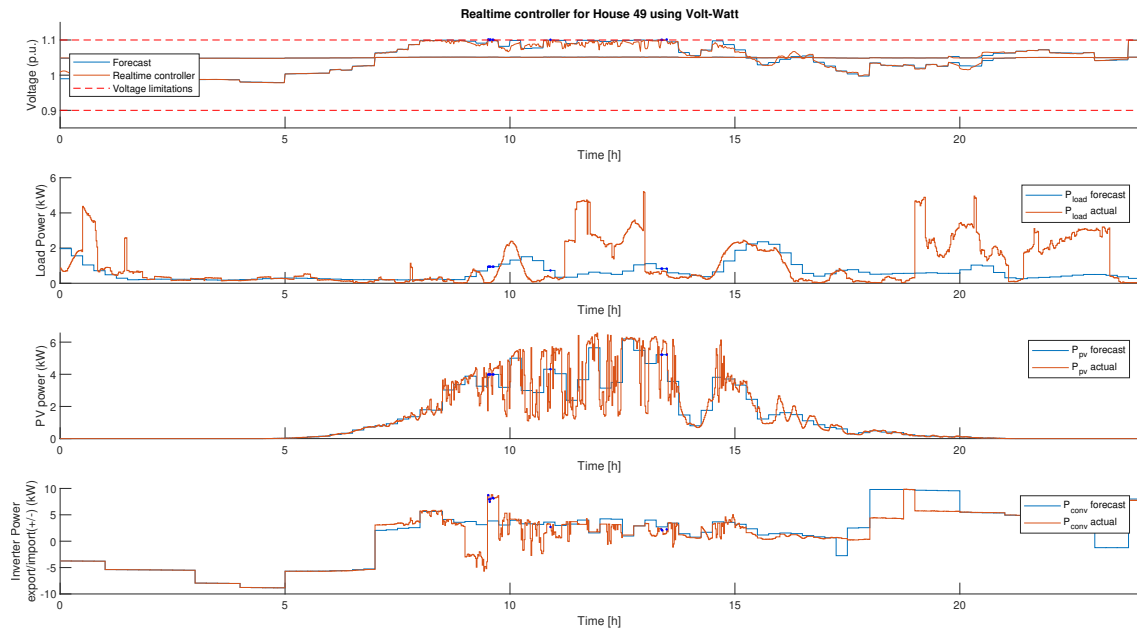


Figure 7.38: Forecasted and real-time voltage profile (top), forecasted and actual load demand at the house (middle top), forecasted and actual PV generation at the house (middle bottom), and forecasted and actual import and export of energy by the multi-port converter (bottom) on day 185 with 20 multi-port converter, using the Volt-Watt correction method for the forecast.

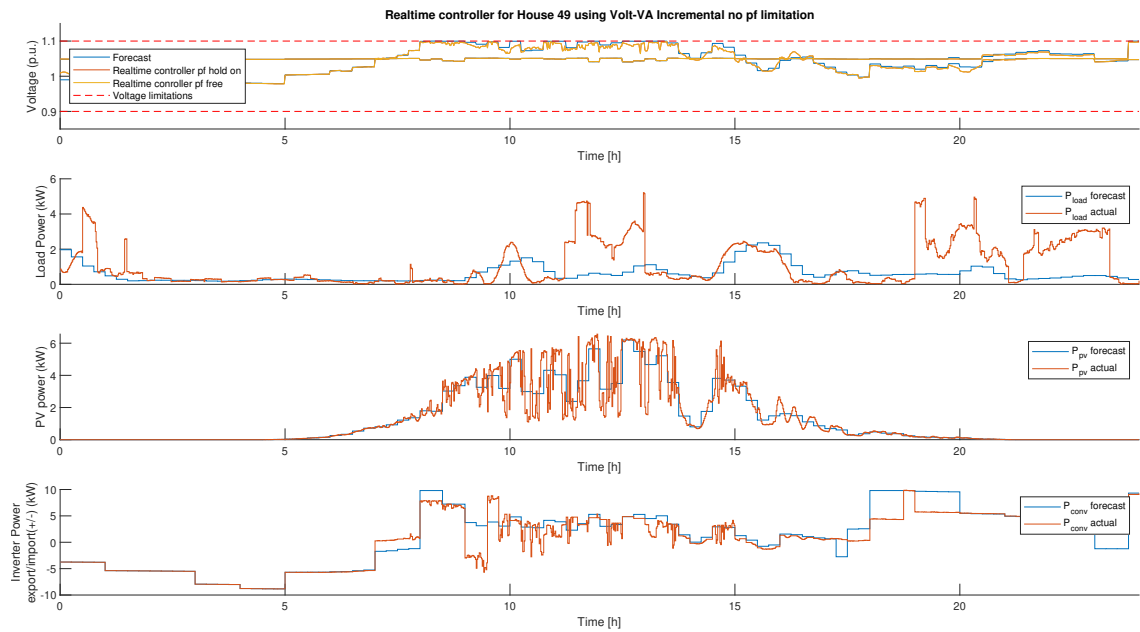


Figure 7.39: Forecasted and real-time voltage profile (top), forecasted and actual load demand at the house (middle top), forecasted and actual PV generation at the house (middle bottom), and forecasted and actual import and export of energy by the multi-port converter (bottom) on day 185 with 20 multi-port converter, using the Volt-VA incremental correction method with no power factor restrictions for the forecast.

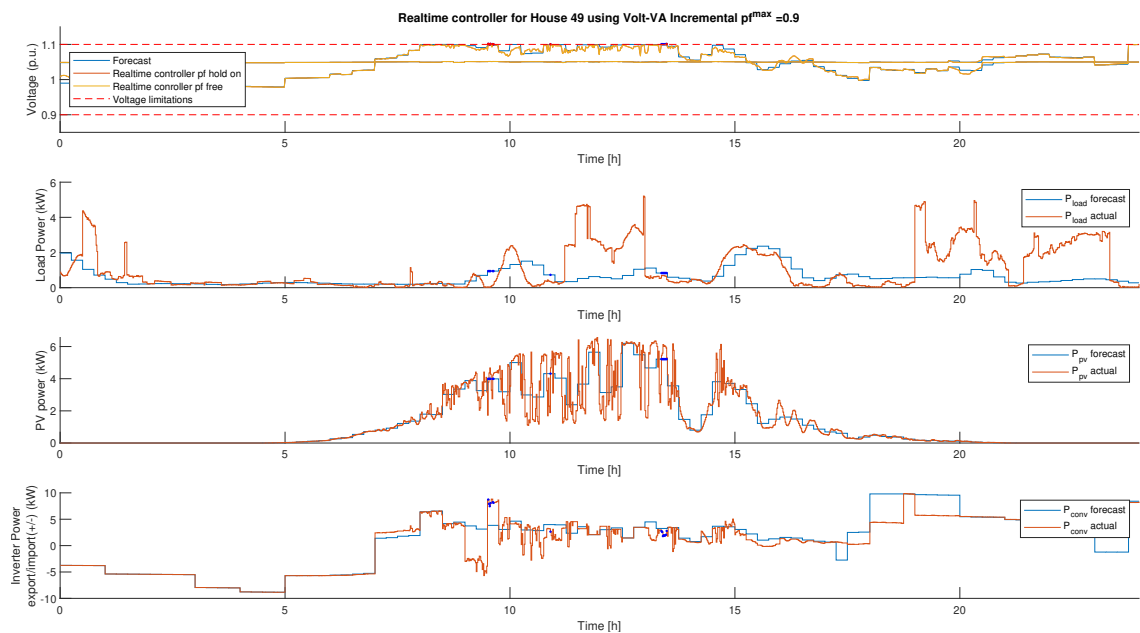


Figure 7.40: Forecasted and real-time voltage profile (top), forecasted and actual load demand at the house (middle top), forecasted and actual PV generation at the house (middle bottom), and forecasted and actual import and export of energy by the multi-port converter (bottom) on day 185 with 20 multi-port converter, using the Volt-VA incremental correction method with power factor restrictions for the forecast. Removal of the voltage violation is only possible if the original reactive power setpoint is used. If the real-time controller obey the power factor, a voltage violation occurs (blue dots). Red dots indicate that even if the power factor is not enforced, a voltage violation still occurs.

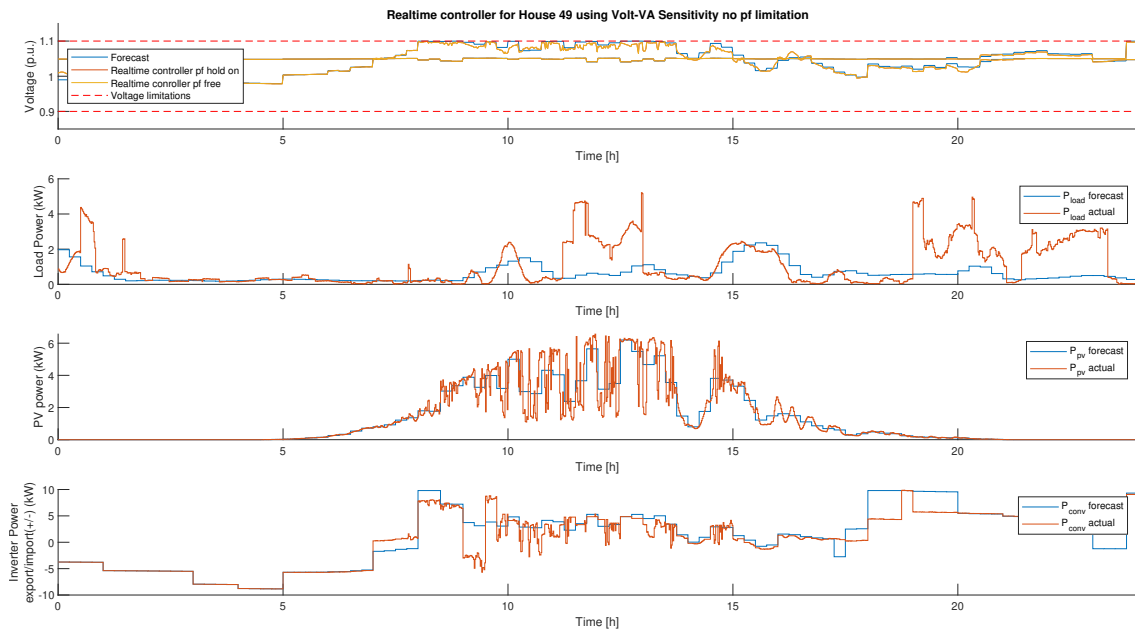


Figure 7.41: Forecasted and real-time voltage profile (top), forecasted and actual load demand at the house (middle top), forecasted and actual PV generation at the house (middle bottom), and forecasted and actual import and export of energy by the multi-port converter (bottom) on day 185 with 20 multi-port converter, using the Volt-VA sensitivity correction method with no power factor restrictions for the forecast.

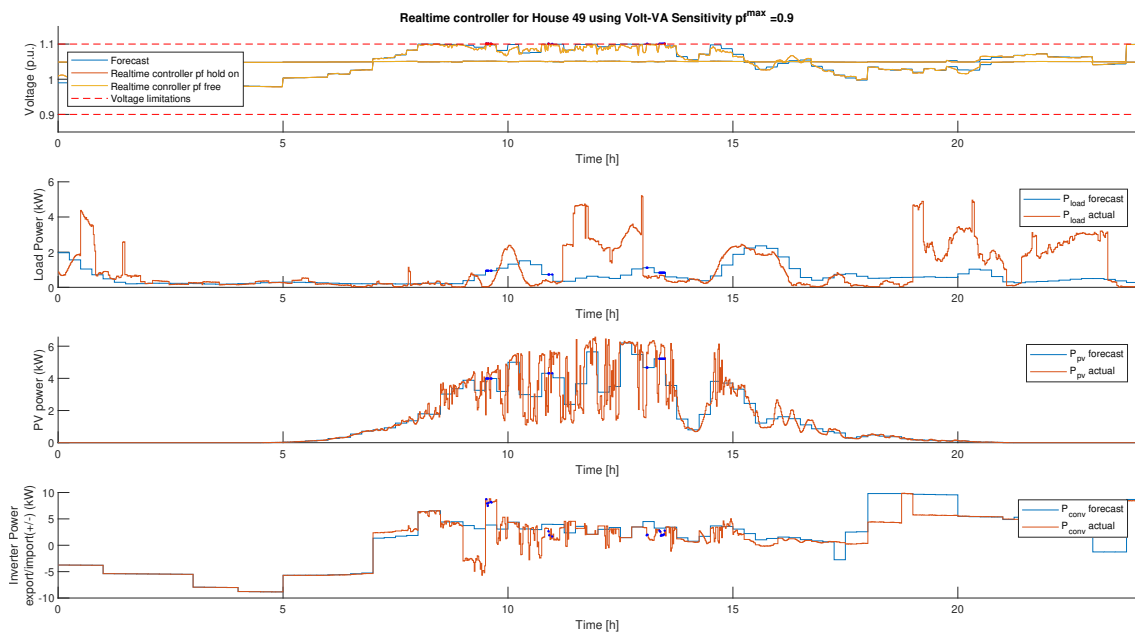


Figure 7.42: Forecasted and real-time voltage profile (top), forecasted and actual load demand at the house (middle top), forecasted and actual PV generation at the house (middle bottom), and forecasted and actual import and export of energy by the multi-port converter (bottom) using the Volt-VA sensitivity correction method with power factor restrictions for the forecast. Removal of the voltage violation is only possible if the original reactive power setpoint is used. If the real-time controller obey the power factor, a voltage violation occurs (blue dots). Red dots indicate that even if the power factor is not enforced, a voltage violation still occurs.

7.3. Winter day

In the winter, voltage violations may occur due to the increase in the energy demand for heating. Two scenarios are picked: scenario one, where the majority (45) of the houses in the distribution network have a multi-port converter and scenario two, where the minority (20) of the houses in the distribution network have a multi-port converter. The numbers 45 and 20 have been randomly picked.

Day 1 has been chosen as winter days have a higher energy demand. The PV generation is shown in Figure 7.43. Figure 7.44 shows the benchmark of the day. As shown, the network without a multi-port converter is insufficient to cope with the energy demand of the EV.

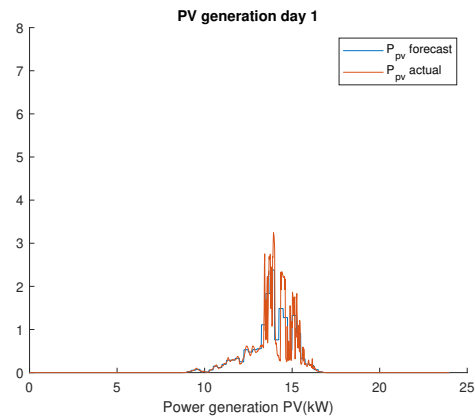


Figure 7.43: The average forecasted and actual PV profile of day 1 (winter).

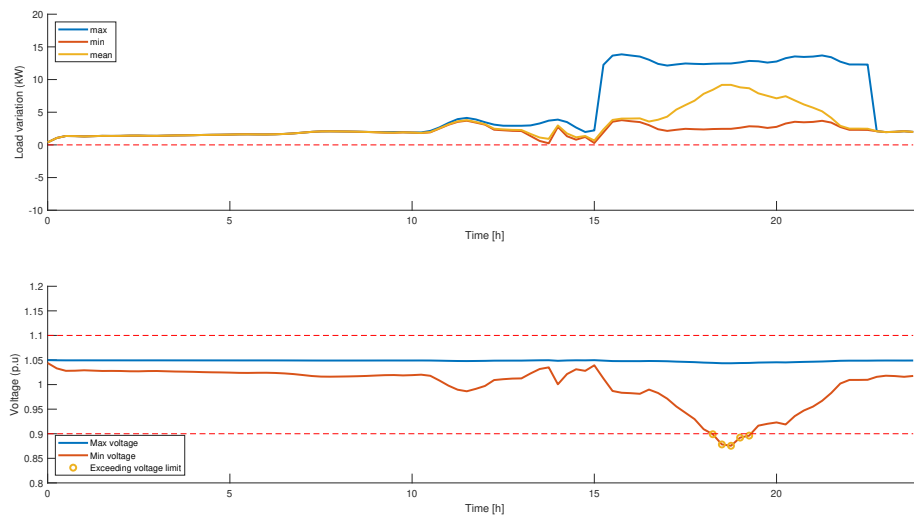


Figure 7.44: Load variation (top) and voltage profile (bottom). The load variation show a large demand of power between 3 PM and 10 PM, caused by EV charging, creating voltage violations.

7.3.1. Winter day with many multi-port converters (45)

Figure 7.45 shows the load variation, voltage profile and price alterations of the VMS before adding P_{conv} of the multi-port converter. This is done, as stated in Section 5.3, to prevent voltage violations in the network. The step is the "Voltage based price" in Figure 5.19. An reduction in energy demand from 4 PM till 11 PM (EV charging). There are no voltage violations, and therefore the price does not have to change.

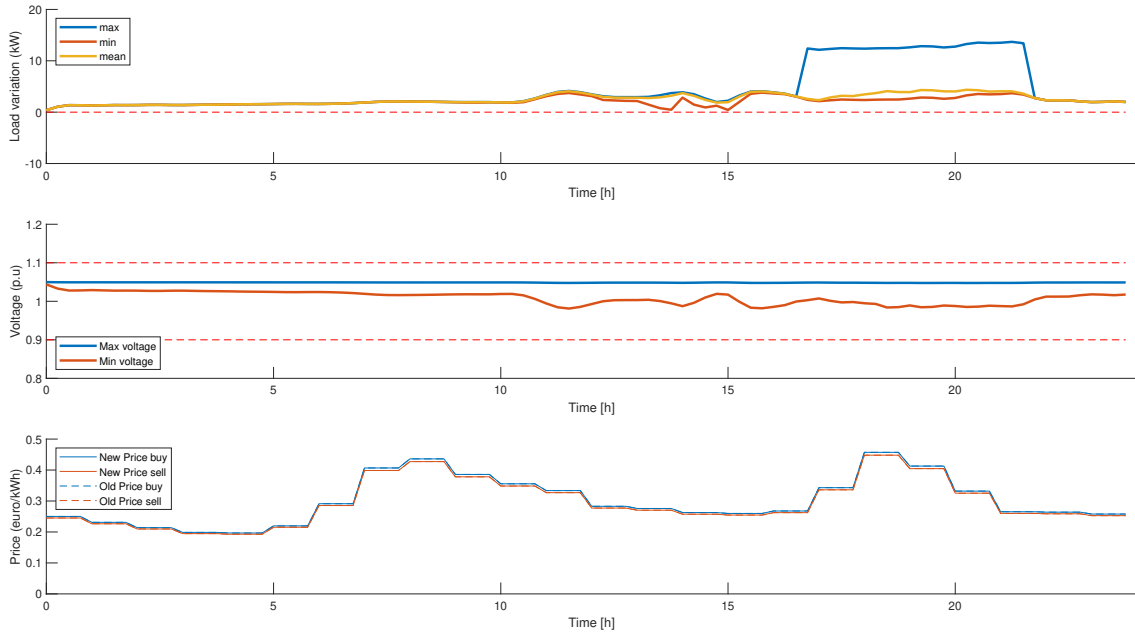


Figure 7.45: Load variation (top), voltage profile (middle), and price correction mechanism (bottom) before the multi-port converter energy demand P_{conv} is added.

Figure 7.46, shows the first iteration of the optimal charging algorithm of house number 49. This is step "EMS House" in Figure 5.19. This house has been randomly selected. No correction has taken place, therefore no variation between the correction methods are obtained.

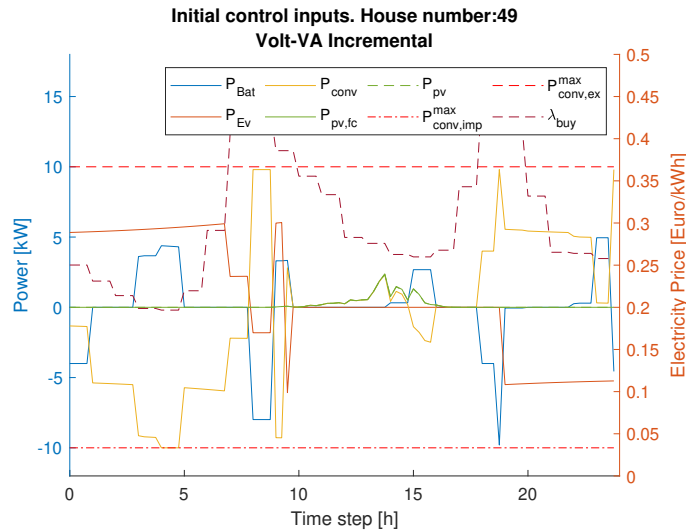


Figure 7.46: The optimal control inputs of the EMS before the correction methods are used.

The Figures 7.47 (Volt-Watt), 7.48 (Volt-VAR Incr (no pf)), 7.49 (Volt-VAR Incr (pf=0.9)), 7.50 (Volt-VAR Sens (no pf)) and 7.51 (Volt-VAR Sens (pf=0.9)) show the initial voltage violations caused by the demand of the multi-port converter.

These figures combine the step "Voltage profile computation" and the correction method step from Figure 5.19. These figures show that if no VMS was designed, all the multi-port converters want to buy energy at the lowest price (see Figure 7.46), resulting in voltage violations.

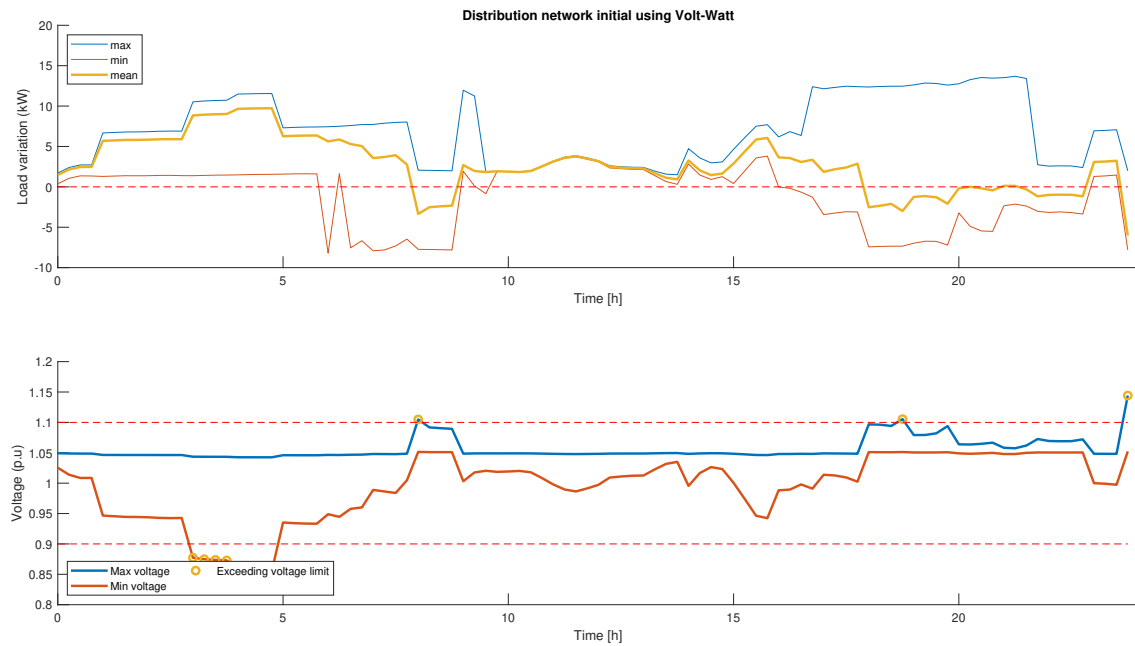


Figure 7.47: Load variation (top) and voltage profile (bottom). Initial voltage profile after adding the multi-port converter energy demand P_{conv} using the Volt-Watt method on day 1 with 45 multi-port converters.

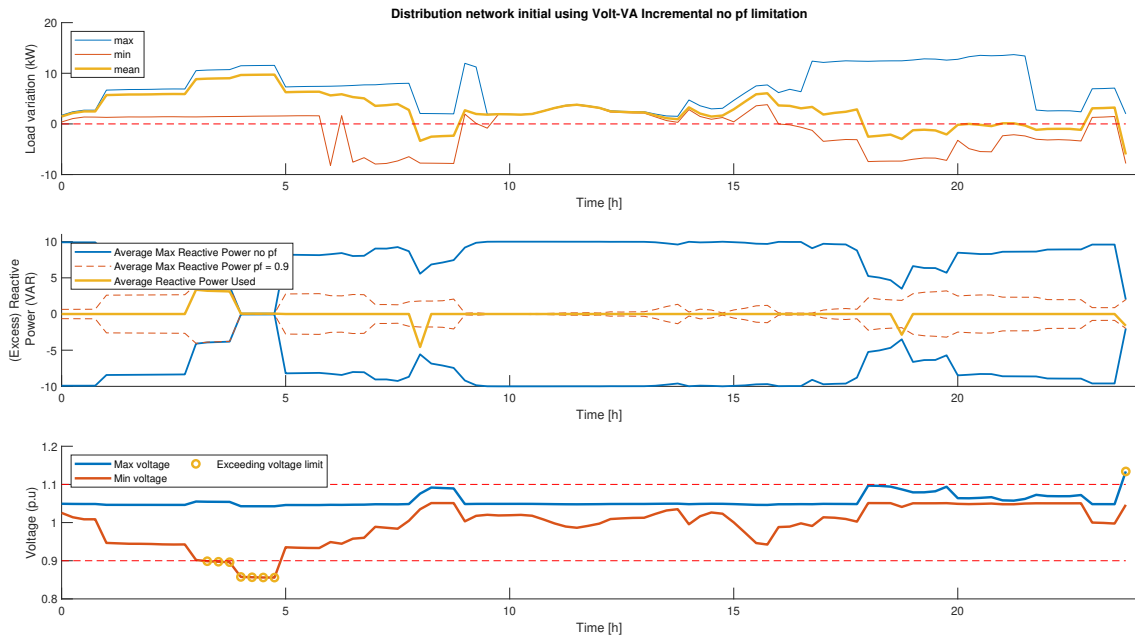


Figure 7.48: Load variation (top), reactive power usage Q_{conv} and availability Q_{conv}^{max} (middle), and voltage profile (bottom). Initial voltage profile after adding the multi-port converter energy demand P_{conv} using the Volt-VAR incremental method on day 1 with 45 multi-port converters. Reactive power compensation, with no restriction, has already been added.

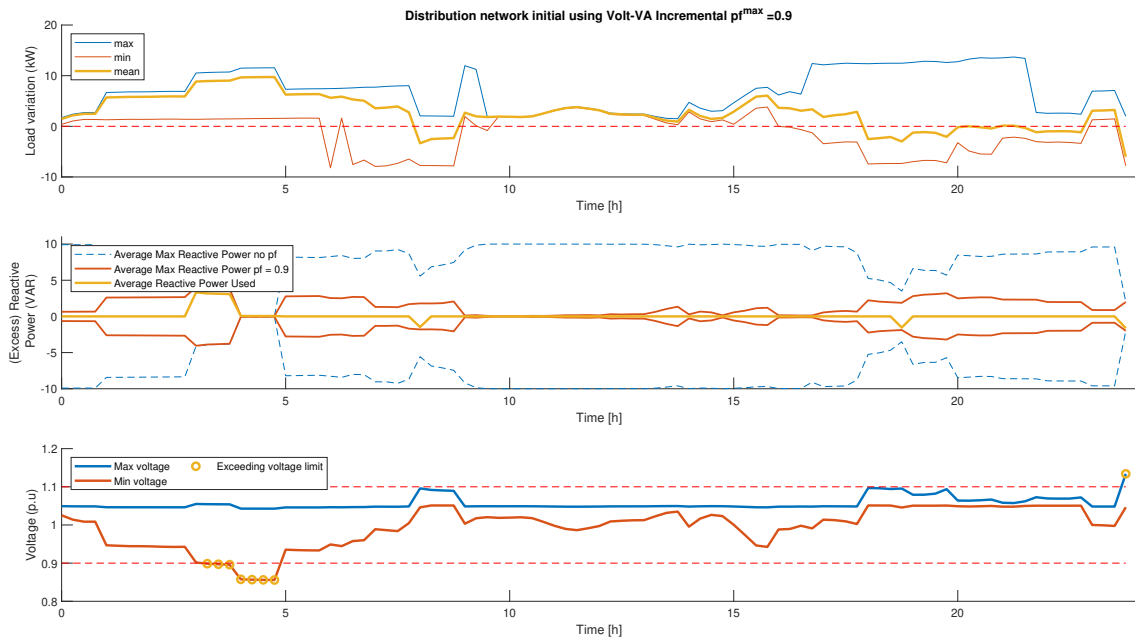


Figure 7.49: Load variation (top), reactive power usage Q_{conv} and availability Q_{conv}^{max} (middle), and voltage profile (bottom). Initial voltage profile after adding the multi-port converter energy demand P_{conv} using the Volt-VAR incremental method on day 1 with 45 multi-port converters. Reactive power compensation, with power factor restriction, has already been added.

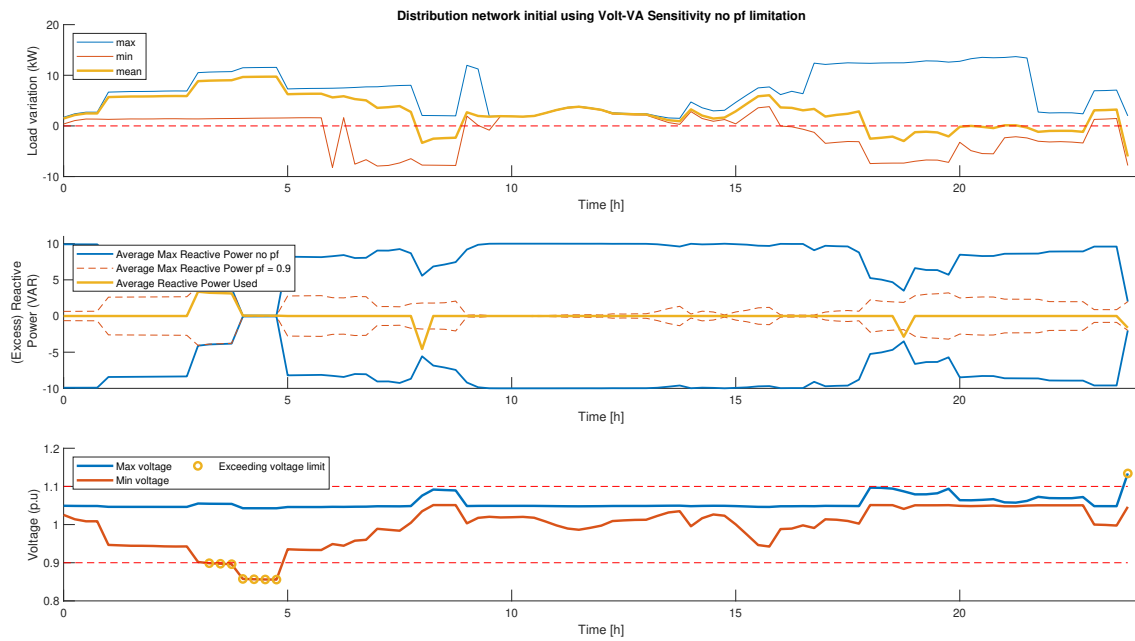


Figure 7.50: Load variation (top), reactive power usage Q_{conv} and availability Q_{conv}^{max} (middle), and voltage profile (bottom). Initial voltage profile after adding the multi-port converter energy demand P_{conv} using the Volt-VAR sensitivity method on day 1 with 45 multi-port converters. Reactive power compensation, with no restriction, has already been added.

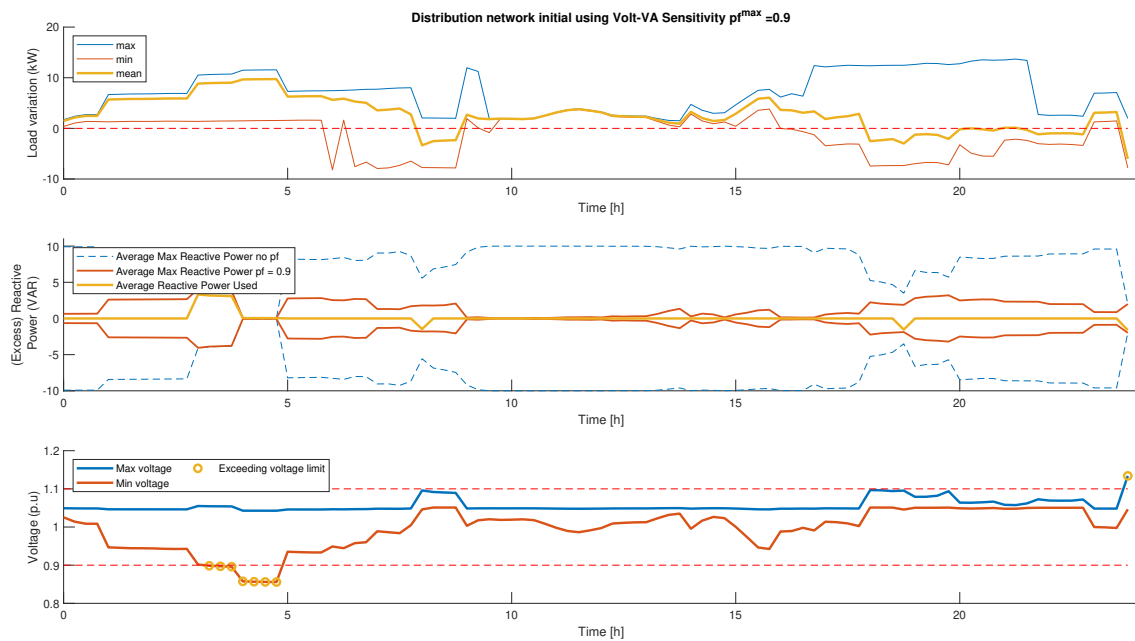


Figure 7.51: Load variation (top), reactive power usage Q_{conv} and availability Q_{conv}^{max} (middle), and voltage profile (bottom). Initial voltage profile after adding the multi-port converter energy demand P_{conv} using the Volt-VAR sensitivity method on day 1 with 45 multi-port converters. Reactive power compensation, with power factor restriction, has already been added.

The Figures 7.52 (Volt-Watt), 7.53a (Volt-VAR Incr (no pf)), 7.53b (Volt-VAR Incr (pf=0.9)), 7.54a (Volt-VAR Sens (no pf)) and 7.54b (Volt-VAR Sens (pf=0.9)), show the final iteration of the optimal charging algorithm of house number 49.

Limited difference can be spotted between Figure 7.52 (Volt-Watt) and the Volt-VA methods shown in Figure 7.53 and 7.54.

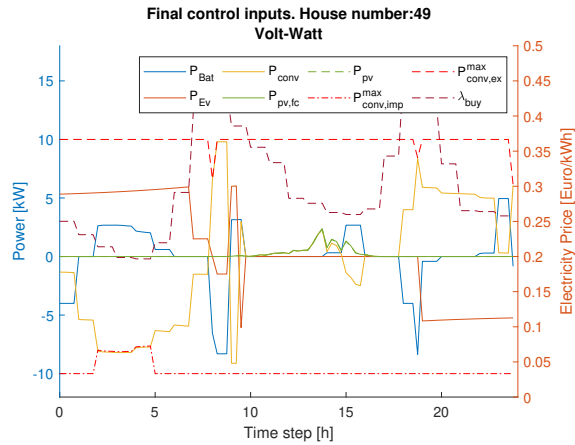
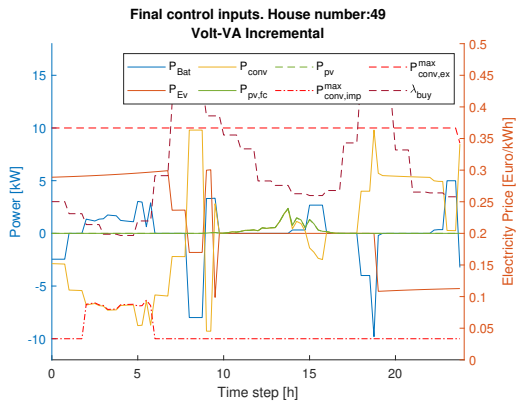
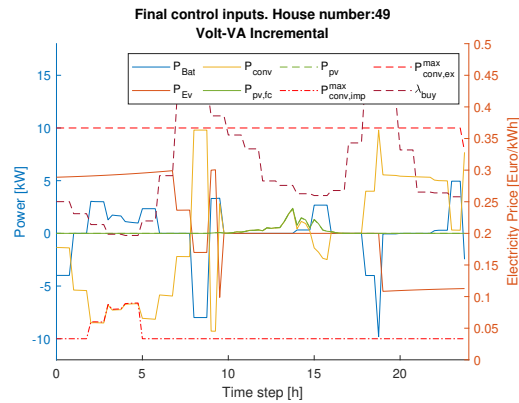


Figure 7.52: The final optimal control inputs using the Volt-Watt correction method.

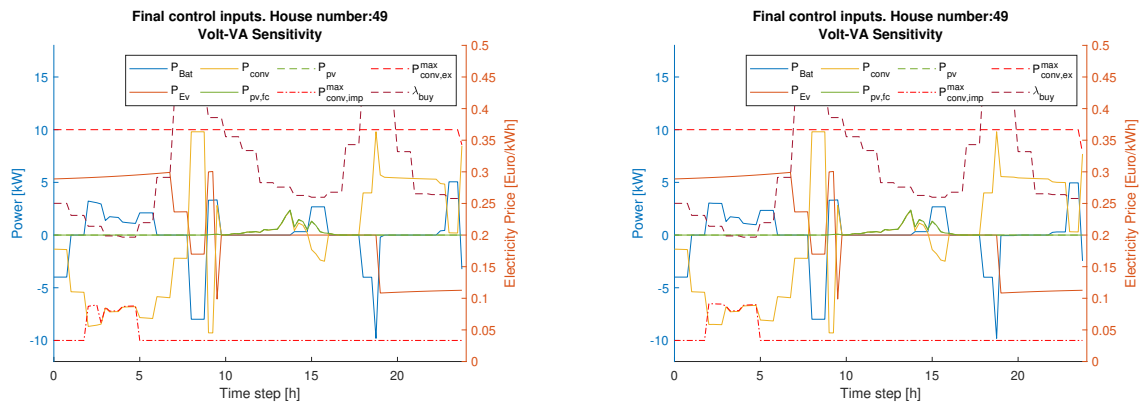


(a) The final optimal control inputs using the Volt-VA incremental correction method with no power factor restriction.



(b) The final optimal control inputs using the Volt-VA incremental correction method with power factor restriction.

Figure 7.53: The final optimal control inputs using the Volt-VA incremental correction method without (Figure 7.53a) and with (Figure 7.53b) power factor restriction.



(a) The final optimal control inputs using the Volt-VA sensitivity correction method with no power factor restriction.

(b) The final optimal control inputs using the Volt-VA sensitivity correction method with power factor restriction.

Figure 7.54: The final optimal control inputs using the Volt-VA sensitivity correction method without (Figure 7.54a) and with (Figure 7.54b) power factor restriction.

The Figures 7.55 (Volt-Watt) ,7.56 (Volt- VAR Incr (no pf)), 7.57(Volt- VAR Incr (pf=0.9)),7.58 (Volt- VAR Sens (no pf)) and 7.59 (Volt- VAR Sens (pf=0.9)) show the forecasted load demands and corrected voltage profile. As all the voltage violations have been corrected, the VMS procedure in Figure 5.19 is done.

No major differences are found between the correction methods.

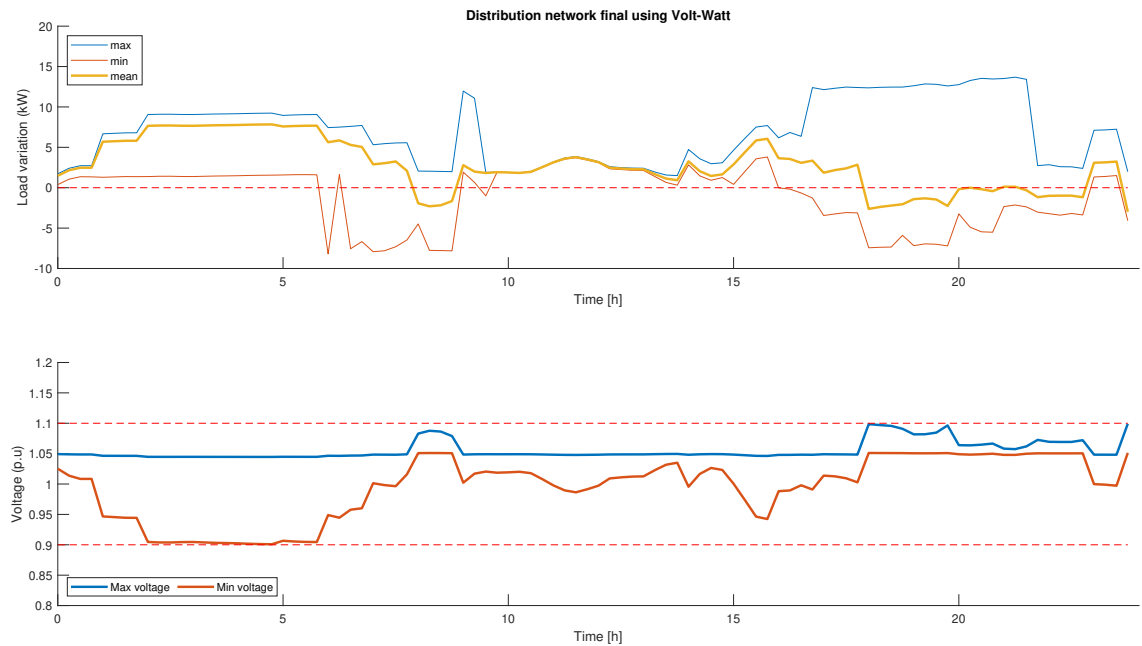


Figure 7.55: Final voltage profile after the correction iterative procedure. All voltage violations in the forecast have been removed by using the Volt-Watt method on day 1 with 45 multi-port converter.

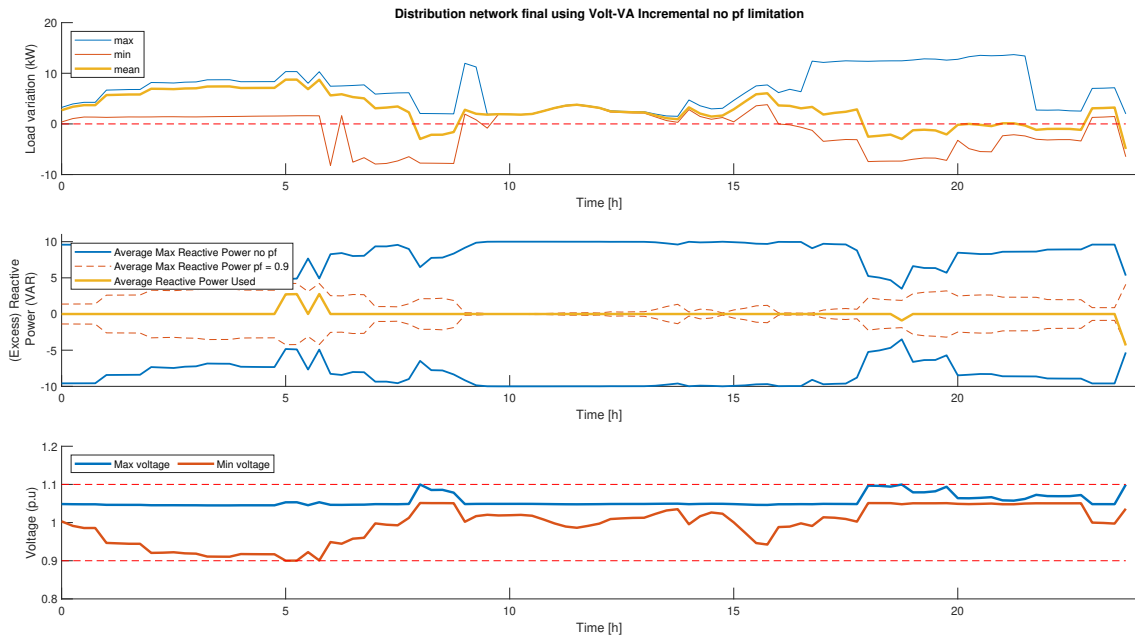


Figure 7.56: Final voltage profile after the correction iterative procedure. All voltage violations in the forecast have been removed by using the Volt-VA incremental method with no power factor restrictions, on day 1 with 45 multi-port converter.

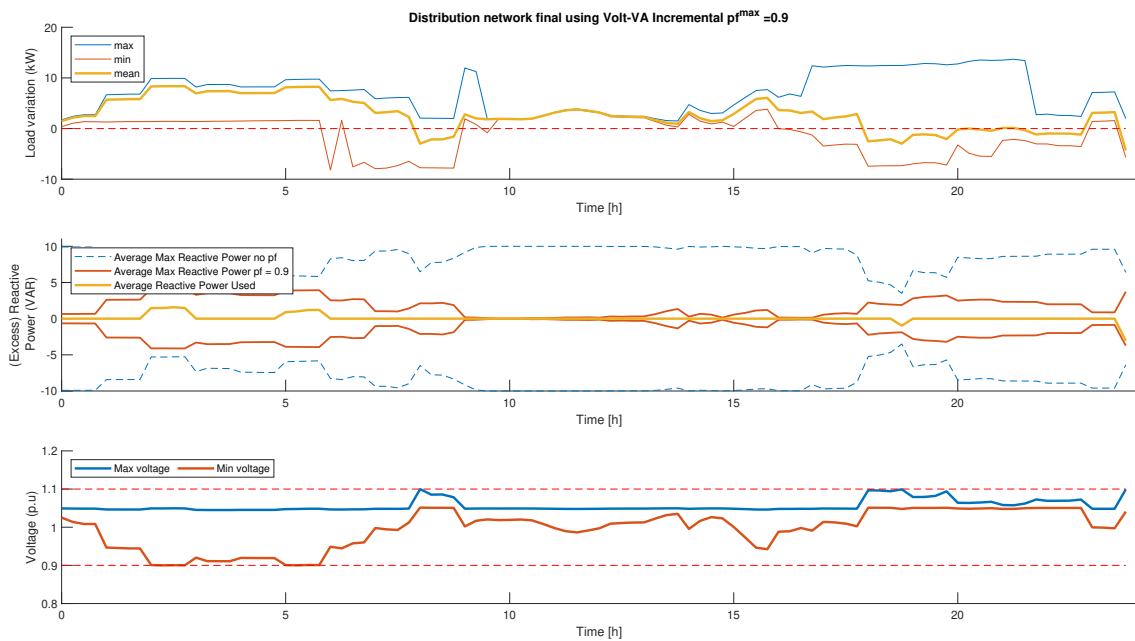


Figure 7.57: Final voltage profile after the correction iterative procedure. All voltage violations in the forecast have been removed by using the Volt-VA incremental method with power factor restrictions, on day 1 with 45 multi-port converter.

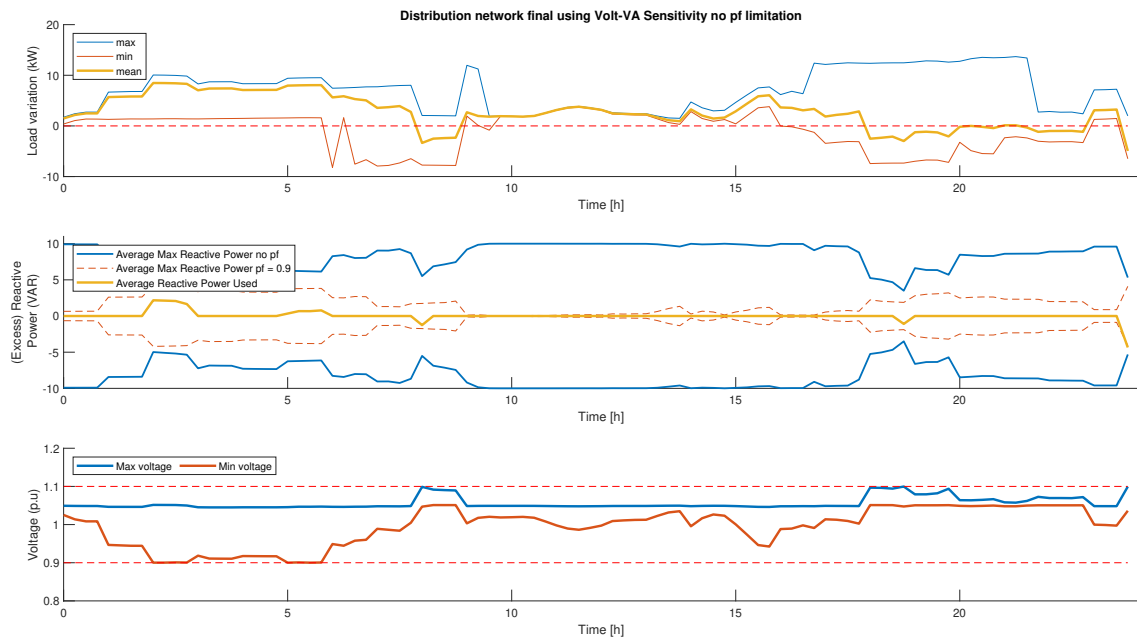


Figure 7.58: Final voltage profile after the correction iterative procedure. All voltage violations in the forecast have been removed by using the Volt-VA sensitivity method with no power factor restrictions, on day 1 with 45 multi-port converter.

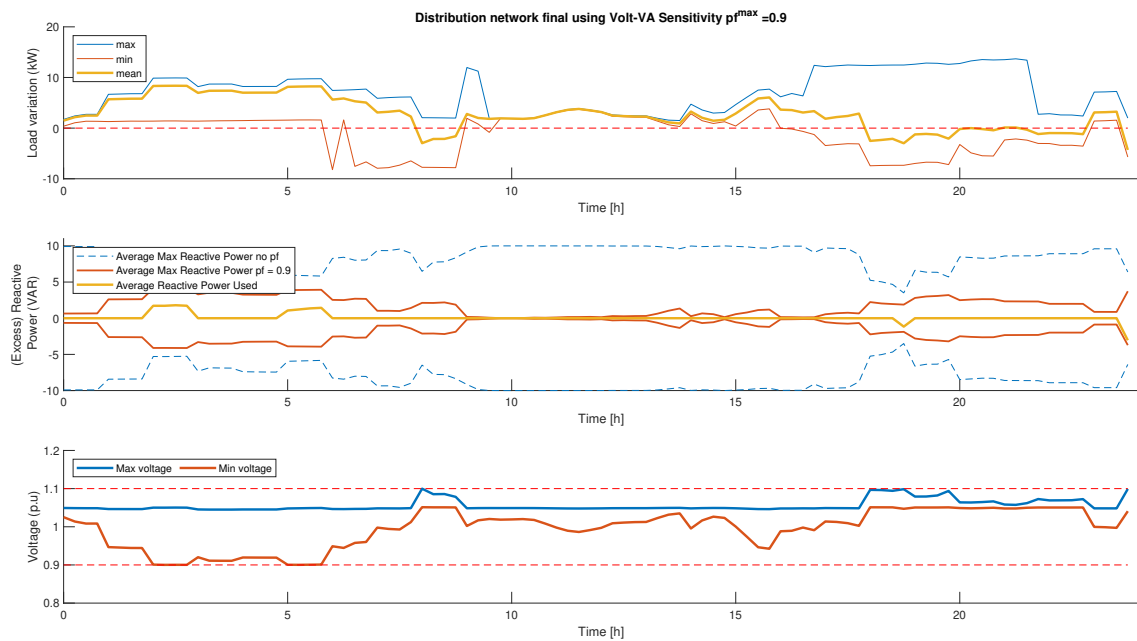


Figure 7.59: Final voltage profile after the correction iterative procedure. All voltage violations in the forecast have been removed by using the Volt-VA sensitivity method with power factor restrictions, on day 1 with 45 multi-port converter.

The Figures 7.60 (Volt-Watt), 7.61 (Volt-VAR Incr (no pf)), 7.62(Volt-VAR Incr (pf=0.9)), 7.63 (Volt-VAR Sens (no pf)) and 7.64 (Volt-VAR Sens (pf=0.9)) show the final result after the real-time controller. Volt-Watt, Volt-VA incremental (no pf) and Volt-VA sensitivity (no pf) can remove most of the voltage violation using the real-time controller. An example where the real-time controller cannot correct the voltage is shown in the right corner of Figure 7.60 till 7.64. This error is possible as the multi-port converter can only correct their house load error, as they do not know anything about the other houses. In practice, this particular error will not occur. As the moving horizon continues, the control input will change, and the corresponding energy demand will too. The voltage violations of Volt-VA incremental and Volt-VA sensitivity are negligible.

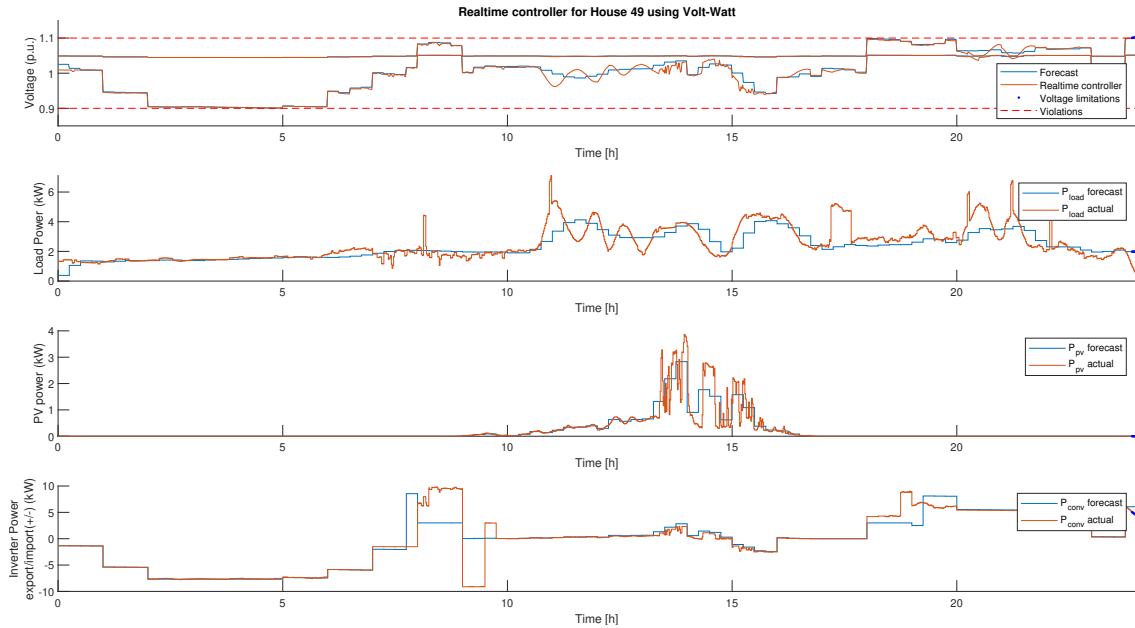


Figure 7.60: Forecasted and real-time voltage profile (top), forecasted and actual load demand at the house (middle top), forecasted and actual PV generation at the house (middle bottom), and forecasted and actual import and export of energy by the multi-port converter (bottom) on day 1 with 45 multi-port converter, using the Volt-Watt correction method for the forecast.

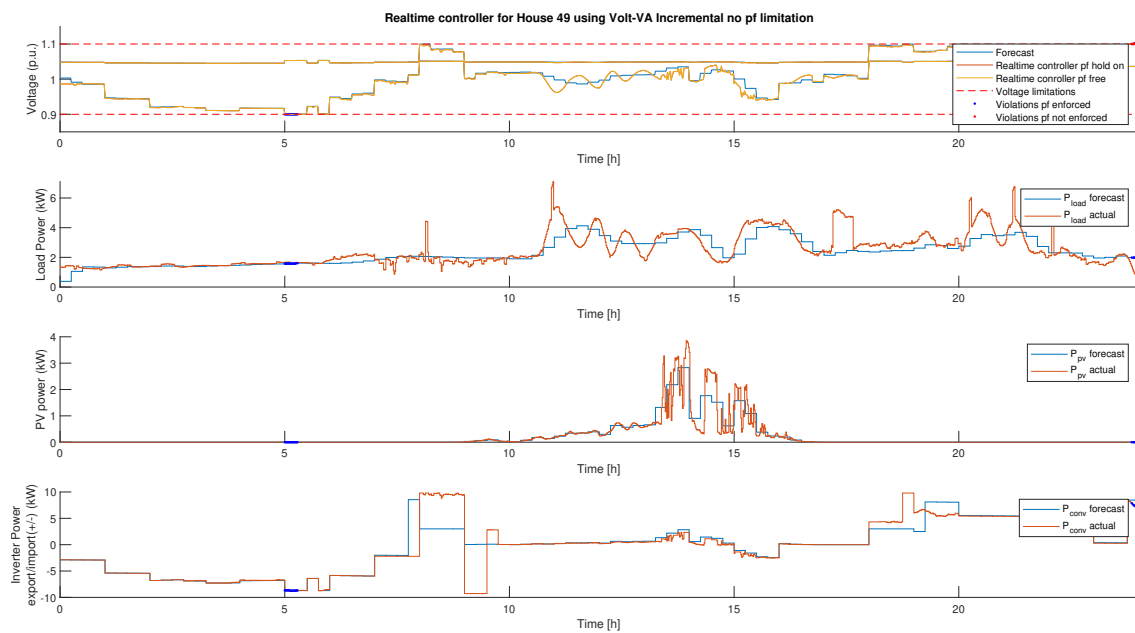


Figure 7.61: Forecasted and real-time voltage profile (top), forecasted and actual load demand at the house (middle top), forecasted and actual PV generation at the house (middle bottom), and forecasted and actual import and export of energy by the multi-port converter (bottom) on day 1 with 45 multi-port converter, using the Volt-VA incremental correction method with no power factor restrictions for the forecast.

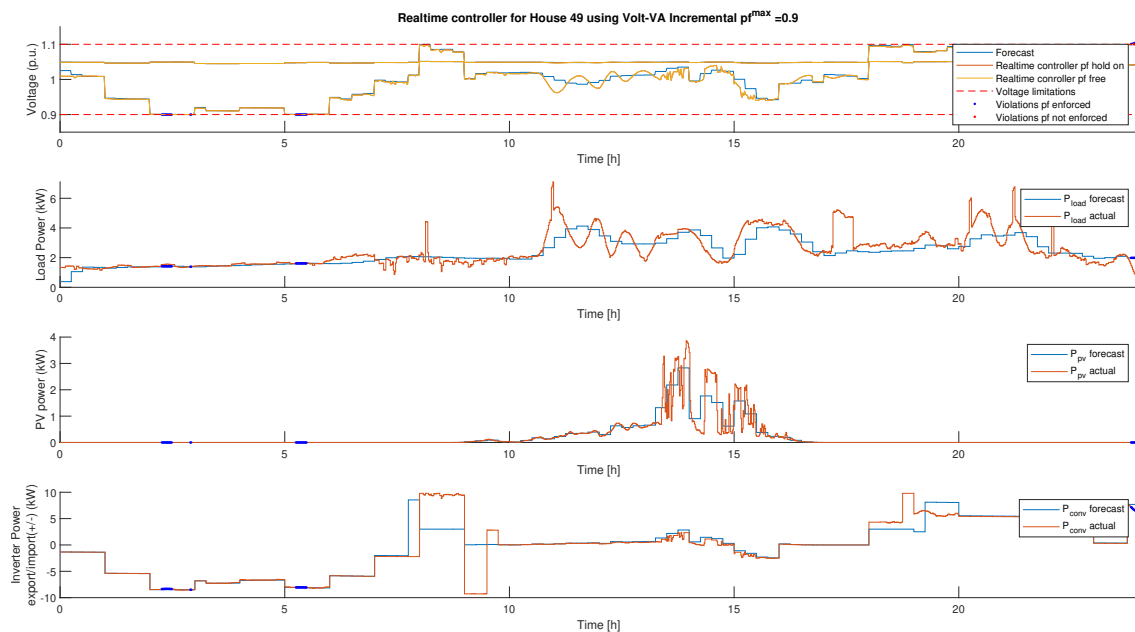


Figure 7.62: Forecasted and real-time voltage profile (top), forecasted and actual load demand at the house (middle top), forecasted and actual PV generation at the house (middle bottom), and forecasted and actual import and export of energy by the multi-port converter (bottom) on day 1 with 45 multi-port converter, using the Volt-VA incremental correction method with power factor restrictions for the forecast. Removal of the voltage violation is only possible if the original reactive power setpoint is used. If the real-time controller obey the power factor, a voltage violation occurs (blue dots).

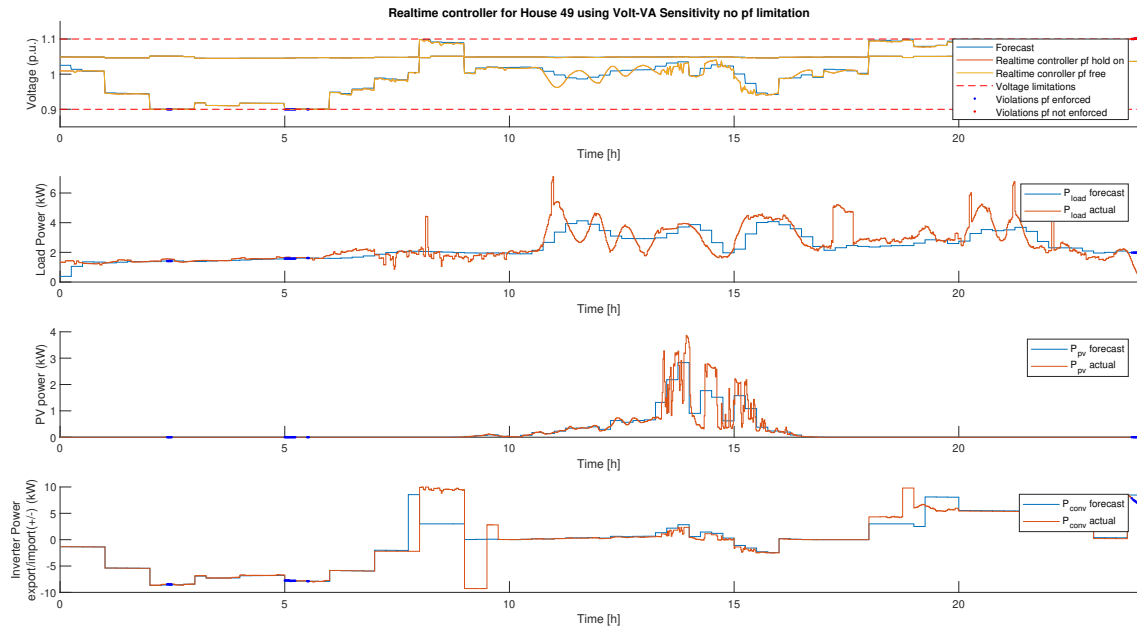


Figure 7.63: Forecasted and real-time voltage profile (top), forecasted and actual load demand at the house (middle top), forecasted and actual PV generation at the house (middle bottom), and forecasted and actual import and export of energy by the multi-port converter (bottom) on day 1 with 45 multi-port converter, using the Volt-VA sensitivity correction method with no power factor restrictions for the forecast.

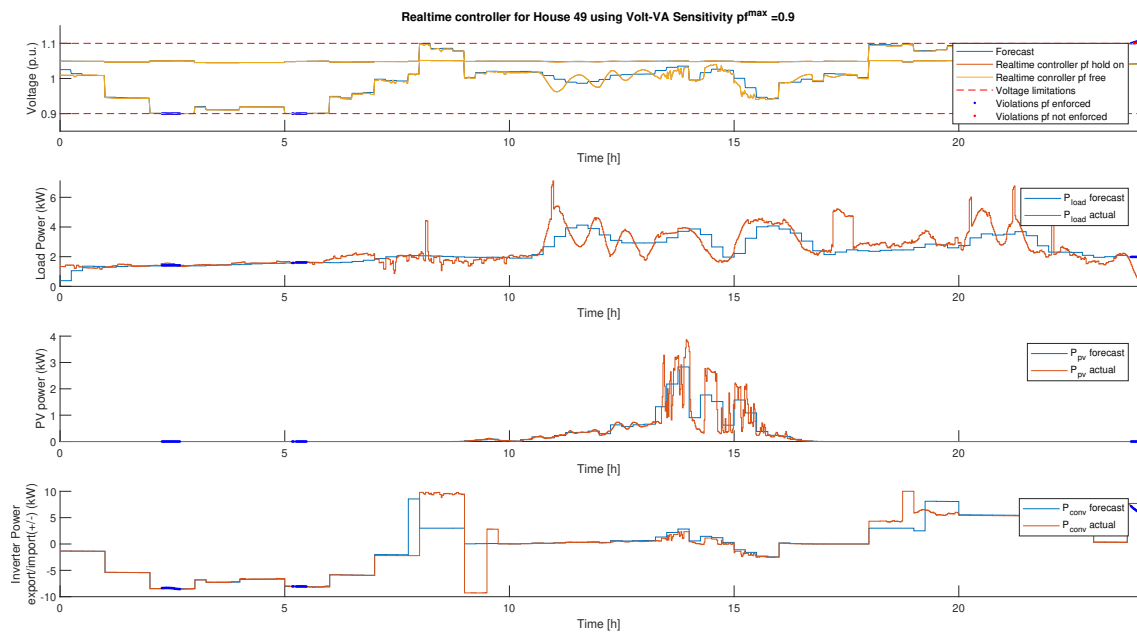


Figure 7.64: Forecasted and real-time voltage profile (top), forecasted and actual load demand at the house (middle top), forecasted and actual PV generation at the house (middle bottom), and forecasted and actual import and export of energy by the multi-port converter (bottom) using the Volt-VA sensitivity correction method with power factor restrictions for the forecast. Removal of the voltage violation is only possible if the original reactive power setpoint is used. If the real-time controller obey the power factor, a voltage violation occurs (blue dots).

7.3.2. Winter day with few multi-port converters(20)

Figure 7.65 shows the load variation and the voltage profile after adding the demand of the multi-port converters P_{conv} . As shown in the Figure no possible voltage violations can occur. No corrections are necessary. The real-time controller output is shown in Figure 7.66

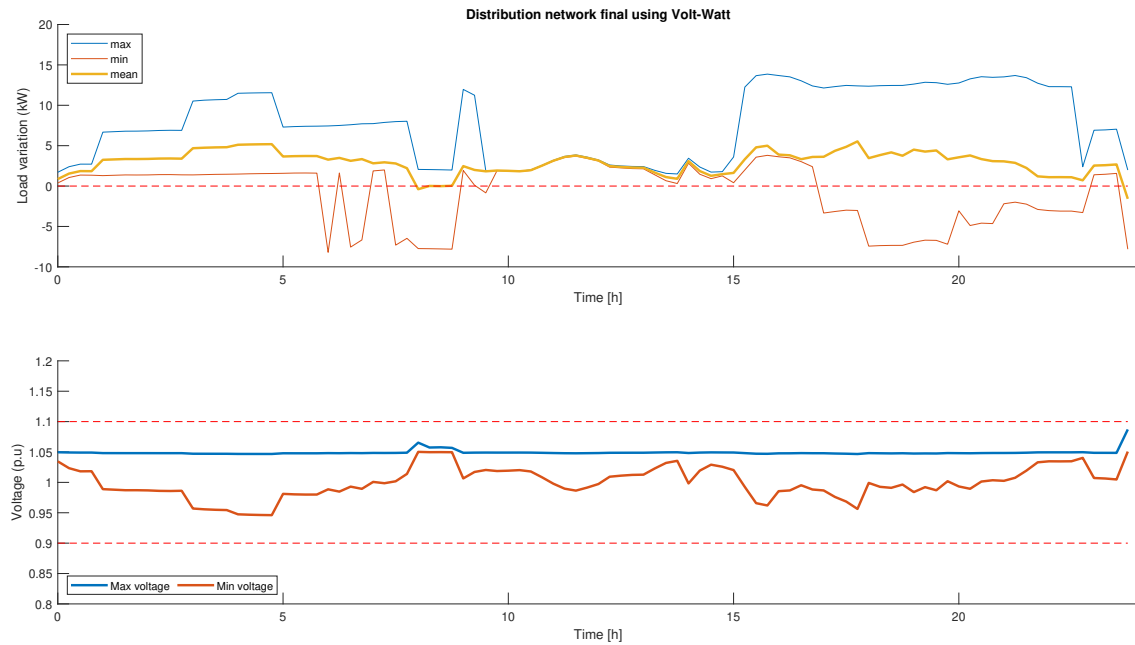


Figure 7.65: Load variation (top), voltage profile (bottom). No voltage violation occurs.

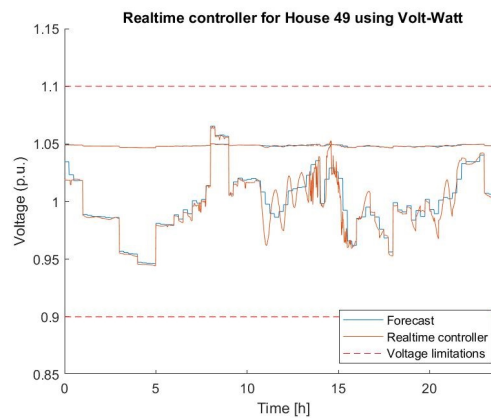


Figure 7.66: The real-time voltage profile on day 1 with 20 multi-port converters.

7.4. Moving horizon window

An essential requirement for voltage prevention and deviation is that the values in the system are continuously updated. Using a moving horizon window makes this possible. Figures 7.67,7.68,7.69,7.70, and 7.71 show the impact of the PV error on the components of the multi-port converter and the limited impact on the BESS and EV charge state. In this scenario, day 185 has been picked with 20 multi-port converters.

All figures show the forecasted and actual inputs of the BESS state (top-left), the EV state (top-right), the (dis)charging rate of BESS (middle-left), the (dis)charging rate of EV (middle-right), the PV generation (bottom-left), and the import and export of the multi-port converter (bottom-right).

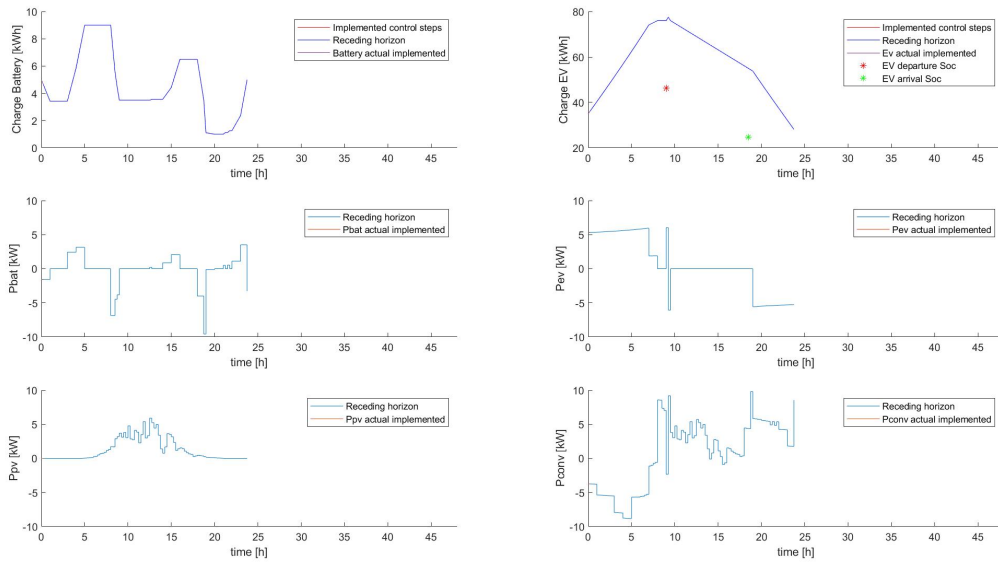


Figure 7.67: Moving horizon at timestep 1.

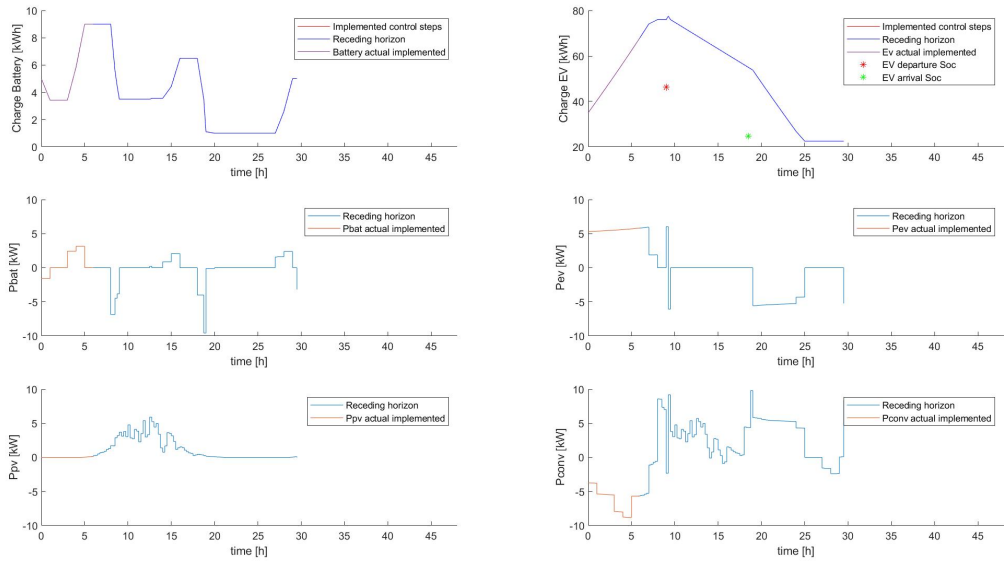


Figure 7.68: Moving horizon at timestep 24 (6AM)

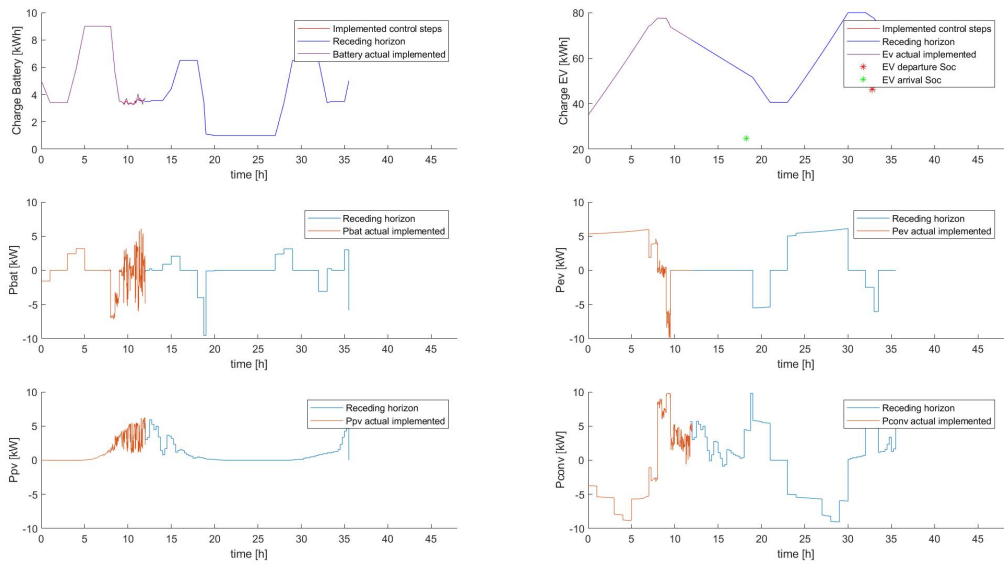


Figure 7.69: Moving horizon at timestep 48 (12AM)

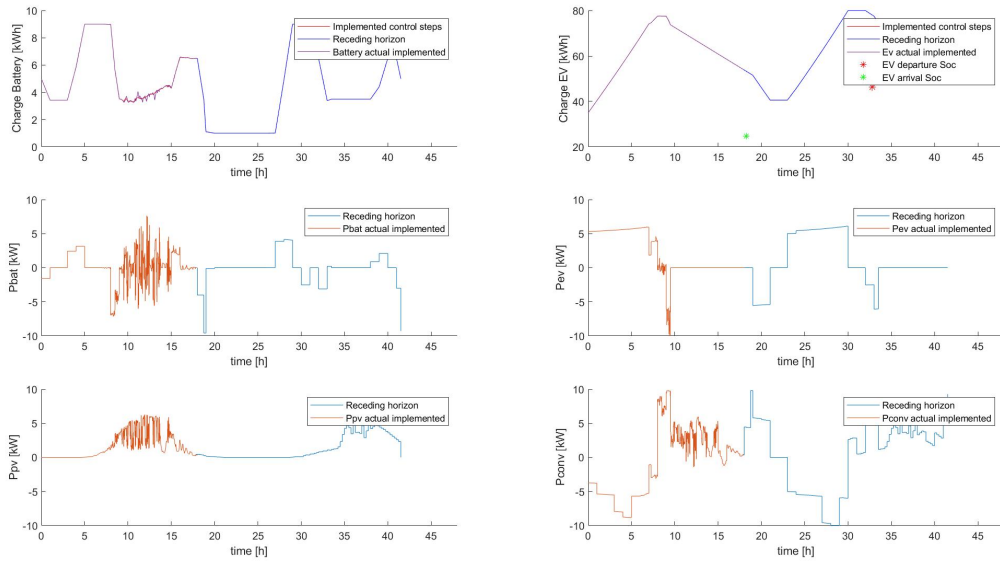


Figure 7.70: Moving horizon at timestep 72 (6PM)

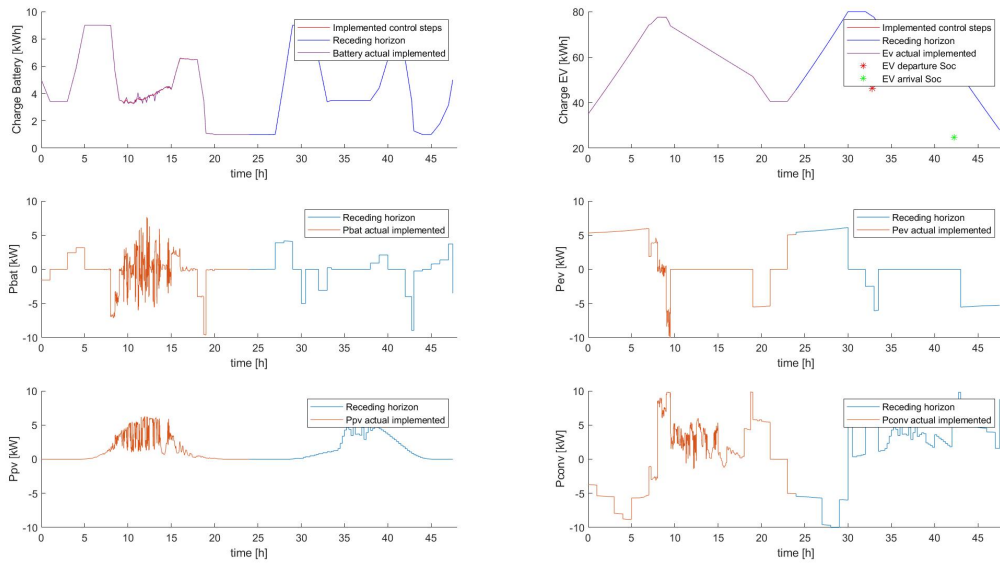


Figure 7.71: Moving horizon at timestep 96 (12PM)

Conclusion and Future work

8.1. Conclusions

The expected increase in energy consumption and generation in the distribution network will threaten voltage stability if not properly managed. If the DSO does not want to enhance the current grid, the network capacity needs to be optimally used.

This thesis aims to develop a control structure that can utilise this capacity while preventing voltage violations. By using a multi-port converter, a structure is available for various voltage correction and prevention methods. Furthermore, the converter's energy management system optimises costs for the users, creating an initiative for both DSO and consumers. The multi-port converter can combine the Volt-Watt and Volt-VAR correction methods, which is absent in the literature. Moreover, by using a moving horizon window, many of the hazards can be averted in advance. Due to the uncertainty in forecasting data, additional real-time controllers and reference trackers had to be made.

The combination of using Volt-Watt and Volt-VAR usually is unheard of due to the loss of energy, as its primarily used in PV systems. More control over the voltage has been achieved by using the multi-port converter than the popular Volt-VAR method.

Numerical experiments have shown that Volt-Watt, Volt-VA sensitivity (with or without power factor restrictions), and Volt-VA incremental (with or without power factor restrictions) can correct the voltage in the forecast. The difference between the sensitivity and incremental Volt-VA show no considerable advantages. The Volt-VAR as a correction method is less capable of preventing voltage deviation. Furthermore, enabling price fluctuations to facilitate multi-port converters to buy excess energy or feed-in power during peak hours prevents voltage violations.

The first sub-goal of this thesis, making it gradually possible, has succeeded. Even with a reduced amount of multi-port converters, the voltage can be rectified. However, this is heavenly dependent on the accuracy of the data. The second sub-goal is to implement real-time control to correct the voltage over a short period. The real-time controller showed capable of removing voltage hazards by compensating using active power. Reducing the power factor can result in miscalculation by the real-time controller due to a mismatch between the real-time converter and the reactive power setpoints.

8.2. Future Work

This section list the possibilities for future work:

- In this thesis, various parameters (e.g. battery size, converter limits) have a predefined value. An optimisation could be made to calculate the amount of capacity needed for the converter to guarantee stability.
- The heat pump in this thesis is considered a non-flexible load. An optimisation scheme could be integrated into the EMS to incorporate the energy demand and schedule the heating and cooling of the house. Furthermore, the heat pump could be used to decrease the impact of the forecasting error by using the heat pump as a load if too much PV energy is generated.
- Using voltage unbalance. In this thesis, the voltage is assumed to be balanced. This is assumed as all the significant loads are balanced (heat pump, P_{conv} with multi-port converter and P_{ev} and P_{pv} without multi-port converter). As most residential loads (e.g. appliances) are unbalanced, it can be assumed the network is unbalanced too. Additional work can be done as the amount of power through each line can be measured. As the multi-port converter in almost all scenarios has extra

power left in the converter, it can be optimally divided, amongst the phases, to counteract the voltage unbalance.

- Although a large time scale from 24h to real-time has been considered in this thesis, the voltage spikes are not considered. A significant benefit of the proposed control structure is the additional V_{mag} that is sent to each house. This information can prevent such voltage spikes, as the multi-port converter has a reference voltage it should obey. Future work could include a control scheme that uses the V_{mag} computed by the VMS to prevent voltage spikes.
- In this thesis, only voltage violations have been taken into account. To prevent congestion in a distribution network, the current flow should also be taken into consideration. However, this can be implemented quickly due to the correlation between voltage and current. Additionally to the voltage correction in the VMS, the current is calculated and corrected using an adaption of the VMS.
- The compensation for real-time control is done by using a linear coefficient. This works by using the selection method applied in this thesis but would not work if the houses were randomly selected. Future work would include composing a method that can determine this needed ratio.
- When the EV is unavailable, the reserved BESS capacity to guarantee maximum (dis)charging capacity is not always needed. A scheme can be developed to reserve the needed capacity based on additional factors.

A

IEEE European Low Voltage Test Feeder

The Line characteristics are summarised in Table A.1. Figure A.1 shows the single line diagram of the IEEE European Low voltage Test Feeder by cable type.

Table A.1: Cable types used in the IEEE European Low voltage test feeder with corresponding Resistance and Admittance.[57] Here, R_1/X_1 are the Positive-Sequence resistance/reactance per unit length and R_0/X_0 are the Zero-Sequence resistance/reactance per unit length. Due to the short distance the capacitance of C_1 and C_0 are zero.

Name	phases	$R_1(\Omega/km)$	$X_1(\Omega/km)$	$R_0(\Omega/km)$	$X_0(\Omega/km)$	$C_1(F)$	$C_0(F)$
2c_.007	3	3.97	0.099	3.97	0.099	0	0
2c_.0225	3	1.257	0.085	1.257	0.085	0	0
2c_16	3	1.15	0.088	1.2	0.088	0	0
35_SAC_XSC	3	0.868	0.092	0.76	0.092	0	0
4c_.06	3	0.469	0.075	1.581	0.091	0	0
4c_.1	3	0.274	0.073	0.959	0.079	0	0
4c_.35	3	0.089	0.0675	0.319	0.076	0	0
4c_185	3	0.166	0.068	0.58	0.078	0	0
4c_70	3	0.446	0.071	1.505	0.083	0	0
4c_95_SAC_XC	3	0.322	0.074	0.804	0.093	0	0

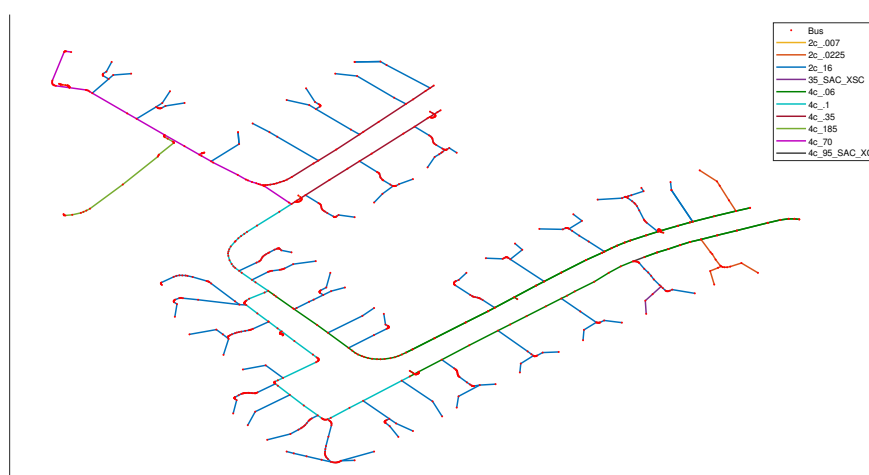


Figure A.1: A single line diagram of the IEEE European LV Test Feeder by cable type.

Figure A.2 shows a bar graph, of the positive-sequence R/X ratio, of the distribution lines used in the IEEE European low voltage test Feeder.

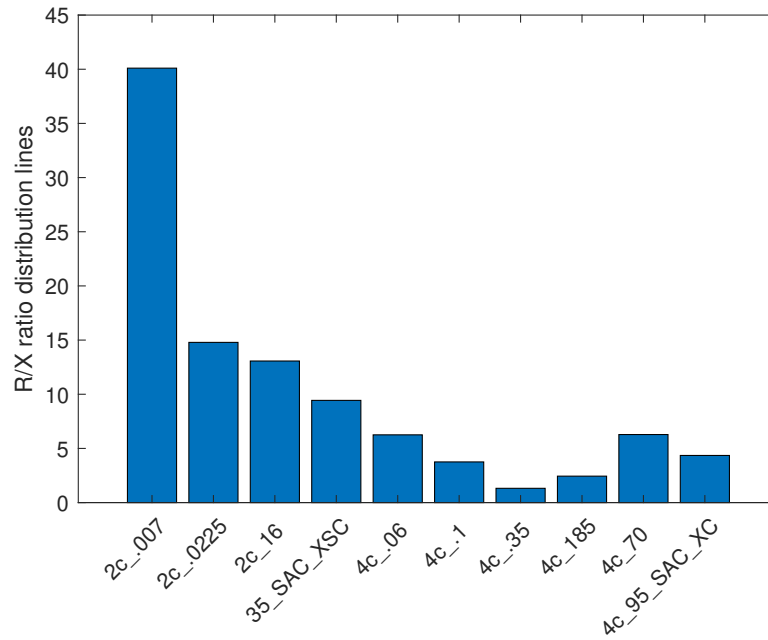


Figure A.2: Bar graph of the positive-sequence R/X ratio of the cables of the IEEE European Low voltage test Feeder.

B

Newton-Raphson Power flow equations

The current through a line, is described by:

$$I = YV \quad (\text{B.1})$$

Here, Y is the admittance, I the current and V the voltage. If this extended to a n bus system, the equation in matrix form becomes:

$$\begin{bmatrix} I_1 \\ I_2 \\ \vdots \\ I_i \\ \vdots \\ I_n \end{bmatrix} = \begin{bmatrix} Y_{11} & Y_{12} & \cdots & Y_{1i} & \cdots & Y_{1n} \\ Y_{21} & Y_{22} & \cdots & Y_{2i} & \cdots & Y_{2n} \\ \vdots & \vdots & \ddots & \vdots & & \vdots \\ Y_{i1} & Y_{i2} & \cdots & Y_{ii} & \cdots & Y_{in} \\ \vdots & \vdots & & \vdots & \ddots & \vdots \\ Y_{n1} & Y_{n2} & \cdots & Y_{ni} & \cdots & Y_{nn} \end{bmatrix} \begin{bmatrix} V_1 \\ V_2 \\ \vdots \\ V_i \\ \vdots \\ V_n \end{bmatrix} \quad (\text{B.2})$$

A single line of Equation B.2 can be written as:

$$I_i = \sum_{j=1}^n Y_{ij} V_j \quad (\text{B.3})$$

where n is the total buses in the network. Written in Polar form, this becomes:

$$I_i = \sum_{j=1}^n |Y_{ij}| |V_j| \angle \theta_{ij} + \delta_j \quad (\text{B.4})$$

where δ_j is the angle of the Voltage V_j and θ_{ij} is the angle of the admittance Y_{ij} .

The complex power at bus i is described as:

$$P_i - jQ_i = V_i^* I_i \quad (\text{B.5})$$

when Equation B.4 is filled in Equation B.5, this results in:

$$P_i - jQ_i = |V_i| \angle -\delta_i \sum_{j=1}^n |Y_{ij}| |V_j| \angle \theta_{ij} + \delta_j \quad (\text{B.6})$$

By separating the equation into a real and imaginary parts, the power flow equations are obtained. These are described as:

$$\begin{aligned} P_i &= \sum_{j=1}^n |Y_{ij}| |V_i| |V_j| \cos(\theta_{ij} + \delta_j - \delta_i) \\ Q_i &= - \sum_{j=1}^n |Y_{ij}| |V_i| |V_j| \sin(\theta_{ij} + \delta_j - \delta_i) \end{aligned} \quad (\text{B.7})$$

Acronyms

AC Alternating Current.
ADN active distribution network.
APC active power control.
BESS battery energy storage system.
CB capacitor bank.
DC Direct Current.
DER distributed energy resources.
DG distributed generation.
DN distribution network.
DSM demand side management.
DSO distribution system operator.
DVR Dynamic voltage restorer.
EMS energy management system.
ESS energy storage system.
EV electric vehicle.
FACTS Flexible alternating current transmission systems.
GAMS General Algebraic Modeling System.
HVCS Hierarchical voltage control structure.
MPC model predictive controller.
MPPT Maximum power point tracking.
NLP non linear programming.
OLTC on-load tap changer.
p.u. per unit.
PCC Point of common coupling.
PV Photovoltaics.
RES renewable energy sources.
RPC reactive power control.
SCADA supervisory control and data acquisition.
STATCOM static compensators.
SVC Static VAR compensator.
SVR step voltage regulators.
TN Transmission network.
TSO transmission system operator.
V2G vehicle-to-grid.
VMS Voltage management system.
VVC Volt-VAR control.

Nomenclature

$\Delta E_{bat,dcap}$	Battery degradation per time step [kWh/h]
$\Delta E_{bat,dcap}$	Total battery degradation over a day [kWh]
Δk	Optimisation time step interval [h]
ΔP_{bat}	Real-time variation in BESS (dis)charging [kW]
ΔP_{conv}	Real-time variation in export/import of the multi-port converter [kW]
ΔP_{ev}	Real-time variation in EV (dis)charging [kW]
$\Delta P_{load,error}$	Real-time load error in the distribution network [kW]
ΔP_{load}	Real-time variation in load demand [kW]
$\Delta P_{pv,error}$	Real-time PV error in the distribution network [kW]
ΔP_{pv}	Real-time variation in PV generation [kW]
$\Delta P_{total,error}$	Real-time total error in the distribution network [kW]
ΔV_i	Difference in voltage at bus i [V]
η_{bat}	(Dis)charging efficiency BESS [%]
η_{conv}	Importing/Exporting Converter efficiency [%]
η_{ev}	(Dis)charging efficiency EV [%]
η_{grid}	Cable efficiency [%]
η_{MPPT}	Efficiency of MPPT [%]
λ_{buy}	Buying price electricity [Euro]
λ_{sell}	Selling price electricity [Euro]
$\bar{\lambda}_{buy}$	Altered buying price [Euro]
$\bar{\lambda}_{sell}$	Altered selling price [Euro]
$C_{bat,soft}$	Total cost BESS soft constraint
C_{bat}	Total operational cost BESS [Euro]
C_{dev}	Cost charge deviation
$C_{ev,soft}$	Total cost EV soft constraint
C_{ev}	Total operational cost EV [Euro]
C_{grid}	Total energy cost [Euro]
C_{pv}	Total cost PV [Euro]
C_{total}	Total cost of operation multi-port converter [Euro]
E_{bat}^{max}	Maximum BESS capacity [kWh]
E_{ev}^{max}	Maximum EV capacity [kWh]

$E_{bat,1}$	Battery charge reference tracker [kWh]
$E_{bat,dev}$	Penalised charge deviation [kWh]
$E_{bat,final}$	Final capacity BESS [kWh]
$E_{bat,init}$	Initial capacity BESS [kWh]
$E_{bat,lim}$	Reserved capacity BESS [kWh]
$E_{bat,np}$	Maximum possible charge deviation without penalty [kWh]
$E_{bat,soft}$	Soft constraints BESS [kWh]
$E_{dep,soft}$	Soft constraint for departure of EV
$E_{ev,arr}$	EV charge at arrival [kWh]
$E_{ev,dep}$	EV charge at departure [kWh]
$E_{ev,final}$	Final capacity EV [kWh]
$E_{ev,init}$	Initial capacity EV [kWh]
$E_{ev,soft}$	Soft constraints EV [kWh]
EV_{avail}	Availability of the EV
I_{bat}	BESS cell current [A]
I_{ij}	Current flow from bus i to j [A]
I_{ij}	Current through the line from bus i to j [A]
k	Optimisation time index
$k_{ev,arr}$	Time index step of arrival
$k_{ev,dep}$	Time index step of departure
k_{res}	Time step index for power reservation
$N_{bat}^{parallel}$	Number of battery cells in parallel for BESS
$N_{ev}^{parallel}$	Number of battery cells in parallel for EV
N^{series}	Number of battery cells in series
P	Active Power [kW]
$P^{conv,pv,res}$	Maximal curtailment capacity PV [kW]
$P^{max,ex}$	The maximum allowed export of active power from the multi-port converter [kW]
$P^{max,imp}$	The maximum allowed imp of active power to the multi-port converter [kW]
P_{bat}^{max}	Maximum BESS (dis)charging power [kW]
$P_{conv,bat,ch}^{max}$	Maximal charging capacity BESS [kW]
$P_{conv,bat,dis}^{max}$	Maximal discharging capacity BESS [kW]
$P_{conv,conv,ex}^{max}$	Maximal export capacity BESS [kW]
$P_{conv,conv,imp}^{max}$	Maximal import capacity BESS [kW]
$P_{conv,ev,dis}^{max}$	Maximal Charging capacity EV [kW]
$P_{conv,ev,dis}^{max}$	Maximal Discharging capacity EV [kW]
P_{ev}^{max}	Maximum EV (dis)charging power [kW]

P_{pv}^{rated}	Installed PV capacity Power [kWp]
P_{bat}	Energy to/from the BESS from/to the multi-port converter [kW]
$P_{cap,ex}$	Maximal export capacity for each multi-port converter [kW]
$P_{cap,imp}$	Maximal import capacity for each multi-port converter [kW]
P_{conv}	Import to/from the AC/DC converter of the multi-port converter [kW]
P_{drive}	Power used when EV is not available at the house [kW]
$P_{ev,fc}$	Forecasted energy demand for EV with houses without a multi-port converter [kW]
P_{ev}	Energy to/from the EV from/to the multi-port converter [kW]
$P_{grid,ex}$	Power exchange multi-port converter to the distribution network [kW]
$P_{grid,imp}$	Power exchange multi-port converter from the distribution network [kW]
P_{grid}	Power exchange multi-port converter with distribution network [kW]
P_{ij}^{loss}	Active power losses from bus i to j [kW]
$P_{load,act}$	Actual load demand [kW]
$P_{load,fc}$	Forecasted load demand [kW]
$P_{pv,act}$	Actual PV generation [kW]
$P_{pv,fc}$	Forecasted PV generation [kW]
P_{pv}	Energy from the solar panels to the multi-port converter [kW]
P_{res}	Reserved Power exchange by the DSO [kW]
pf	Power factor angle [rad]
Q	Reactive Power [kVAR]
Q_{conv}^{max}	Maximum amount of reactive power support [kVAR]
Q_{conv}	Reactive power output multi-port converter [kVAR]
R_{ij}	Resistance from bus i to j [Ω]
r_{pv}	Ratio PV generation in multi-port converters and total PV generation
S	Apparent Power [kVA]
S_{conv}^{max}	Maximum apparent power rating of the multi-port converter [kVA]
SoC _{bat}	State of charge BESS [%]
SoC _{depart}	State of charge EV at departure [%]
SoC _{ev}	State of charge EV [%]
V_i	Voltage at bus i [V]
V_{bat}	Value of BESS battery per kWh [Euro]
V_{bat}^0	Initial value of BESS battery per kWh [Euro]
V_{ev}	Value of EV battery per kWh [Euro]
V_{ev}^0	Initial value of EV battery per kWh [Euro]
V_{mag}	Voltage magnitude computed by VMS [V]
$V_{oc,bat}$	Open circuit Voltage BESS [kVA]
X_{ij}	Reactance from bus i to j [Ω]
Y_{ij}	Admittance from bus i to j [S]

Bibliography

- [1] Eurostat, “Renewable energy in the eu in 2018.” [Online]. Available: <https://ec.europa.eu/eurostat/documents/2995521/10335438/8-23012020-AP-EN.pdf/292cf2e5-8870-4525-7ad7-188864ba0c29>
- [2] A. Gerbrandy, “Klimaatakkoord (en) en het mededingingsrecht.” Raad van State, 2018.
- [3] Eurostat, “Energy consumption in households.” [Online]. Available: https://ec.europa.eu/eurostat/statistics-explained/index.php?title=Energy_consumption_in_households
- [4] “Hoe lang kan ik nog koken en stoken op gas?” [Online]. Available: <https://www.rijksoverheid.nl/onderwerpen/duurzame-energie/vraag-en-antwoord/hoe-lang-kan-ik-nog-koken-op-gas>
- [5] “Bijna 200 duizend stekkerauto’s,” <https://www.cbs.nl/nl-nl/nieuws/2020/16/bijna-200-duizend-stekkerauto-s>, accessed: 7-12-2020.
- [6] R. Harrabin. (2020) Ban on new petrol and diesel cars in uk from 2030 under pm’s green plan. [Online]. Available: <https://www.bbc.com/news/science-environment-54981425>
- [7] Eurostat, “Final energy consumption in europe by mode of transport.” [Online]. Available: [https://www.eea.europa.eu/data-and-maps/indicators/transport-final-energy-consumption-by-mode/assessment-10#:~:text=Annual%20energy%20consumption%20in%20transport,%25%20in%20EU%2D28\).&text=Road%20transport%20accounts%20for%20the,in%202017%20than%20in%201990.](https://www.eea.europa.eu/data-and-maps/indicators/transport-final-energy-consumption-by-mode/assessment-10#:~:text=Annual%20energy%20consumption%20in%20transport,%25%20in%20EU%2D28).&text=Road%20transport%20accounts%20for%20the,in%202017%20than%20in%201990.)
- [8] “Cbs trends in the netherlands 2018 - energy,” <https://longreads.cbs.nl/trends18-eng/economy/figures/energy/#:~:text=The%20average%20electricity%20consumption%20per,as%20opposed%20to%204%2C120%20kWh.>, accessed: 7-12-2020.
- [9] N. Augusteijn. (2020) Houden we het elektriciteitsnet met miljoenen elektrische auto’s in stand? [Online]. Available: <https://www.nu.nl/auto/5996849/houden-we-het-elektriciteitsnet-met-miljoenen-elektrische-autos-in-stand.html>
- [10] H. Ekker. (2020) Aantal huizen met zonnepanelen tikt 1 miljoen aan. [Online]. Available: <https://nos.nl/artikel/2345132-aantal-huizen-met-zonnepanelen-tikt-1-miljoen-aan.html>
- [11] “Directive 2009/72/ec of the european parliament and of the council of 13 july 2009 concerning common rules for the internal market in electricity and repealing directive 2003/54/ec,” <https://eur-lex.europa.eu/legal-content/en/ALL/?uri=celex%3A32009L0072>, accessed: 18-2-2020.
- [12] S. Parhizi, H. Lotfi, A. Khodaei, and S. Bahramirad, “State of the art in research on microgrids: A review,” *Ieee Access*, vol. 3, pp. 890–925, 2015.
- [13] N. Mahmud and A. Zahedi, “Review of control strategies for voltage regulation of the smart distribution network with high penetration of renewable distributed generation,” *Renewable and Sustainable Energy Reviews*, vol. 64, pp. 582–595, 2016.
- [14] X. Fang, S. Misra, G. Xue, and D. Yang, “Smart grid—the new and improved power grid: A survey,” *IEEE communications surveys & tutorials*, vol. 14, no. 4, pp. 944–980, 2011.
- [15] C. D’Adamo, S. Jupe, and C. Abbey, “Global survey on planning and operation of active distribution networks-update of cigre c6. 11 working group activities,” in *CIGRE 2009-20th International Conference and Exhibition on Electricity Distribution-Part 1*. IET, 2009, pp. 1–4.

- [16] J. R. Roncero, "Integration is key to smart grid management," in *CIREC Seminar 2008: Smart-Grids for Distribution*. IET, 2008, pp. 1–4.
- [17] C. Gao and M. Redfern, "A review of voltage control in smart grid and smart metering technologies on distribution networks," in *2011 46th International Universities' Power Engineering Conference (UPEC)*. VDE, 2011, pp. 1–5.
- [18] G. R. C. Mouli, P. Bauer, T. Wijekoon, A. Panosyan, and E.-M. Bärthlein, "Design of a power-electronic-assisted oltc for grid voltage regulation," *IEEE Transactions on Power Delivery*, vol. 30, no. 3, pp. 1086–1095, 2014.
- [19] W. Vermeer, G. R. Chandra Mouli, and P. Bauer, "Real-time building smart charging system based on pv forecast and li-ion battery degradation," *Energies*, vol. 13, no. 13, p. 3415, 2020.
- [20] P. Chaudhary and M. Rizwan, "Voltage regulation mitigation techniques in distribution system with high pv penetration: A review," *Renewable and Sustainable Energy Reviews*, vol. 82, pp. 3279–3287, 2018.
- [21] "Power factor file: Lagging-leading," https://en.wikipedia.org/wiki/Power_factor#/media/File:Lagging-Leading.jpg, accessed: 18-2-2020.
- [22] "Netcode elektriciteit," <https://wetten.overheid.nl/jci1.3:c:BWBR0037940&hoofdstuk=2¶graaf=2.4&sub-paragraaf=2.4.1&artikel=2.4.1.2&z=2017-01-01&g=2017-01-01>, accessed: 18-2-2020.
- [23] A. M. Nour, A. Y. Hatata, A. A. Helal, and M. M. El-Saadawi, "Review on voltage-violation mitigation techniques of distribution networks with distributed rooftop pv systems," *IET Generation, Transmission & Distribution*, vol. 14, no. 3, pp. 349–361, 2019.
- [24] M. N. I. Sarkar, L. G. Meegahapola, and M. Datta, "Reactive power management in renewable rich power grids: A review of grid-codes, renewable generators, support devices, control strategies and optimization algorithms," *IEEE Access*, vol. 6, pp. 41 458–41 489, 2018.
- [25] M. M. Haque and P. Wolfs, "A review of high pv penetrations in lv distribution networks: Present status, impacts and mitigation measures," *Renewable and Sustainable Energy Reviews*, vol. 62, pp. 1195–1208, 2016.
- [26] D. J. Rogers and T. C. Green, "A hybrid diverter design for distribution level on-load tap changers," in *2010 IEEE Energy Conversion Congress and Exposition*. IEEE, 2010, pp. 1493–1500.
- [27] M. Guo, Q. Jin, Z. Yao, and W. Chen, "Analysis on the reason of low voltage problem and the effectiveness of voltage regulation in a distribution area," *E&ES*, vol. 440, no. 3, p. 032128, 2020.
- [28] P. V. K. Andersen, S. Georg, K. Gram-Hanssen, P. Heiselberg, A. Horsbøl, K. Johansen, H. Johra, A. Marszal-Pomianowska, and E. S. Møller, "Using residential buildings to manage flexibility in the district heating network: perspectives and future visions from sector professionals," in *IOP Conference Series: Earth and Environmental Science*, vol. 352, no. 1. IOP Publishing, 2019, p. 012032.
- [29] E. Yao, P. Samadi, V. W. Wong, and R. Schober, "Residential demand side management under high penetration of rooftop photovoltaic units," *IEEE Transactions on Smart Grid*, vol. 7, no. 3, pp. 1597–1608, 2015.
- [30] H. Chen, T. N. Cong, W. Yang, C. Tan, Y. Li, and Y. Ding, "Progress in electrical energy storage system: A critical review," *Progress in natural science*, vol. 19, no. 3, pp. 291–312, 2009.
- [31] X. Xi, R. Sioshansi, and V. Marano, "A stochastic dynamic programming model for co-optimization of distributed energy storage," *Energy Systems*, vol. 5, no. 3, pp. 475–505, 2014.

- [32] M. Ban, D. Guo, J. Yu, and M. Shahidehpour, "Optimal sizing of pv and battery-based energy storage in an off-grid nanogrid supplying batteries to a battery swapping station," *Journal of Modern Power Systems and Clean Energy*, vol. 7, no. 2, pp. 309–320, 2019.
- [33] P. M. Carvalho, P. F. Correia, and L. A. Ferreira, "Distributed reactive power generation control for voltage rise mitigation in distribution networks," *IEEE transactions on Power Systems*, vol. 23, no. 2, pp. 766–772, 2008.
- [34] B. Bletterie, S. Kadam, R. Bolgarny, and A. Zegers, "Voltage control with pv inverters in low voltage networks—in depth analysis of different concepts and parameterization criteria," *IEEE Transactions on Power Systems*, vol. 32, no. 1, pp. 177–185, 2016.
- [35] E. Demirok, P. C. Gonzalez, K. H. Frederiksen, D. Sera, P. Rodriguez, and R. Teodorescu, "Local reactive power control methods for overvoltage prevention of distributed solar inverters in low-voltage grids," *IEEE Journal of Photovoltaics*, vol. 1, no. 2, pp. 174–182, 2011.
- [36] J. Seuss, M. J. Reno, M. Lave, R. J. Broderick, and S. Grijalva, "Advanced inverter controls to dispatch distributed pv systems," in *2016 IEEE 43rd Photovoltaic Specialists Conference (PVSC)*. IEEE, 2016, pp. 1387–1392.
- [37] A. Maknouninejad, Z. Qu, J. Enslin, and N. Kutkut, "Clustering and cooperative control of distributed generators for maintaining microgrid unified voltage profile and complex power control," in *PES T&D 2012*. IEEE, 2012, pp. 1–8.
- [38] H.-G. Yeh, D. F. Gayme, and S. H. Low, "Adaptive var control for distribution circuits with photovoltaic generators," *IEEE Transactions on Power Systems*, vol. 27, no. 3, pp. 1656–1663, 2012.
- [39] Y. Xu, Z. Y. Dong, R. Zhang, and D. J. Hill, "Multi-timescale coordinated voltage/var control of high renewable-penetrated distribution systems," *IEEE Transactions on Power Systems*, vol. 32, no. 6, pp. 4398–4408, 2017.
- [40] C. Zhang and Y. Xu, "Hierarchically-coordinated voltage/var control of distribution networks using pv inverters," *IEEE Transactions on Smart Grid*, 2020.
- [41] T. Van Dao, S. Chaitusaney, and H. T. N. Nguyen, "Linear least-squares method for conservation voltage reduction in distribution systems with photovoltaic inverters," *IEEE Transactions on Smart Grid*, vol. 8, no. 3, pp. 1252–1263, 2016.
- [42] T. Ding, C. Li, Y. Yang, J. Jiang, Z. Bie, and F. Blaabjerg, "A two-stage robust optimization for centralized-optimal dispatch of photovoltaic inverters in active distribution networks," *IEEE Transactions on Sustainable Energy*, vol. 8, no. 2, pp. 744–754, 2016.
- [43] C. Zhang, Y. Xu, Z. Y. Dong, and R. Zhang, "Multi-objective adaptive robust voltage/var control for high-pv penetrated distribution networks," *IEEE Transactions on Smart Grid*, vol. 11, no. 6, pp. 5288–5300, 2020.
- [44] C. Li, V. R. Disfani, H. V. Haghi, and J. Kleissl, "Coordination of oltc and smart inverters for optimal voltage regulation of unbalanced distribution networks," *Electric Power Systems Research*, vol. 187, p. 106498, 2020.
- [45] C. Zhang, Y. Xu, Z. Dong, and J. Ravishankar, "Three-stage robust inverter-based voltage/var control for distribution networks with high-level pv," *IEEE Transactions on Smart Grid*, vol. 10, no. 1, pp. 782–793, 2017.
- [46] D. He, D. Shi, and R. Sharma, "Consensus-based distributed cooperative control for microgrid voltage regulation and reactive power sharing," in *IEEE PES Innovative Smart Grid Technologies, Europe*. IEEE, 2014, pp. 1–6.

- [47] A. Bidram, A. Davoudi, F. L. Lewis, and J. M. Guerrero, "Distributed cooperative secondary control of microgrids using feedback linearization," *IEEE Transactions on Power Systems*, vol. 28, no. 3, pp. 3462–3470, 2013.
- [48] A. Parisio, E. Rikos, and L. Glielmo, "A model predictive control approach to microgrid operation optimization," *IEEE Transactions on Control Systems Technology*, vol. 22, no. 5, pp. 1813–1827, 2014.
- [49] —, "Stochastic model predictive control for economic/environmental operation management of microgrids: An experimental case study," *Journal of Process Control*, vol. 43, pp. 24–37, 2016.
- [50] Y. Li, L. Li, C. Peng, and J. Zou, "An mpc based optimized control approach for ev-based voltage regulation in distribution grid," *Electric Power Systems Research*, vol. 172, pp. 152–160, 2019.
- [51] Z. Ji, X. Huang, C. Xu, and H. Sun, "Accelerated model predictive control for electric vehicle integrated microgrid energy management: A hybrid robust and stochastic approach," *Energies*, vol. 9, no. 11, p. 973, 2016.
- [52] M. Brandstetter, A. Schirrer, M. Miletić, S. Henein, M. Kozek, and F. Kupzog, "Hierarchical predictive load control in smart grids," *IEEE Transactions on Smart Grid*, vol. 8, no. 1, pp. 190–199, 2015.
- [53] A. Parisio, C. Wiezorek, T. Kytäjä, J. Elo, K. Strunz, and K. H. Johansson, "Cooperative mpc-based energy management for networked microgrids," *IEEE Transactions on Smart Grid*, vol. 8, no. 6, pp. 3066–3074, 2017.
- [54] N. Holjevac, T. Capuder, N. Zhang, I. Kuzle, and C. Kang, "Corrective receding horizon scheduling of flexible distributed multi-energy microgrids," *Applied Energy*, vol. 207, pp. 176–194, 2017.
- [55] F. Kennel, D. Görge, and S. Liu, "Energy management for smart grids with electric vehicles based on hierarchical mpc," *IEEE Transactions on industrial informatics*, vol. 9, no. 3, pp. 1528–1537, 2012.
- [56] A. Bemporad and M. Morari, "Control of systems integrating logic, dynamics, and constraints," *Automatica*, vol. 35, no. 3, pp. 407–427, 1999.
- [57] "Ieee european low voltage test feeder," <https://site.ieee.org/pes-testfeeders/resources/>, accessed: 18-2-2020.
- [58] A. I. Nousedilis, A. I. Chrysochos, G. K. Papagiannis, and G. C. Christoforidis, "The impact of photovoltaic self-consumption rate on voltage levels in lv distribution grids," in *2017 11th IEEE International Conference on Compatibility, Power Electronics and Power Engineering (CPE-POWERENG)*. IEEE, 2017, pp. 650–655.
- [59] H. Saadat *et al.*, *Power system analysis*. McGraw-hill, 1999, vol. 2.
- [60] "Electric power research institute, opendss, distribution system simulator [online].," <http://sourceforge.net/projects/electricdss/>.
- [61] L. Saputelli, M. Nikolaou, and M. Economides, "Real-time reservoir management: A multi-scale adaptive optimization and control approach," *Computational Geosciences*, vol. 10, no. 1, pp. 61–96, 2006.
- [62] G. R. C. Mouli, J. H. Schijffelen, P. Bauer, and M. Zeman, "Design and comparison of a 10-kw interleaved boost converter for pv application using si and sic devices," *IEEE Journal of Emerging and Selected Topics in Power Electronics*, vol. 5, no. 2, pp. 610–623, 2016.

- [63] “Lg chem resu 10h—400v lithium-ion storage battery.” <https://www.europe-solarstore.com/lg-chem-resu-10h-400v-lithium-ion-storage-battery.html>.
- [64] G. R. C. Mouli, “Charging electric vehicles from solar energy: Power converter, charging algorithm and system design,” 2018.
- [65] W. Khan, F. Ahmad, and M. S. Alam, “Fast ev charging station integration with grid ensuring optimal and quality power exchange,” *Engineering Science and Technology, an International Journal*, vol. 22, no. 1, pp. 143–152, 2019.
- [66] J. Wang, J. Purewal, P. Liu, J. Hicks-Garner, S. Soukazian, E. Sherman, A. Sorenson, L. Vu, H. Tataria, and M. W. Verbrugge, “Degradation of lithium ion batteries employing graphite negatives and nickel–cobalt–manganese oxide+ spinel manganese oxide positives: Part 1, aging mechanisms and life estimation,” *Journal of Power Sources*, vol. 269, pp. 937–948, 2014.
- [67] I. Baccouche, S. Jemmali, B. Manai, N. Omar, and N. E. B. Amara, “Improved ocv model of a li-ion nmc battery for online soc estimation using the extended kalman filter,” *Energies*, vol. 10, no. 6, p. 764, 2017.
- [68] G. R. C. Mouli, M. Leendertse, V. Prasanth, P. Bauer, S. Silvester, S. van de Geer, and M. Zeman, “Economic and co2 emission benefits of a solar powered electric vehicle charging station for workplaces in the netherlands,” in *2016 IEEE Transportation Electrification Conference and Expo (ITEC)*. IEEE, 2016, pp. 1–7.
- [69] “Antigone, algorithms for continuous / integer global optimization of nonlinear equations, is a deterministic general mixed-integer nonlinear global optimization framework,” https://www.gams.com/latest/docs/S_ANTIGONE.html.